ANALYSIS OF THE PERFORMANCE FOR A HIGH FLUX HEAT EXCHANGER

By

JAMES MICHAEL CUTBIRTH

Bachelor of Science

in Mechanical Engineering

Oklahoma State University

Stillwater, Oklahoma

1994

Submitted to the Faculty of the
Graduate College of the
Oklahoma State University
in partial fulfillment of
the requirements for
the Degree of
MASTER OF SCIENCE
May, 1996

ANALYSIS OF THE PERFORMANCE FOR A

HIGH FLUX HEAT EXCHANGER

Thesis Approved:

A. J. Ghajar

Thesis Advisor

Ronald L. Daugherty

Thomas C. Collins

Dean of the Graduate College

ACKNOWLEDGMENTS

I wish to declare greatest appreciation to my advisor, Dr. A. J. Ghajar, for his confidence in my ability to perform this novel heat transfer study, and providing me the opportunity to do so. In addition, I give special thanks for his continuous patience, for his boundless guidance, for his endless encouragement, and his support.

I am deeply indebted to the members of my committee, Dr. R. L. Dougherty and Dr. F. Chambers for their valuable help and constructive criticisms and wish to express my gratitude to them. I am privileged to have had a committee that consisted of the cornerstones of the Mechanical Engineering Department.

This analysis for the High Flux Heat Exchanger was conducted under sponsorship of the Air Force Wright Laboratory, Aero Propulsion and Power Directorate, Wright Patterson AFB, Ohio, with Dr. Jerry E. Beam and Dr. John E. Leland as Project Managers.

A special thanks to Don Reinmuller of Wright Laboratories for his essential assistance in developing and building the test setup for this research.

In the development of the data reduction program LAB,

I wish to thank my father Dr. Jim Cutbirth, whose understanding of FORTRAN far outweighs mine.

To both my parents, Jim and Denise Cutbirth, who never waived in their support of me, who allowed their ears to be continually bent, and who always emanated confidence in my abilities, I wish to express my warmest appreciation.

My final and most deserved thanks is reserved for my fiancee Michelle, who has tolerated the many hours and days I have spent at the laboratory completing the requirements of this investigation without complaint, and indeed has given the support and love which has carried me throughout.

TABLE OF CONTENTS

Chapter Page

LIST OF TABLES

LIST OF FIGURES

Figure Page

NOMENCLATURE

A	cross-sectional area of the individual channels of the CHIC, m^2
b	spacing in a dead-weight tester, cm
C	constant relating the Reynolds number and the friction factor for laminar flow
C_n	constants in the curve fit for the pressure, with n =1,2
d	diameter of the piston in the dead-weight tester, cm
D	diameter of the individual channels in the CHIC, m
f	friction factor for pipe flow, dimensionless
g	gravitational acceleration, m^2/s
g_c	gravitational constant, kg-m/N-s^2
h	enthalpy, N-m/kg
h_f	total frictional head loss, m
k	thermal conductivity of the HFHE (copper), 300 W/m-°C
k_i	minor loss coefficient for the CHIC for pipe flow, dimensionless
l	length of the piston in the dead-weight tester, cm
L	length of the individual tubes in the CHICs, m
$\dot{m}$	mass flow rate of the fluid, kg/hr
p	pressure, psi
Q	volumetric flow rate, m^3/s

$\dot{Q}$ heat transfer, W/cm^2 or W per CHIC (each CHIC has a surface area of 1 cm^2)

Re Reynolds number (= $\rho VD/\mu$), dimensionless

R_{xy} thermal resistance from x to y, $°C/(W/cm^2)$

r_n distance from CHIC center to symmetry boundary in n-direction, m

t conduction thickness of the target plate, 0.001143 m

T_n temperature of n, where n is a subscript referring to the coolant fluid, surface of the HFHE, wall of the CHIC, and the junction, °C

v volume of fluid, mL

V velocity of the fluid in the test section, m/s

w work, J/kg

$\dot{W}$ power, W/s

z potential energy term, m

Greek letter symbols

Δp pressure drop across the HFHE, psi

ε error term, dimensionless

ϕ_n constant in the $\dot{Q}_{loss}/\dot{Q}_{applied}$ curve fit, n=1,...,7

γ specific weight of the coolant fluid, N/m^3

λ_n constant in the wall temperature curve fit, n=0,1,2,3

μ absolute viscosity of the coolant fluid, $N\text{-}s/m^2$

ν kinematic viscosity of the coolant fluid, m^2/s

θ_n constant in the surface temperature curve fit, n=1,2,3

ρ density of the coolant fluid, kg/m^3

ξ dummy variable to express the direction of the radial heat flow, cm

ψ temporary coefficient for the wall temperature, dimensionless

Subscripts

c refers to the case housing of the electronics

e exit of the control volume

f refers to the coolant fluid

i inlet to the control volume

j refers to the junction of the case housing and the electronic chip

mech mechanical (i.e. mechanical work)

s refers to the surface of the HFHE

s_τ Viscous stress

w refers to the outer wall of the CHIC in the HFHE

CHAPTER I

INTRODUCTION

This chapter will first present background as it relates to the study of the hydraulic and thermal performance of the High Flux Heat Exchanger. The purposes of the investigation will be given and a summary of the performed experimental work will be included. Finally, brief statements about the previous work of other investigations, relating to the development of the High Flux Heat Exchanger, will justify the need for experimentation such as this.

1.1 Background

Modern aircraft has seen an increase in dependence on electronics. New on-board electronics require more data processing units for improvements in navigation and high-powered radar. In addition, computer technology is constantly creating more powerful electronic chips without increasing the surface area. The combination of these factors has created a need for improved coolant systems to dissipate the increasing amount of thermal energy created by

the electronics. In past electronic components that have low power densities, the preferred cooling approach was air cooling due to its simplicity, leakage tolerance, and reliability. However, with the increase of electronic chip technology, processors have higher heat fluxes; thus, liquid cooling becomes more attractive even though the liquid cooling systems add an intermediate cooling loop. One of the most effective processes for liquid cooling is jet impingement. However, an analysis can be made that leads to the conclusion that a multiple number of small jets will be more effective in cooling the same area than a single large jet. Furthermore, the cooling performance can be enhanced by extending the surface areas. Therefore, a greater surface density per unit volume can be achieved leading to higher fin efficiencies all resulting from the use of shorter conduction path lengths that are vigorously scrubbed by high heat transfer coolant jets. The shorter path lengths are a result from using thin lamination plates in close proximity to the heat source. This concept of using multiple jet impingement with the enhancement of multiple plates let to Sundstrand's Compact High Intensity Cooler, CHIC. However, this concept only satisfies the requirement for higher heat fluxes caused by modern electronics. To meet the need for the increased number of electronic processors, McDonnell Douglas developed the High Flux Heat

Exchanger, HFHE. The HFHE consists of 20 CHICs arranged in parallel flow, with each CHIC being 1 cm^2 in contact area and capable of absorbing 100 W/cm^2.

Because of this need for liquid cooling to absorb higher heat fluxes, additional considerations must be introduced. With the added intermediate cooling loop, in the aircraft, associated with liquid cooling, leaking and handling of the liquid coolant are of immense concern. Also, with the increase of emphasis on safety and environmental hazards, this liquid coolant must be non-toxic, non-corrosive, and be an adequate dielectric. Because of these concerns, the Navy and Air Force have replaced Coolanol, a silicate based ester that forms flammable components when exposed to water, with polyalphaolefin, PAO, a synthetic oil.

1.2 Objectives

The long range goal of this investigation is to accurately model the thermal and hydraulic performance of the High Flux Heat Exchanger, HFHE, under actual performance conditions. The specific objectives of this research are:

1. To investigate the influence of the coolant flow rate and temperature on the pressure drop across the inlet and outlet of the HFHE. This

investigation should result in a hydraulic performance equation and corresponding performance curve with the flow rate and temperature as the dependent variables.

2. To investigate the influence of the coolant flow rate and temperature on the heat flux removal capabilities of the HFHE for steady-state heat loads. This investigation should result in a thermal performance curve and correlating equation for the necessary coolant flow rate with respect to the coolant temperature to achieve a given amount of heat flux removal (e.g. one performance curve for 100 Watts of heat flux removal, one performance curve for 80 Watts of heat flux removal, etc.)

3. To investigate the influence of the coolant flow rate and temperature on the heat flux removal capabilities of the HFHE for transient heat loads. This investigation should result in graphical presentation of the thermal lag of the HFHE.

4. To develop a guideline for the overall performance of the HFHE. This will consist of a performance chart and correlating equation combining the

hydraulic performance and the steady-state performance curves.

1.2.1 Long Term Goals

This thesis details the preparations of a suitable experimental apparatus with inherent versatility for the successful fulfillment of all long term objectives. In addition, this thesis concerns itself with both the methodology and the analysis of accurate modeling of the High Flux Heat Exchanger. The methodology was developed to be used not only on the HFHE but any other high flux heat exchanger developed for the purpose of cooling the avionics' electronic system. The common methodology will allow for comparison between the different proposed cooling systems. Furthermore, the test loop was designed to accommodate any heat exchanger that fits the SEM-E configuration (the SEM-E configuration is described in detail in the literature review).

1.2.2 Data Base

This thesis discusses the hydraulic and thermal performance of the High Flux Heat Exchanger over a wide range of mass flow rates, coolant temperatures, and heat loads. To provide the necessary data base, 104 experimental

runs were performed for the hydraulic tests, 1236 experimental runs were performed for the steady-state thermal tests, and 150 experimental runs were performed for the transient thermal tests. At the beginning of the research, it was determined that for each run, a minimum of fifteen data points were necessary for sufficient accuracy, due to the fluctuations of the data collection equipment. This reasoning is shown in Appendix A.

The hydraulic tests were performed over the following ranges: coolant temperature, -10°C to 50°C by an increment of 10°C, with the addition of -15°C to fully cover the effects of sub-zero coolant temperature, and mass flow rate, 1.0 kg/min to 4.0 kg/min by an increment of 0.25 kg/min.

The steady-state thermal tests were performed on six of the twenty CHICs in the HFHE, shown in Figure 1.1. The first three CHICs tested (CHICs: A, B, C) were evaluated in full to develop all of the correlations, and covered the following ranges: a coolant temperature of -10°C to 40°C by an increment of 10°C, a mass flow rate of 1.0 kg/min to 4.0 kg/min by an increment of 0.25 kg/min, and a heat load of 20 W to 100 W by an increment of 20 W. However, due to the constraints explained below, the flow rate and heat load ranges were truncated for certain coolant temperatures. One of the constraints states that the maximum HFHE wall

temperature be 50°C; therefore, the 100 W heat load for the 30°C coolant temperature and the 80 W and the 100 W heat load for the 40°C coolant temperature were eliminated. In addition, for these coolant temperatures, the minimum mass flow rate was raised to 2.0 kg/min. Also, due to the constraint of high pressure, the maximum flow rate was lowered to 3.0 kg/min for the 0°C and 10°C coolant temperatures.

The last three CHICs (CHICs: D, E, F) were then evaluated in part to cross-correlate with the first three CHICs. For these CHICs, the coolant temperature and heat load ranges were retained from the first three CHICs. However, the flow rate range was truncated to contain the following data points: the lowest flow rate, the lowest flow rate increased by 0.5 kg/min, the median flow rate, the highest flow rate decreased by 0.5 kg/min, and the highest flow rate for the corresponding coolant temperature (e.g. 1.0, 1.5, 2.5, 3.5, and 4.0 kg/min for a coolant temperature of 10°C).

Finally for the transient tests, the full coolant range, -10°C to 40°C, was retained. In addition, the flow rate data points were the same as the flow rate data points for the last three CHICs; the lowest flow rate, the lowest

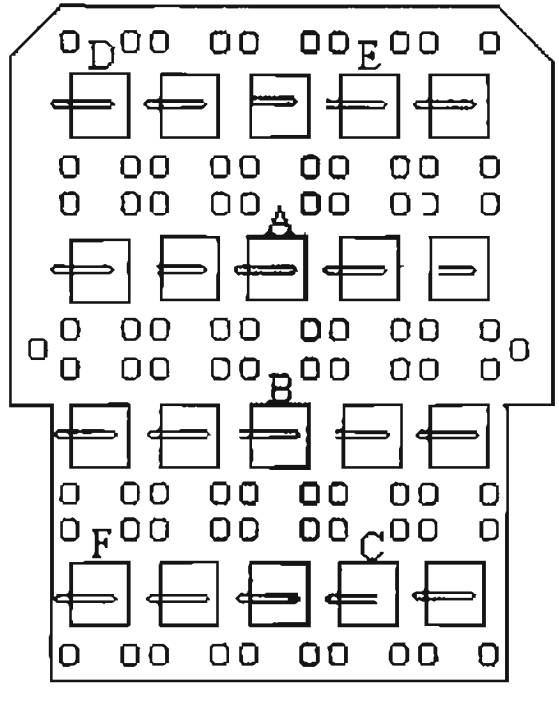

Figure 1.1. The Location of the Tested CHICs.

flow rate increased by 0.5 kg/min, the median flow rate, the highest flow rate decreased by 0.5 kg/min, and the highest flow rate for the corresponding temperature, as shown in the example above. Finally, the heat load range was reduced to 10 W to 50 W by an increment of 10 W.

1.2.3 Correlation Comparisons

For this data base, few correlations are possible due to the small amount of existing data on the High Flux Heat Exchanger.

For the hydraulic tests, Sundstrand has existing computer programs that are capable of predicting the hydraulic performance of the Compact High Intensity Cooler in any geometric arrangement. However, these programs only predict the hydraulic performance for the turbulent flow regime. In addition, the experimental analysis backing these existing performances are for fluids other than polyalphaolefin. For this research, only the combination of the extreme end of the flow range, 4.0 kg/min, and the extreme end of the coolant temperature, 50°C, results in non-laminar flow. For these parameters, the Reynolds number is 2176 which is slightly in the transitional flow region. Therefore, the flow regime and the fluid used in this research have not previously been examined in detail, and

all previous predictions for the HFHE must be used roughly.

In addition, the thermal performance, both steady-state and transient, have been previously examined by McDonnell Douglas. However, this previous research covered only three discrete flow rates and a temperature range of 10°C to 40°C. Furthermore, the stacking of the laminates for the HFHE examined by McDonnell Douglas differs from the stacking of the laminates for the HFHE used in this research. Therefore, the thermal data in this research should theoretically differ from the thermal performance data recorded by McDonnell Douglas. In conclusion, the data collected in this research is unique, and all previous results for the HFHE are used as very rough approximations.

1.3 Literature Survey

Modern aircraft has seen an increase in dependence on electronics. Mackowski [1] performed an industrial survey to determine future requirements for the high flux heat removal in advanced electronics systems. The study focused on the technology requirements for military avionics systems. The results of this survey can be sorted into four broad application categories: commercial digital systems, military data processors, power processors and radar and optical systems. The commercial digital systems can be

divided into sub-categories, the first being the central processor units (CPUs) and gate arrays (customizable processors). Some thermal management researchers predict that future power dissipation in these devices will increase to 100 W per device, while each device's surface area will decrease to 1 cm^2; thereby creating a maximum heat flux of 1 W/cm^2. However, Mackowski states that these devices will have power consumptions that remain under 30 W.

The second sub-category is the mainframe computer. The modern mainframe itself can have power consumption of 500 W; however, the thermal load per individual chip is low due to the large number of chips used. One example given by Mackowski is a Motorola multi-chip module that can accommodate a heat load of up to 500 W. However, this module is 4 inches by 4 inches, yielding a heat flux of 14 W/cm^2. The second category includes military data processors. These processors range from the general data processor to missiles and smart weapons. However, even though it is predicted that the total power for each board may go as high as 400 W for these digital systems, the localized heat flux should not exceed 50 W/cm^2.

The third category, which includes general power processors, low-voltage power supplies, high-power systems, and neutral particle beam, require a cooling capability of at least 100 W/cm^2. However, the cooling capability could

be even higher because the solid state power switching devices can produce a pulsed heat flux of over 400 W/cm^2. The final category includes conventional radar, solid state RF arrays, laser radar, optical sensors, and laser communications. The most likely driver for high flux cooling from this category will be the solid state RF arrays and laser device. However, the localized heat fluxes for both of these devices are under 25 W/cm^2. As seen, the most challenging thermal problems were found to lie with the power controllers. The power controllers contain steady-state heat fluxes reaching at least 100 to 200 W/cm^2. In addition, pulsed heat loads of short duration, on the order of a second or less, could exceed 400 W/cm^2. The heat dissipation of future high-performance data processors was predicted to be somewhat lower, with steady-state levels reaching perhaps 50 to 100 W/cm^2.

Flynn [2] made an evaluation of cooling concepts for high power avionics applications. Based on the results of Mackowski [1], a steady-state chip heat flux of 100 W/cm^2 and a maximum chip junction temperature of 90°C was selected as representative thermal requirements for the near-future high power avionics. Several additional constraints were also imposed on the cooler due to the intended application of cooling fighter aircraft electronics. These constraints included a practical lower limit on coolant supply

temperature, the preference for a non-toxic, nonflammable, and nonfreezing coolant, the need to minimize weight and volume, and operation in an accelerating environment. Evaluation factors included aircraft system impact, cooler development status, and qualitative assessments of life cycle cost, reliability, maintainability, and safety. Among the emerging cooling technologies, seven concepts were identified which could meet the cooling requirements. The evaluated cooling concepts were: Compact High Intensity Cooler (CHIC), Curved Channel Flow with Subcooled Boiling, Evaporative Spray Cooler, Heat Pipe, Jet Impingement with Subcooled Boiling, Microchannel Cooler, and Pumped Capillary Evaporator. These seven cooling concepts were investigated in detail and an assessment of their performance was made against the evaluation factors. The Compact High Intensity Cooler (CHIC) concept was selected to meet the demanding thermal requirements foreseen for near-future avionics.

The CHIC device was first introduced by Sundstrand in 1983 (Bland, et al. [3]). The original CHIC was developed to provide a heat rejection of 50 W to a 1 cm by 1 cm surface, which results in a heat flux intensity of 50 W/cm^2 of heat removal with tight requirements for surface isothermality. This liquid single phase cooler combines the thermal efficiency of multiple jet impingement with a large

fin area to produce a high effective heat transfer coefficient.

In the development of the multi-CHIC High Flux Heat Exchanger, Flynn, et al. [4] made a comparison of a single jet impingement to multiple jet impingement. Ordinary jet impingement for a single jet can be divided into three zones: the stagnation zone, the turning region and the wall jet region. For jet impingement with multiple jets a fourth region occurs, the jet interaction zone. These four zones can be seen in Figure 1.2. The heat transfer rates are high for both of the inner regions. This leads to the conclusion that a multiple number of small jets will be more effective in cooling the same area than a single large jet.

Furthermore, the cooling performance can be enhanced by extending the surface areas. Therefore, a greater surface area density per unit volume can be achieved leading to higher fin efficiencies resulting from the shorter conduction path lengths. This is accomplished by using thin lamination plates in close proximity to the heat source being vigorously scrubbed by high heat transfer coolant jets. This maximizing the surface area and fin effectiveness is in actuality minimizing the thermal

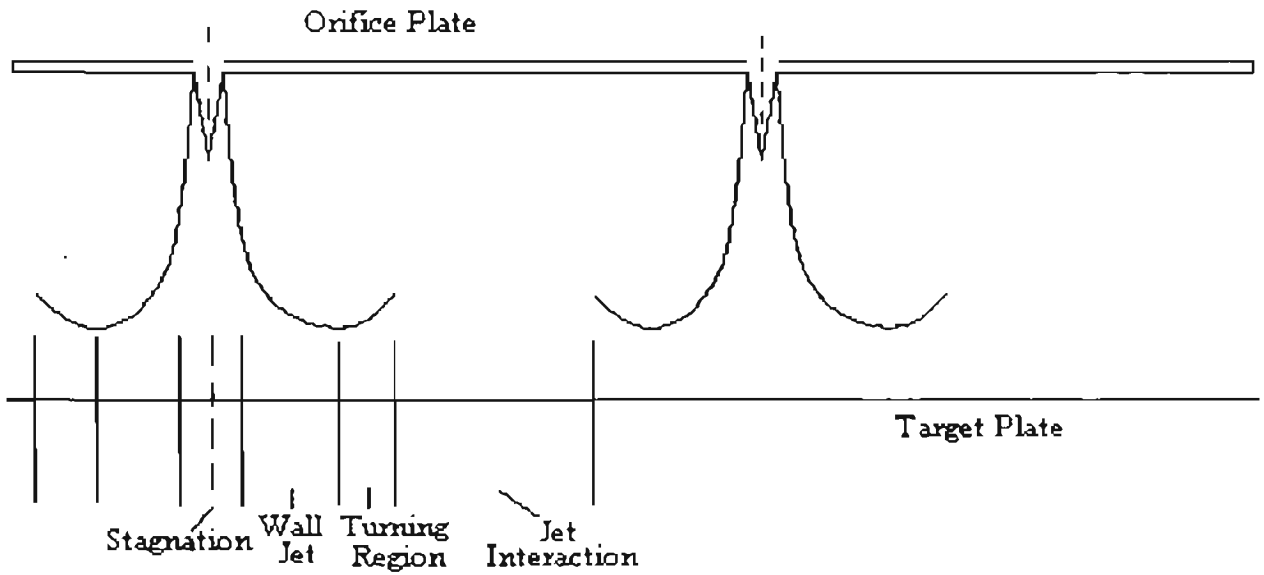

Figure 1.2. Four Characteristic Regions for Multiple Jet Impingement Heat Exchanger.

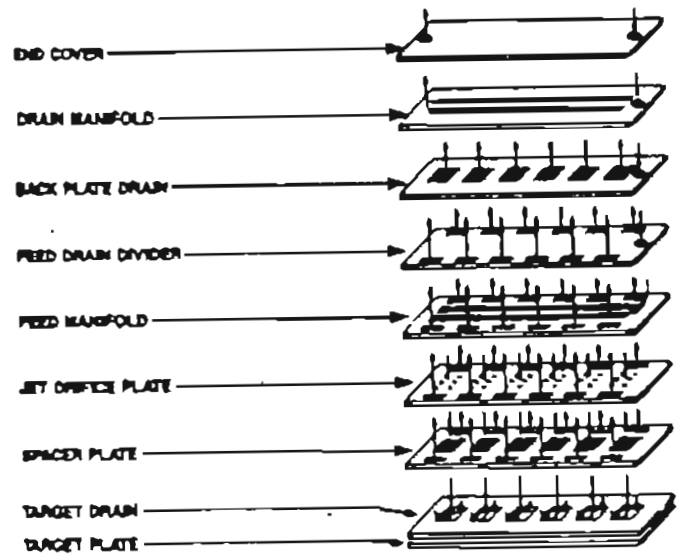

Figure 1.3. CHIC Basic Elements and Operating Principle [4].

resistance. This concept of using multiple jet impingement with the enhancement of multiple plates is the basis for Sundstrand's development of the CHIC.

The operating principle of a CHIC device is relatively simple, as shown in Figure 1.3. The liquid enters the inlet port in the end cover, flows through a succession of thin laminates towards the heat acquisition surface, or target plate. The liquid impinges on the target plate, and then isdirected back to the drain manifold attached and ultimately to the exit port of the end cover. The electronics device is attached to the opposite side of the target plate. As shown in Figure 1.3, the fluid en route to the target plate passes through a jet orifice plate and a spacer plate. The jet orifice plate usually contains about 50 to 200 small circular holes. In a typical CHIC device, the orifice plate and the spacer plate are repeated several times, with each successive orifice plate acting as a target for the jets from the orifice plate immediately upstream. The orifices are offset by one-half their pitch from plate to plate, so that the liquid impinges on solid metal, then cascades downward as it passes through subsequent orifice plates. The jet interaction of the multiple jets increases the turbulence and mixing, enhancing the heat transfer. Increasing the number of orifice plates, increases the fin

area and produces a higher effective heat transfer coefficient. The penalty for a larger number of orifice plates is higher pressure drop and a thicker heat exchanger. Since the 1983 prototype [3], several versions of CHICs have been built from copper and aluminum. The devices have been tested with Freon-11 [3], Freon-113 [5], and water [6].

However, this concept only satisfies the requirement for higher heat fluxes caused by modern electronics. To meet the need for an increase in the number of electronic processors, McDonnell Douglas developed the High Flux Heat Exchanger, HFHE. The HFHE consists of 20 CHICs arranged in parallel flow, with each CHIC being 1 cm^2 and capable of absorbing 100 W/cm^2. The HFHE was designed to integrate into the Lockhart LOC-E-JECT liquid cooled Navy Standard Electronic Module (SEM-E) used for F-2 avionics cooling. The actual design requirement used for the development of the HFHE is that size must fit the SEM-E, approximately 15 by 17 cm, on 1.5 cm pitch, for a total of 200 cm^2 mounting area per side. Furthermore, the module must absorb 2180 W of steady-state heat load, distributed as 100 W/cm^2 to 20 cm^2 of board surface area, consisting of the 20 one cm^2 CHICs, and 1.0 W/cm^2 heat flux over the remaining 180 cm^2 of surface area. Further details of the high flux heat exchanger design are documented in [4]

To ease the process of manufacturing this complex array of CHICs, Sundstrand has developed a process [7] of photo-etching laminae allowing for very accurate location of the orifices on the plates. The laminae are then stacked and bonded. Diffusion bonding was used for the copper boards and vacuum brazing was used for the aluminum boards. This photo-etching process allows virtually anything that can be drawn to be fabricated.

Because of this need for liquid cooling to absorb higher heat fluxes, additional considerations must be introduced. With the added intermediate aircraft cooling loop associated with liquid cooling, leaking and handling create a selection process for the liquid coolants. And with the increase of emphasis on safety and the environment, this liquid coolant must be non-toxic, non-corrosive, and be an adequate dielectric. In the past, silicate-ester based fluids, Coolanol 25R, were widely used as the liquid coolant in military avionics systems. These fluids have caused significant and sometimes catastrophic problems due to their hygroscopic nature and subsequent formation of flammable alcohols and silica gel. The alcohol by-product lowers the fluid flash point, increasing the risk of aircraft fires. The gelatinous precipitate called the "black plague", deposits on the surfaces of the electronics components, causing avionics equipment to malfunction. In order to

solve the problems associated with Coolanol, the Air Force and the Navy investigated the possibility of direct replacement of silicate-ester based fluids with hydrogenated polyalphaolefin based fluids. Their studies concluded that polyalphaolefin (PAO) fluids are chemically more stable, (do not hydrolyze to form either silica gel or alcohol by-products), are less costly, offer equal or improved dielectric characteristics, and meet or exceed military requirements for a dielectric coolant [8,9]. Due to these desirable properties of PAO, the Air Force and the Navy, for some selected fighter aircraft, have both replaced the liquid coolant, Coolanol, used in their fighter aircraft electronic cooling systems with PAO.

In a recent study [10], the hydraulic and thermal performance of PAO and Coolanol 25R in different flow regimes, laminar and turbulent, were compared. The results indicated that at normal operating temperatures the two coolants were reasonably close and fairly independent of the flow regime. However, at low temperatures, dependent on the flow regime, there could be a substantial difference between the hydraulic and thermal performance of the two fluids. Particularly, at temperatures below 0°C, PAO's hydraulic performance in the laminar flow region, and its thermal performance in the turbulent flow region, are inferior to those of Coolanol 25R at comparable conditions.

Coolanol has been a standard coolant of fighter aircraft, but is currently being phased out by PAO, which is much less prone to decomposition. Therefore, in this study of the performance for the High Flux Heat Exchanger, PAO was selected as the liquid coolant.

In the following chapters, the experimental setup, the experimental procedure, and the presentation of the completed objectives are presented.

CHAPTER II

EXPERIMENTAL APPARATUS

Because of the extreme ranges of pressure and temperature and the wide array of information garnered, the analysis of the hydraulic and thermal performances of the High Flux Heat Exchanger, HFHE, required a specialized experimental setup. A schematic diagram of the top view of the laboratory setup is shown in Figure 2.1. Also, presented in this chapter is a description of the experimental apparatus used in the laboratory test setup, including the necessary instrumentation details on the individual components. Following the apparatus descriptions, an explanation of the necessary calibration procedures is given ensuring the accuracy of each data processing component. Next, the operational procedure of the test setup for the hydraulic, steady-state thermal, and the transient thermal tests are given. The final section of this chapter is concerned with the detailing of the reduction of the raw data output from the data processing

components of the experimental setup to a presentable form, including the software incorporated in this process.

2.1 Test Section

The test section consisted of the following materials: circular steel tubing and Swegelock fittings, a variable speed motor and gear pump, a reservoir for the loop coolant, a shell and tube heat exchanger, a mass flow meter, a filter, two analog pressure gauges, a differential pressure transducer, a cold temperature bath, four metering valves, power supply and heat source, fifteen surface thermocouples, the HFHE, and a data acquisition system.

The test loop and its components rest upon a wooden table, with the exception of the reservoir, filter, and flow meter, in order to keep the fluid in a horizontal plane. This allows for the elimination of the change in potential energy throughout the test loop. The reservoir, filter, and flow meter are all suspended from the tubing from the edges of the table. Furthermore, to reduce vibrations from the motor/pump causing inaccuracies in the data measurements, rubber mats were placed under the motor/pump, HFHE, and the differential pressure transducer.

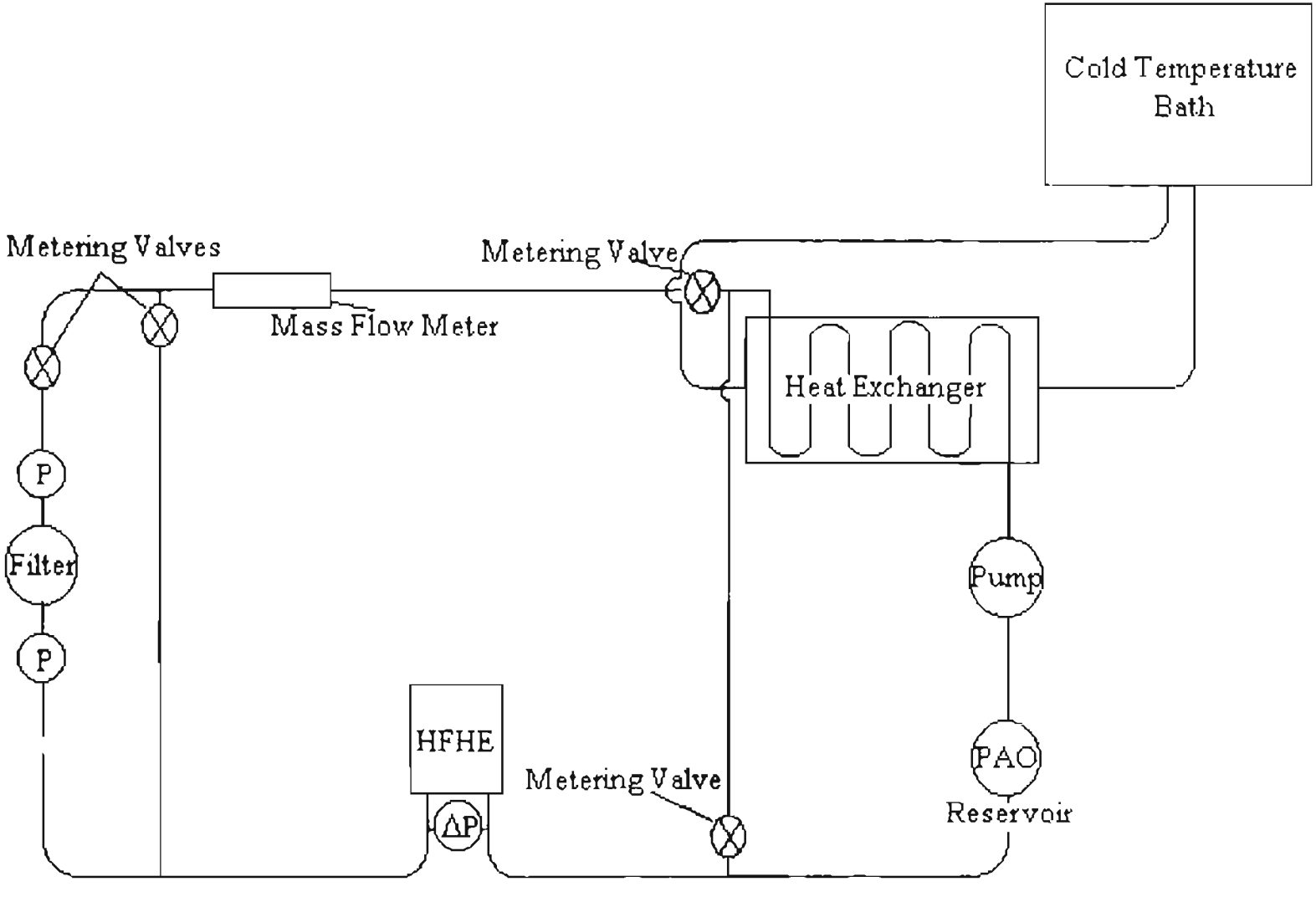

Figure 2.1. Schematic of the Experimental Apparatus.

2.1.1 Tubing

The test section consisted of seamless 316 stainless steal circular tube with an average inside diameter of 15.850 ± 0.0127 mm (0.624 ± 0.0005 inches) and outside diameter 18.999 ± 0.0127 mm (0.748 ± 0.0005 inches). The connections for the joints of the tubing and the setup components consisted of Swegelock™ compression fittings. The test setup is arranged in a rough rectangular shape. The dimensions of the test setup are 1.8288 m (6 ft) by 1.2192 m (4 ft). These dimensions are adhered to because of the need for a large length to diameter ratio, L/D, for the mass flow meter. Figure 2.2 shows the compression fittings and the individual dimensions of the piping throughout the test loop. Furthermore, because one bypass loop must transverse the heat exchanger, the tubing was bent out of the horizontal plane as shown in Figure 2.3.

2.1.2 Pump-motor

The pump-motor combination consisted of a variable speed DC Scott motor magnetically coupled with a gear pump from Tuthill. The coupling for the motor and pump was capable of handling pressures up to 150 psi. The variable speed DC motor allowed for the necessary variation in the

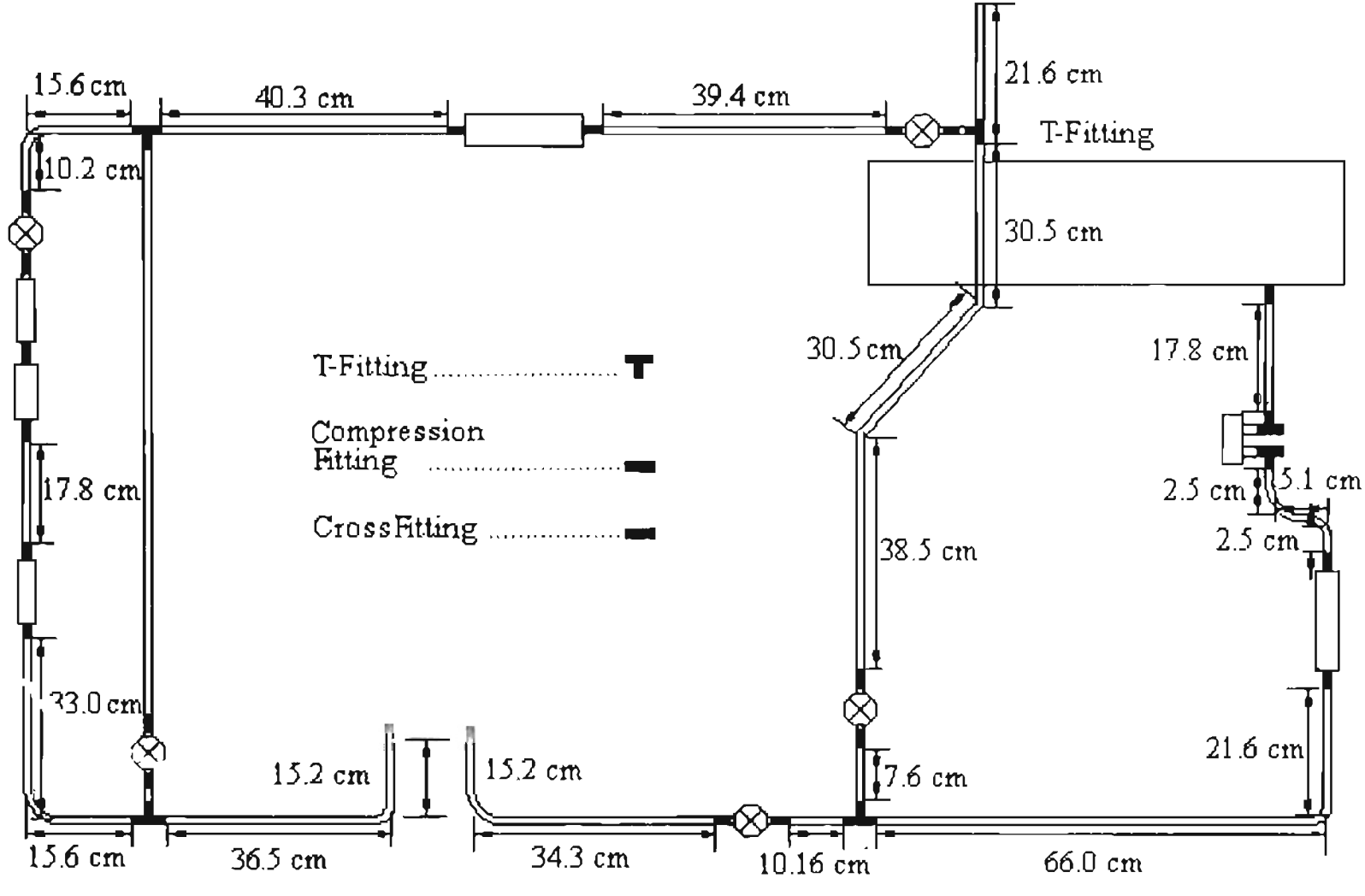

Figure 2.2. Dimensions and Fittings for the Test Loop.

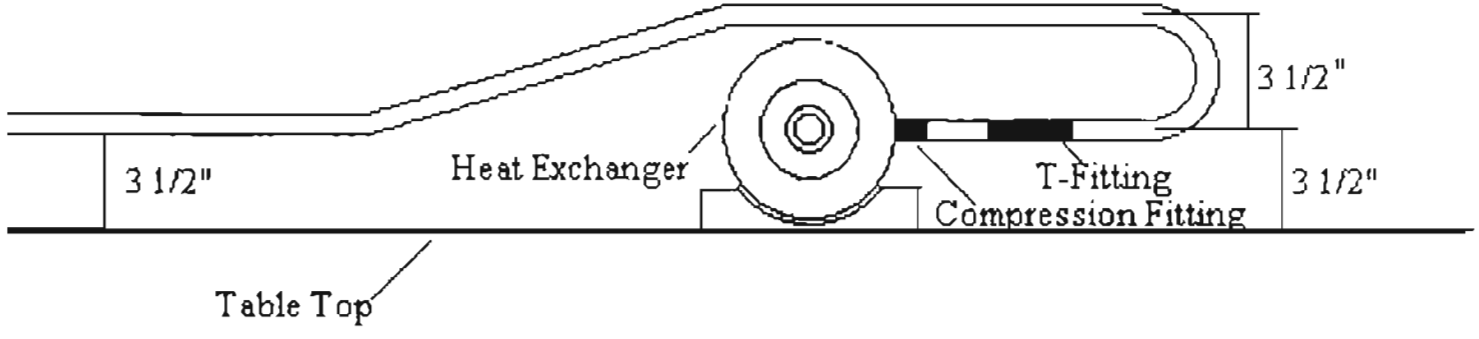

Figure 2.3. Side View of the Bypass Loop in the Test Section.

range of flow rates analyzed. The pump-motor was capable of a range of flow rates from 0.50 to 4.5 kg/min.

2.1.3 Reservoir

The reservoir for the test loop coolant consisted of the shell casing of a large flow rate filter with the capability of containing two liters of fluid. Because of the placement of the reservoir before the pump in the test loop, the fluid flow was induced flow. In addition to the induced flow, the physical design of the filter used for the reservoir, shown in Figure 2.4, in which the exiting fluid was from the bottom of the container, allowed for air pockets to be alleviated from the test loop.

Because of the weight of the reservoir, support must be provided to alleviate any deflection of the pipe. For this support, a wooden block with a cross section of 1 inch by 1 inch was attached to the table top by the use of 3/8 inch diameter wood screws with a length of 2 inches. Two 5/8 inch holes were drilled four inches apart through this wooden block. A four inch u-bolt was then attached to the block and secured by two lock nuts. This support system can be seen in Figure 2.5.

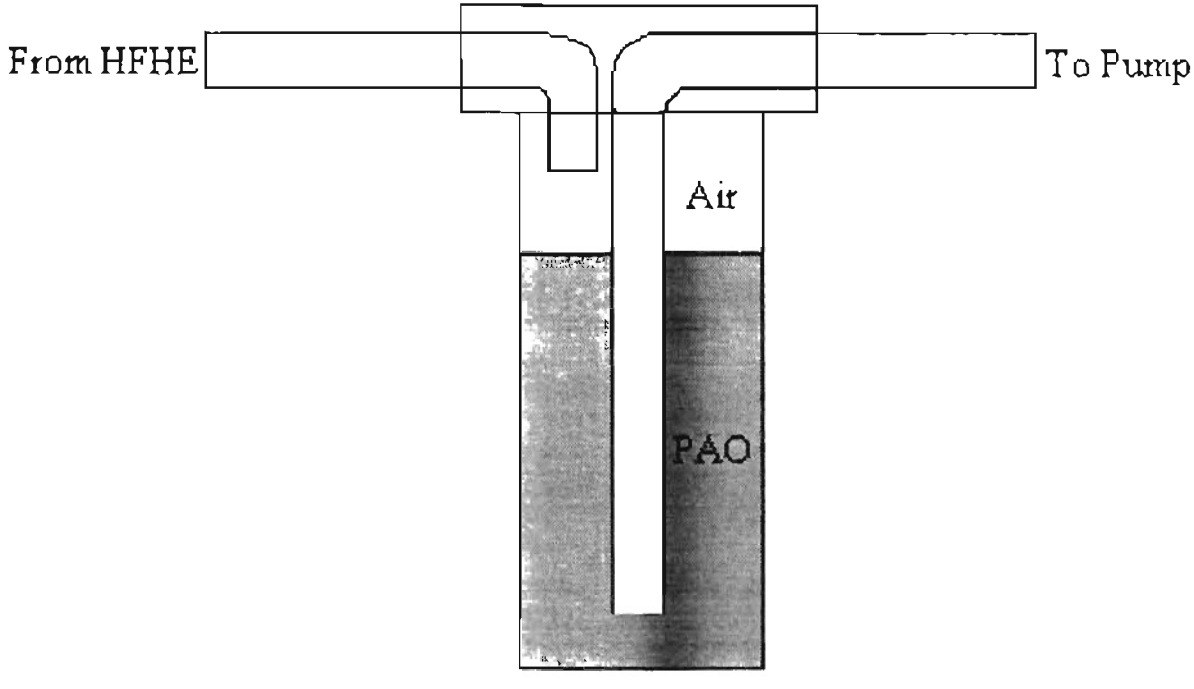

Figure 2.4. PAO Reservoir for the Experimental Setup.

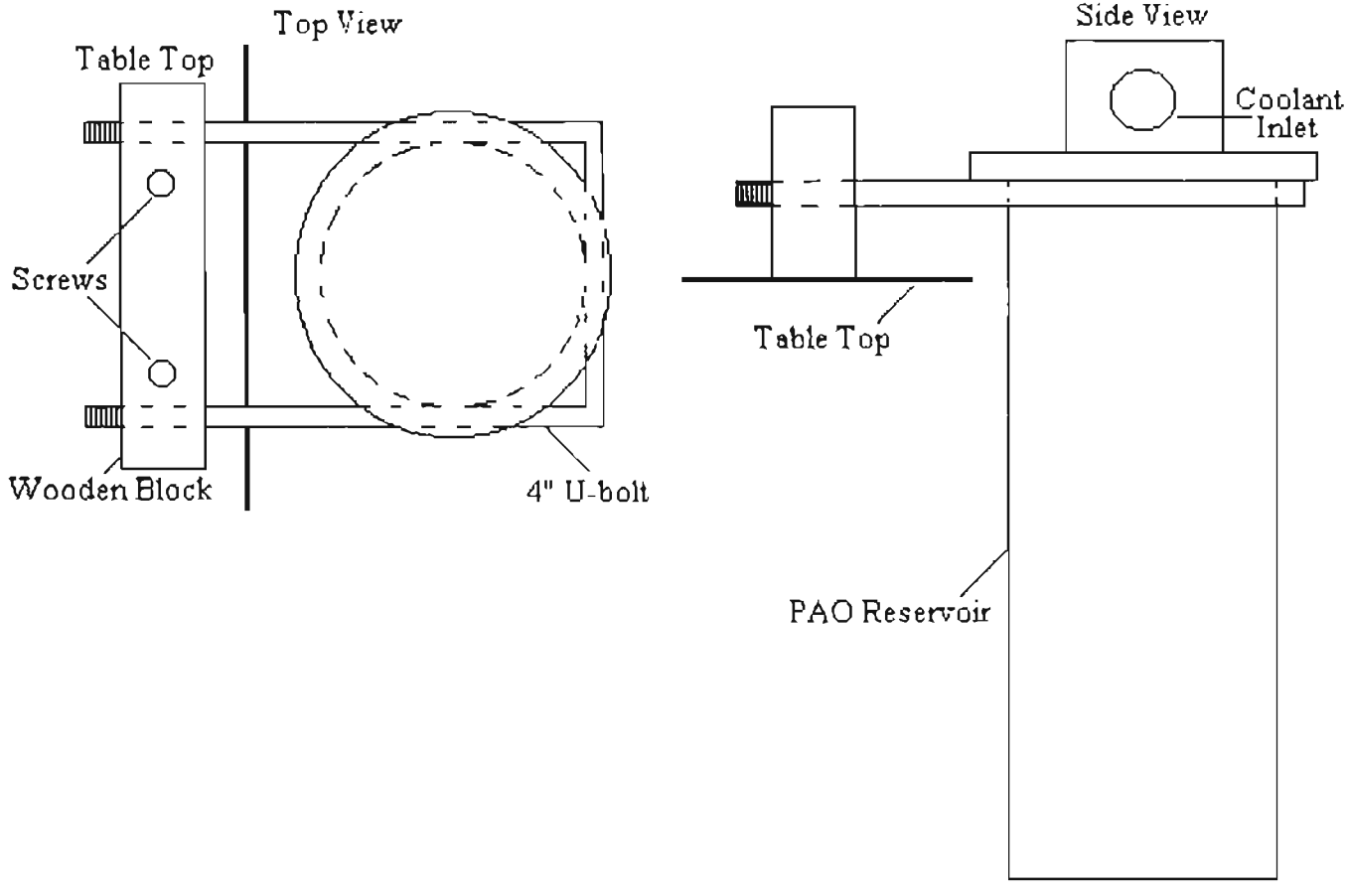

Figure 2.5. Support System for the PAO Reservoir.

2.1.4 Heat Exchanger

Because the coolant for the HFHE was required to be PAO, the test section fluid was also required to be PAO. However, because this fluid is a light hydraulic oil, it was deemed that it not be used inside the cold temperature bath. Therefore, an additional in-loop heat exchanger was needed. This heat exchanger consisted of a shell and tube counter flow heat exchanger appropriated from Wright Laboratories. The purpose of this heat exchanger was to remove the heat flux added to the PAO from the applied heat load and from the frictional forces induced by the test loop and its components.

2.1.5 Flow Meter

One of the three dependent variables used for the spectrum of analysis is the flow rate. Therefore a flow meter was included into the test loop. The flow meter consisted of a MicroMotion DS25 mass flow meter that delivers an output of 4 to 24 mA of current. This current output was directly monitored by the data acquisition system. The mass flow meter is capable of a density range from 0.0 to 5.0 g/cm^3, with a minimum span of 0.1 g/cm^3 and a maximum span of 5.0 g/cm^3. In addition the flow meter has

a temperature range of -240°C to 450°C with a minimum span of 20°C and a maximum span of 690°C. The flow meter has a turn-on time of 15 seconds and reaches stable operation within 30 minutes.

For the MicroMotion mass flow meter, the flow meter is flagged upward for gases and downward for liquids. Therefore, for the coolant PAO, the mass flow meter must be flagged downward in this test loop. A mass flow meter was chosen, as opposed to a volumetric flow meter, due to dependency of the density of PAO on temperature. A mass flow meter allowed for accurate measurements of the mass flow rate for all operating coolant temperatures.

2.1.6 Filter

Because of the relatively small diameter of the orifices in the HFHE, any substantial particulates will clog the passages of the HFHE causing higher pressure losses and reduced flow through some of the impingement jets. This partial loss of flow through the impingement jets will cause unequal cooling throughout the HFHE. Therefore, a 20 micron HYCON filter was used to remove particulates large enough to do damage to the HFHE.

2.1.7 Analog Pressure Gauges

Two 250 psi analog pressure gauges were included in the test loop immediately upstream and downstream of the filter to monitor the pressure drop across the filter. A high pressure drop would indicate that the filter needed to be cleaned. However, because the test loop is closed to the atmosphere, after a large number of hours of testing, all of the particulates should be filtered out of the test loop and the filter can be removed from the fluid path to reduce the pressure loss in the test loop.

2.1.8 Differential Pressure Transducer

One substantial element of the analysis of the HFHE is its hydraulic performance. This hydraulic performance corresponds to the pressure drop across the HFHE. Therefore, a pressure tap was formed immediately before the inlet and after the exit of the HFHE and connected by a differential pressure transducer. Both pressure taps were constructed by using a cross fitting with a 0.635 cm (0.25 inches) inside diameter attached vertically into the test section. The in-line legs of the cross fitting allowed for the flowing coolant, the bottom leg allowed for a thermocouple probe, and the top leg was used as a pressure tap. These cross fittings are shown in Figure 2.6. Vinyl

tubing with an inner diameter of 0.635 cm (0.25 inches) was used to connect the pressure tap and the pressure transducer. A Validyne P305D-50 wet-wet pressure transducer provided the pressure drop measurements with an output of ± 5.0 V at 0.5 mA and a pressure range of 0-861.75 kPa (0-125 psi) with a possible overpressure of 200% of full scale with less than a 0.5% zero shift. The P305D is a differential pressure transducer with symmetrical pressure cavities of stainless steel. Fluid pressures act directly on a central diaphragm in a balanced variable reluctance design which eliminates the need for internal isolation fluids. The transducer diaphragm is replaceable. The transducer has an accuracy of ± 0.25% of full scale including linearity, hysteresis, and repeatability. In addition, the transducer is capable of an operating temperature range of -53.89°C (-65°F) to 121.11°C (250°F).

2.1.9 Cold Temperature Bath

The second of the three dependent values that was used for the spectrum of tests was the inlet coolant temperature. Therefore, a cold temperature bath was included into the test loop via the heat exchanger. The cold temperature

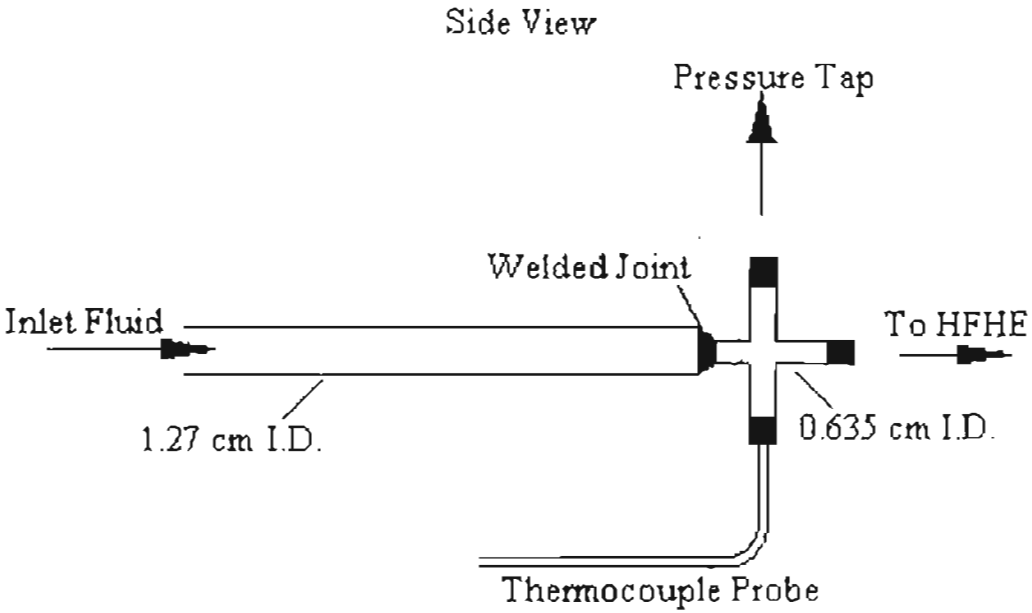

Figure 2.6. Cross Fitting for the Inlet and Outlet of the HFHE.

bath, a RC-50LT with the deluxe control package, was selected from FTS Systems because of its capability of holding the bath fluid temperature constant from -40 °C to 75 °C. This increased range was necessary to hold the PAO temperature constant from -15 °C to 50 °C. The losses in temperature are due to the inefficiencies of the heat exchanger. Three-eighths inch vinyl tubing was used to complete the secondary cooling loop with the heat exchanger. The coolant used, HT-30 silicone oil heat transfer fluid, remained in liquid state well beyond the range of temperatures resulting from the temperature bath, and was purchased from FTS Systems.

2.1.10 Metering Valves

The test loop configuration contains two sets of metering valves. The first set of valves are for the filter. During the initial hours of testing, the filter needs to be part of the test loop to remove any particulates from the fluid. However, because the test setup is a closed loop, the filter becomes unnecessary after the initial hours of testing are complete. Therefore, the additional loss of pressure from the filter can be removed by taking the filter out of the test loop. This removal of

pressure losses decreases the burden on the motor by allowing the pump to operate at a lower pressure. The second set of metering valves were used for the modeling of the hydraulic startup of the HFHE. Because the PAO is cooled by the HT-30 fluid in the heat exchanger, the PAO must have an actual flow rate to achieve any cooling. Therefore, to achieve the low temperatures the motor-pump must be operating. However, to test the start-up capabilities of the HFHE, the test must begin with no flow rate through the HFHE. Therefore, to accommodate both the cooling of the PAO and zero flow rate through the HFHE, a set of metering valves are used to separate the refrigeration cycle of the PAO from the rest of the test setup.

2.1.11 Heat Source

The last dependent variable used for the spectrum of tests is the applied heat load. Therefore, the test setup must include a power source and heat source for the HFHE capable of handling a heat flux of 100 W/cm^2. This high heat flux eliminates most conventional heat sources. Therefore, McDonnell Douglas developed a heat flux amplifier, similar to the one used by Grote, et al. [6]. The heat flux amplifier is designed to increase the contact

surface from 1.0 cm^2 to 40.3 cm^2. Therefore, a low heat flux heating element can be used to produce a high heat flux at the amplifier/HFHE interface.

This amplifier is shown in Figure 2.7. The lower 1.3 cm of the amplifier has a constant area of 1.0 cm^2 . In this section, there are three parallel planes of thermocouples spaced 0.25 cm apart. Eight thermocouples were placed in each of the three planes of the constant cross-sectional area "neck" of the amplifier. These thermocouples were 36 gage type T, copper/constantan, from Omega. A 0.5 mm diameter hole was drilled 0.5 mm deep at each thermocouple location. The thermocouple bead was peened into each hole. A hole was also drilled to the center of each plane, and each thermocouple was covered with Ecco-Bond 56C epoxy and inserted. The other thermocouples were also bonded with epoxy and their leads secured with Kapton tape. The ninth temperature in each plane was extrapolated during the data reduction process. The temperature at the amplifier/HFHE interface plane A, from Figure 2.7, will be calculated by projecting the temperatures in planes "B", "C", and "D" using a linear least squares fit. This technique provides very accurate temperature estimates at the interface correlating with the measured temperature in the HFHE wall.

To provide the actual heat source for the steady-state thermal tests, a Minco mica heater, 5.08 cm (2 inches) in diameter, with a resistance of 19 ohms was used as the heat source. For the transient thermal tests a 32 ohm MiniSystems thick filmed resistor was used. A Variac was used to regulate the AC wall voltage for the mica heater. The voltage output of the Variac and the amperage, measured by a current shunt, was sent directly to the data acquisition system.

2.1.12 Thermocouples

In addition to the 24 thermocouples that are located in the heat flux amplifier, the experimental setup contains fifteen more surface thermocouples and two thermocouple probes. The surface thermocouples consist of Omega 30 gage type T (copper/constantan) thermocouples. These thermocouples are necessary to both measure the wall temperature of the High Flux Heat Exchanger and estimate the radial heat loss due to conduction through the HFHE. This radial heat loss is caused by the simplification of applying a heat load to one CHIC at a time. When only one heat load is applied, heat is lost to the surrounding CHICs. Therefore, the actual heat flux through the tested CHIC is less than the heat load applied. Hence, it is necessary to

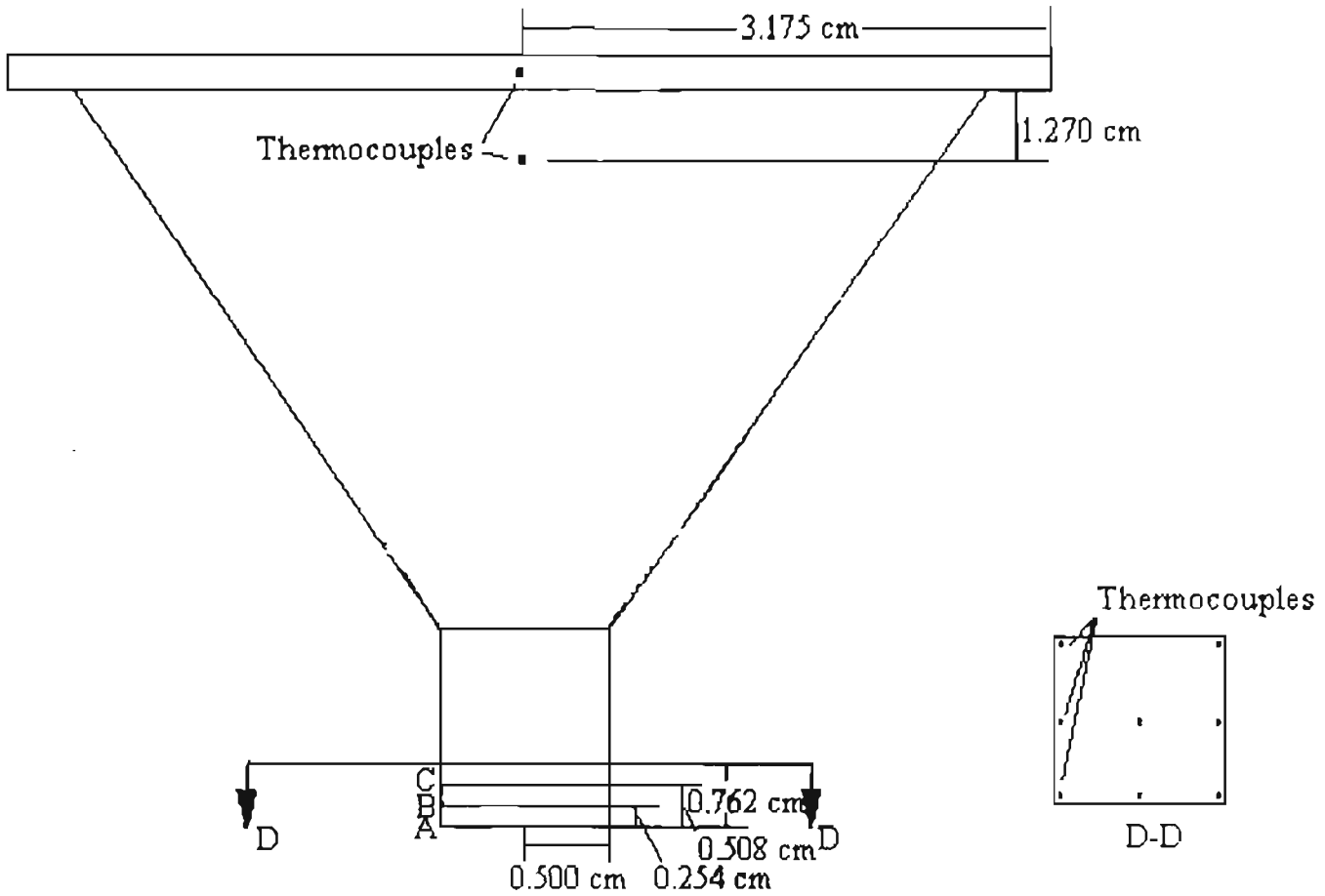

Figure 2.7. Heat Flux Amplifier.

estimate the difference in heat flux. To obtain this difference, the wall temperature profile must be calculated. Therefore, the thermocouples are placed on the HFHE surface using Omega's Omegabond 101. This bond is a high heat conducting epoxy used to temporarily cement the thermocouples onto the HFHE. This placement can be seen in Figure 2.8. For the thermocouple underneath the amplifier, a groove was made in the HFHE for each CHIC. The groove consisted of a channel cut 0.05 cm deep and 0.6 cm long. This length of channel allows for the placement of the thermocouple wire under the amplifier. The channel does not reach the center of the CHIC footprint; however, the heat flux should be uniform across the entire surface area of the footprint. Therefore, the wall temperature should also be uniform across the entire surface of the CHIC footprint. The channel cut was made with a 1/16 inch router bit.

The thermocouple probes consisted of a type T Cole-Parmer general-purpose temperature probe. These 0.3175 cm (0.125 inch) diameter, 20.32 cm (8 inch) long probes consisted of 316 stainless steel with a maximum temperature of 399°C (750°F) and a time constant of 10 seconds. These probes were placed at the inlet and outlet of the HFHE, shown in Figure 2.6. The temperature probes are placed into

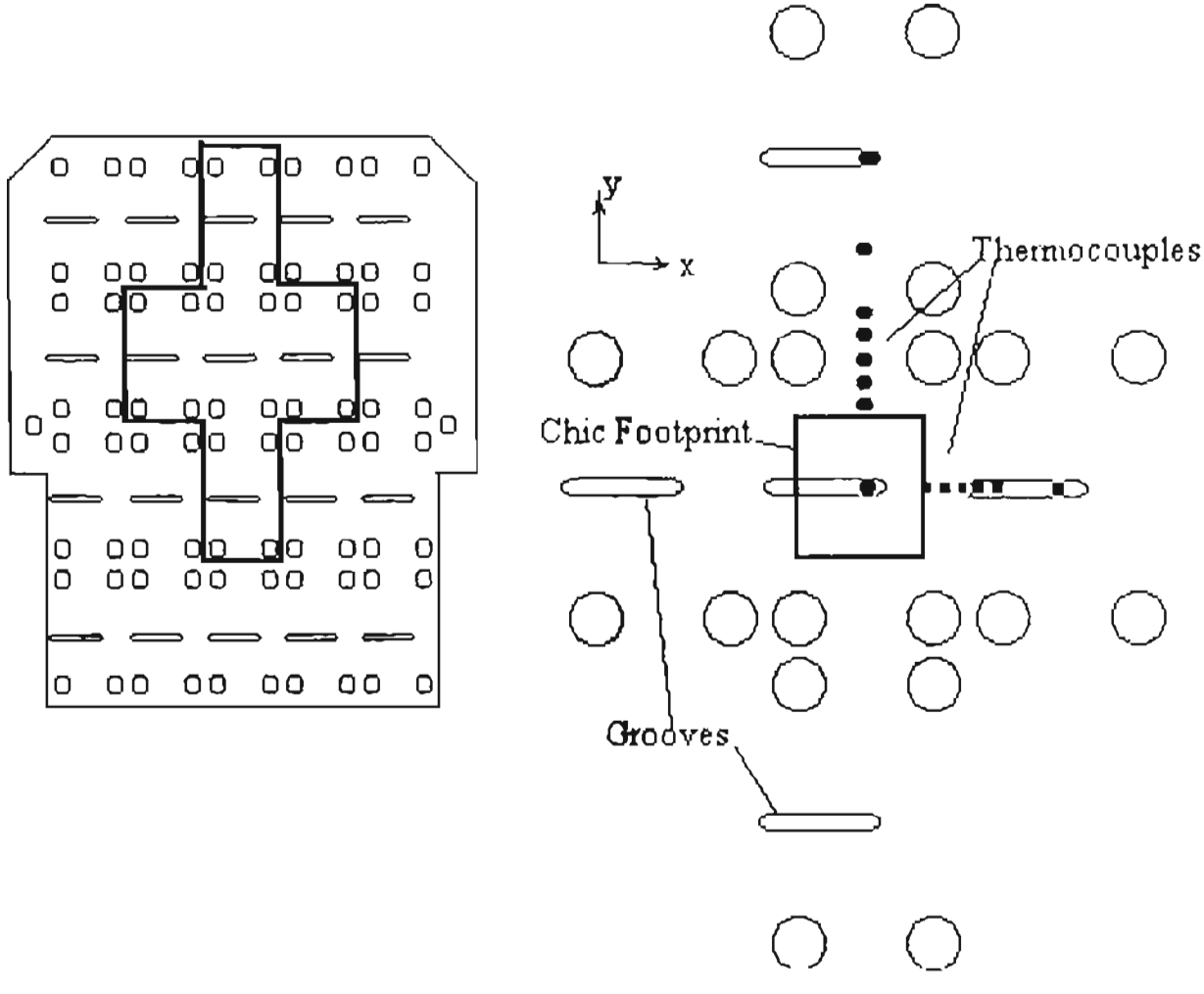

Figure 2.8. Placement of the Surface Thermocouples.

the cross fitting, to where 0.3175 cm (0.125 inch) of the probe extends into the fluid flow, thereby ensuring sufficient immersion into the fluid without causing a large obstruction of the flow. The inlet and outlet temperature measurements are necessary for varying the coolant temperature and heat addition to the fluid, respectively.

2.1.13 Securing Plate

To guarantee sufficient contact pressure between the amplifier and the CHIC surface, the amplifier was bolted onto the HFHE. This was accomplished by four 1/4 inch bolts and a securing plate. The plate consisted of an aluminum sheet 6.35 cm (2.5 inch) by 6.35 cm (2.5 inch) with 0.9525 cm (0.375 inch) holes designed to align with the amplifier holes and the HFHE. In addition, a 1.905 cm (0.75 inch) notch was made to keep from damaging the lead of the mica heater under compression. This securing plate can be seen in Figure 2.9. In addition, thermal grease was applied to the amplifier and HFHE interface.

2.1.14 High Flux Heat Exchanger

The High Flux Heat Exchanger, HFHE, originally was designed to consist of a copper alloy insert into a stainless steel header-frame. The outer dimensions of the

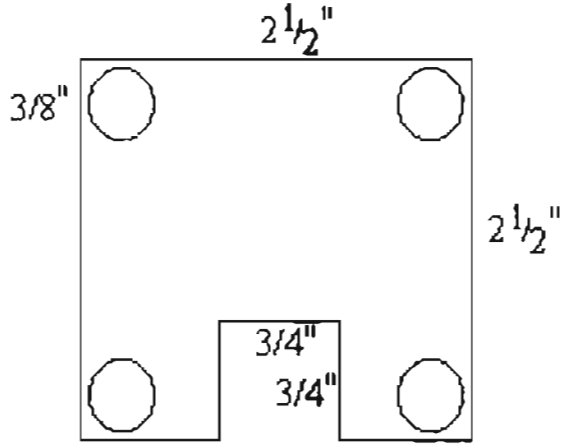

Figure 2.9. Configuration of the Securing Plate.

header-frame was required to meet SEM-E, Standard Electronics Module, Type E, specification, or 15 cm by 17 cm. Because a SEM-E size liquid flow-through module was recently developed under a separate Air Force program, McDonnell Douglas and the maker of the module, Lockhart Industries, Inc., combined to modify the SEM-E liquid cooled module (part number 101456, shown in Figure 2.10) by blocking the normal active flow zone and instead porting the flow into a flush-mounted removable CHIC plate. The porting locations and sizes are shown in Figure 2.11. Because the Lockhart module is fabricated from aluminum alloy, a departure from the original design was necessary.

The overall assembly of the HFHE consists of two principal components: an aluminum header-frame and a copper insert which contains the twenty high flux cooling locations. The header and the insert are then bolted together. The entire assembly measures 14.9 cm by 15.6 cm, with a total thickness of 1.52 cm. The copper insert contains the CHIC coolers, and the aluminum frame adds stiffness to the overall assembly and extends the outer dimensions to SEM-E specifications. To seal the copper insert and header-frame a VITON-A gasket seal was used. The copper insert contains twenty CHIC coolers arranged in a four-by-five array and coolant distribution channels in an

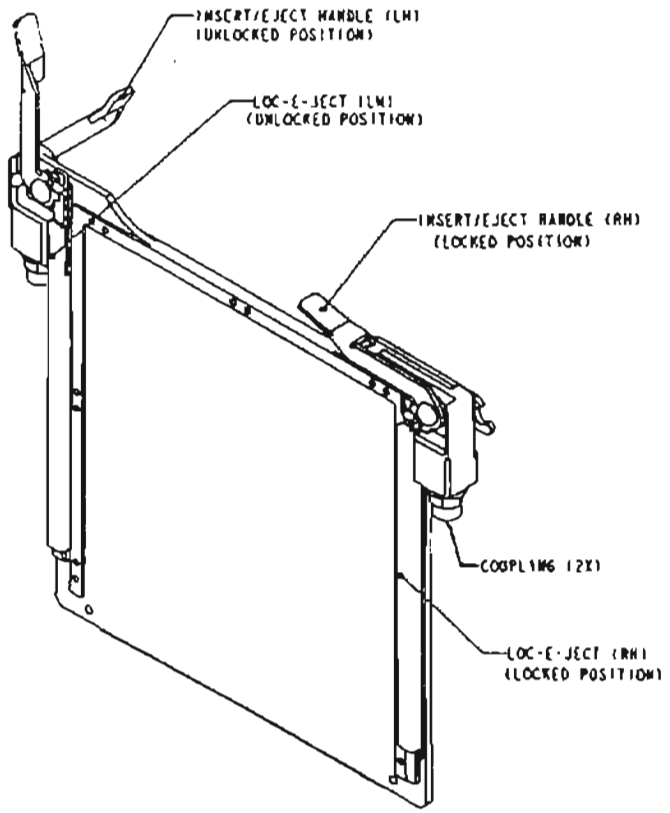

Figure 2.10. Modification to the SEM-E Module.

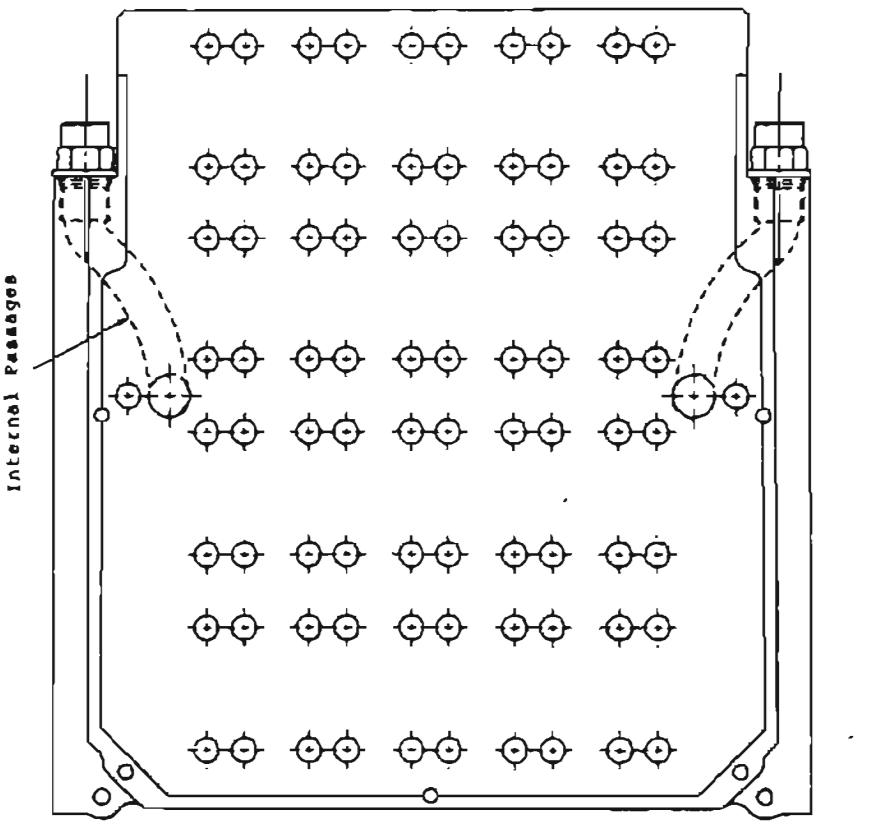

Figure 2.11. Porting Locations and Sizes.

integral structure. It was formed by stacking 24 photo-etched copper alloy laminates, each of 0.010 or 0.038 cm thickness, and diffusion bonding them to create a platelet heat exchanger. Total thickness of the insert is 0.467 cm. The alloy is CDA 15100 (copper, 0.10% zirconium). The module is designed for single-sided heat application. Each CHIC cools a surface area of 1.0 cm^2, contains nine orifice plates, and sixty holes per plate arranged in three parallel slots, and is fed coolant in parallel.

The HFHE design and performance requirements were based on a maximum local heat flux of 100 W/cm^2 (steady or transient) for each 1 cm^2 CHIC surface area and 1.0 W/cm^2 heat flux over the remaining 180 cm^2 for a total heat flux capability of 2180 W. In addition, the HFHE designs were based on a maximum junction temperature of 90°C, and PAO as the liquid coolant. Other constraints included a lower limit on the coolant supply temperature (0°C), an upper limit on the flow rate (1000 kg/hr), and pressure drop (690 kPa for a cold start and 311 kPa at the design point). The HFHE consists of a set of bonded laminates using 8 different types of plates and a total of 24 plates. Appendix B shows each type of plate as well as the configuration of the bonded plates for the HFHE tested. Depending on the number of orifice plates that are used, the thermal performance,

cost , heat exchanger thickness, and pressure drop vary. Therefore, the results shown in chapter III are dependent on the stacking of the individual plates.

2.1.15 Data Acquisition

The final component of the test loop is the data acquisition system. This system consists of two parts, the data logger and a personal computer. The Fluke 1703 data logger was capable of containing individual programs to record the different data needed by the separate tests. These programs require no computer programming. Instead, the Fluke programs consist of listing the channels to be recorded, indicating the name and units for each channel, and calculating any pseudochannel (channel 82 (Wattage) = channel 81 (voltage) x channel 82 (amperage)). In addition, the programs include the mode of recording (a time interval scan of the channels or continuous scan of the channels) and the device for the output file (a printed output or disk file). All of these parameters of the Fluke program are prompted by the Fluke. The output of the Fluke program consists of an ASCII data file. This data file is then input into a DOS data reduction routine on a Pentium-60 personal computer. Finally, all of the final calculations were made with the use of Microsoft Excel and MathCad.

2.2 Experimental Calibrations

Upon the completion of the experimental setup construction, calibrations of all the data processing equipment were performed. The following sections outline the details of the calibrations for the cold temperature bath, the thermocouples, the mass flow meter, and the differential pressure transducer.

2.2.1 Cold Temperature Bath

The calibration procedure for the FTS Systems RC50 recirculating cooler is defined in the operating manual. To calibrate the cold bath a previously calibrated temperature indicator and a heater must be present. The calibration setup is then as follows:

- A "short circuit" hose is placed between the fluid inlet and outlet to provide a short fluid path which introduces minimal heat to the process.
- The temperature standard sensor, provided by FTS Systems, is placed in the reservoir inside the fluid return tube. Place the sensor between 2 inches and 4 inches into the tube.
- On larger systems the cooling system may be difficult to stabilize without a heat load. This is due to the high

refrigeration capacity of the equipment causing extreme drops in temperature when activated.

- To eliminate this problem, a heater rated at 50% of the heat removal capacity of the system at 0°C may be immersed in the reservoir and energized. This will provide a load to stabilize the temperature.

After the setup is completed, the actual calibration is performed by the following:

- While turning on the power to the unit, dress the O/I (off/on) button.
- The SP (set point) prompt and present SP will appear on the display. Adjust the SP to 0.0 and press enter (O/I) button.
- By setting the SP to 0.0 the RC (recirculating cooler) will attempt to cool to 0.0°C. Allow the system to stabilize at zero (wait at least 15 minutes to allow electronics to stabilize). Once the O/I button is pressed the display will begin to alternate between "C oS" (cal offset) and the process temperature. At any time while the "C oS" is displayed, the up/down buttons will adjust the measured process temperature up and down, approximately 0.1 degree per step. Adjust the reading to match the temperature standard.

- After the zero has been adjusted, press the O/I button again and the SP prompt will return. The span may be adjusted either using a low temperature or using a high temperature.

Once the zero temperature has been established, the cold bath calibration is performed for low temperatures and high temperatures separately. For the calibration at low temperatures the following procedure was followed:

- If a heater was added for the zeroing procedure it must be removed. Wait for the temperature to stabilize at its maximum low temperature. (Caution, the fluid being used must be pumpable at the maximum low temperature.) Because the thermocouples will be calibrated to -20°C, the cold bath was calibrated to -30°C.

- Adjust the setpoint to it's minimum setting and then press O/I again. The "C Gn" prompt will appear. When the temperature stabilizes adjust the temperature to read the same as your calibration device.

- When complete press O/I. The prompt "rFC" (restore factory calibration?) appears. If the user calibration was unsuccessful then you will want to restore the factory calibration. To save the adjust calibration

answer 0 (no), to restore factory calibration answer 1 (yes) and press O/I.

- The "Fin?" (finished) prompt will appear. If you are finished answer (yes) and press O/I. In not, entering 0 will loop back to the beginning and start over.

To calibrate the cold bath for high temperatures, the following procedure was performed:

- A heater is required to heat the unit up to it's maximum temperature. If the RC is supplied without heat, an external heater must be added to the reservoir. (Caution, the fluid being used must be pumpable at the maximum temperature and must not be flammable.)

- Adjust the setpoint to it's minimum setting and then press O/I again. The "C Gn" prompt will appear. When the temperature stabilizes adjust the temperature to read the same as your calibration device.

- When complete press O/I. The prompt "rFC" (restore factory calibration?) appears. If the user calibration was unsuccessful then you will want to restore the factory calibration. To save the adjust calibration answer 0 (no), to restore factory calibration answer 1 (yes) and press O/I.

- The "Fin?" (finished) prompt will appear. If you are finished answer (yes) and press O/I. In not, entering 0 will loop back to the beginning and start over.

2.2.2 Thermocouples

For all of the thermocouples, including the surface thermocouples, amplifier thermocouples, and temperature probes, the calibration usually consists of three data points. However, because of the difficulty in reaching known steady state temperatures, the thermocouples can usually be calibrated by submersing the thermocouples in ice water,(0°C), using room temperature (25°C), and submersing the thermocouples in boiling water (100°C). However, after the calibration of the cold temperature bath is completed, the cold bath can be used to calibrate the thermocouples. Moreover, because the cold temperature bath was selected to provide the temperature range necessary to complete the experimental tests, the cold temperature bath is capable of providing a suitable temperature range for the calibration of the thermocouples. Therefore, the thermocouples were submersed in the cold temperature bath at steady state temperatures between -20°C and 60°C at an interval of 10°C. As a reference temperature guide, an Omega Platinum DP50

temperature gage was used to correlate the temperature reading of the cold temperature bath. Both the temperature gage and the cold temperature bath were capable of output readings of tenths of a degree Celsius. The output reading of the submersed thermocouples were taken from the Fluke data processor. Finally, a calibration curve was obtained by using least squares in a linear regression. A typical calibration curve is shown for surface thermocouple 15 in Equation (2.1).

$$T_{act} = 1.009 T_{meas} - 0.6048 \qquad (2.1)$$

A complete listing of the calibration curves can be seen in Appendix C. Because the thermocouples yield data directly, the uncertainty results from only two factors. The first factor is the uncertainty from the thermocouple itself. From Omega's catalog, the type T (copper/constantan) thermocouple, between -20°C and 60°C, has an accuracy of ±0.5°C. However, when calibrating the thermocouples, it was evident that the thermocouples had an accuracy of ±0.1°C. The second factor comes from any non-linearity of the curve fit. However, as can be seen from Figure 2.12, when the uncertainty of the thermocouple is factored into the calibration curve, each data point fits within the

confidence interval. Therefore, it can be assumed that the thermocouples have an uncertainty of ±0.1°C.

The curve fitted data for this thermocouple, surface thermocouple 15, has a standard deviation of 0.044 and a maximum error of -0.09°C (at -20°C) from the actual temperature. Both the standard deviation and the maximum error are typical of the calibrations of all of the thermocouples. The standard deviations and the maximum errors for the remaining thermocouples can also be found in Appendix C.

2.2.3 Mass Flow Meter

For calibration of the flow meter, a "bucket and stopwatch" approach was used. First, the test setup was modified by removing the HFHE, leaving an open loop, seen in Figure 2.13. Next, the time to fill a 500 ml graduated cylinder was measured for flow rates ranging from 0.7 kg/min to 4.0 kg/min. This data combined with the density of the PAO was charted, and a linear curve fit was performed. These can be seen in Figure 2.14. However, no measurements are 100% accurate; therefore, an error analysis for both the "bucket and stopwatch" approach and the measured flow was performed. An example of the methodology is as follows:

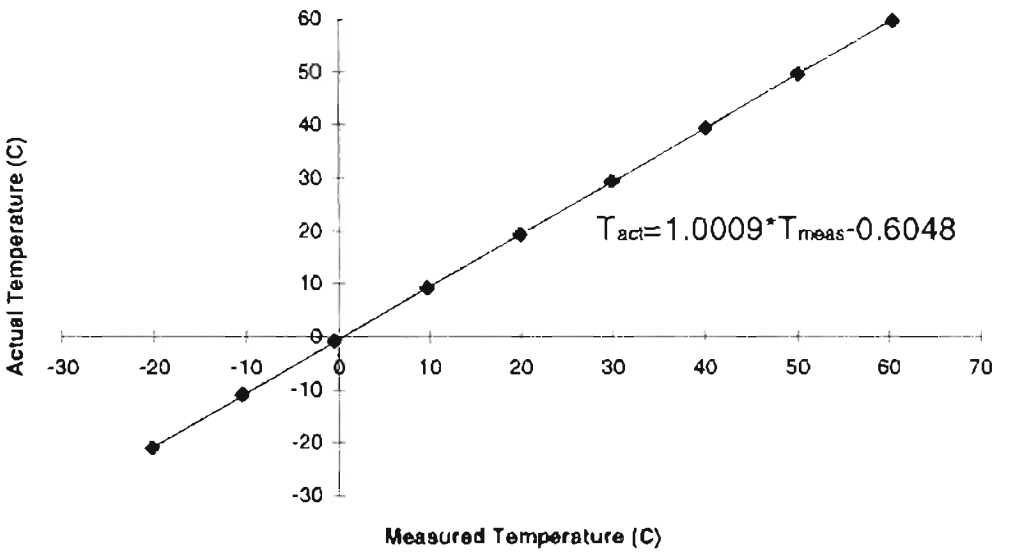

Figure 2.12. Typical Thermocouple Calibration Curve.

For the "bucket and stopwatch" approach, the equation for the mass flow rate is:

$$\dot{m} = \frac{\rho V}{time} \tag{2.2}$$

Next, the uncertainty factor is calculated by the following equation:

$$\varepsilon_m = \left[\left(\frac{\partial \dot{m}}{\partial \rho} \varepsilon_\rho \right)^2 + \left(\frac{\partial \dot{m}}{\partial t} \varepsilon_t \right)^2 + \left(\frac{\partial \dot{m}}{\partial v} \varepsilon_v \right)^2 \right]^{1/2} \tag{2.3}$$

Performing the partial derivatives for each independent variable, dividing by the mass flow rate, and multiplying by 100 to get the percentage yields:

$$\frac{\varepsilon_m}{\dot{m}} = 100 \times \left[\left(\frac{\varepsilon_\rho}{\rho} \right)^2 + \left(\frac{\varepsilon_v}{v} \right)^2 + \left(\frac{\varepsilon_t}{t} \right)^2 \right]^{1/2} \tag{2.4}$$

Next, determine the uncertainty factors for each independent variable.

- The density is calculated as a function of the temperature of the PAO. This function and its'

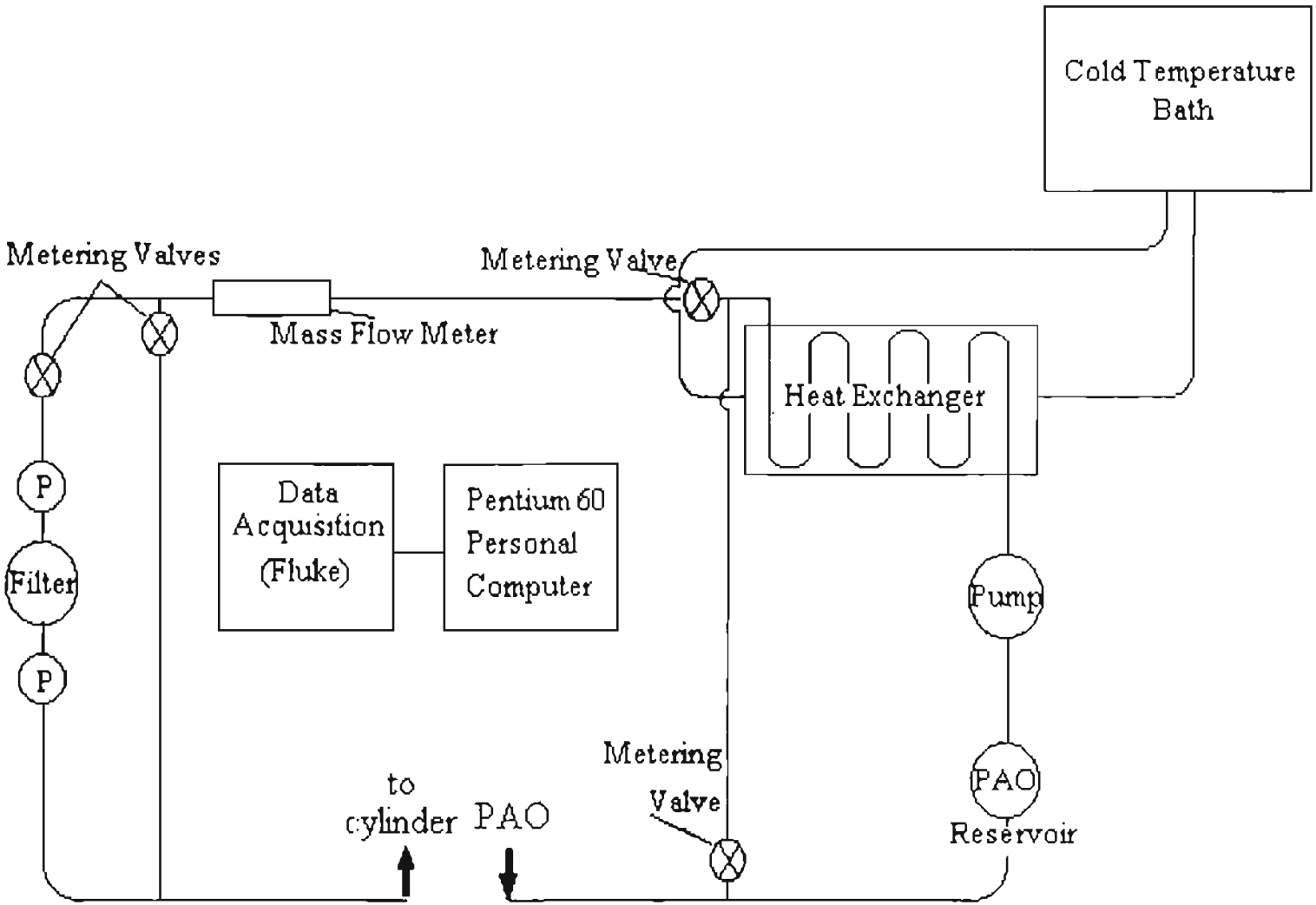

Figure 2.13. Schematic of the Mass Flow Rate Calibration.

uncertainty factor is given by Ghajar [10]. This curve fitted equation for the density has a maximum deviation of less than ±0.5%. For the flow rate measurements, the coolant temperature was room temperature, 25°C. Therefore, then density of the PAO was 0.792 kg/L. A 0.5% deviation from this value represents an uncertainty factor of ± 0.004 kg/L.

- The graduated cylinder used in the measurements consisted of increments of 5 ml. Therefore, the uncertainty of the volume is one half of the smallest increment or 2.5 ml.
- The time was measured with a stopwatch with an increment of 0.01 seconds. However, after many tests, it was concluded that the smallest increment of time that could accurately be measured was 0.25 seconds. Therefore, half of the smallest increment translates to an uncertainty of 0.125 seconds.

Finally, substitute the uncertainty factors and the following independent variables values to achieve a maximum uncertainty into Equation (2.4)

$$\rho = 0.79 \text{ kg/L}$$

$$v = 450 \text{ ml}$$

$$t = 6.5 \text{ s}$$

This yields an uncertainty factor for the measured mass flow rate of 4.09%.

For the error analysis on the flow meter itself, we must look at the fluctuations and perform a least squares analysis for each flow rate. The equation for the least squares analysis is as follows:

$$\varepsilon = \sqrt{\frac{1}{n}\sum_{i=1}^{n}\left[(x_i)_{meas} - (x_i)_{act}\right]^2} \qquad (2.5)$$

Where i is the individual data point and the sum is taken from i = 1 to i = n and x is an individual data point. At a flow rate of 2.5 kg/min, this analysis yields an error of 0.009517 kg/min.

2.2.4 Differential Pressure Transducer

The next data gathering component of the test setup in need of calibration was the differential pressure transducer from Validyne, (Validyne P305D-50) capable of differential pressures up to 125 psi. For the calibration of the pressure transducer, the procedure must be performed in two steps. The two step procedure is necessary due to the large range of possible pressures. The first step, for the low pressures, was performed by using a Dwyer 60-0-60 inch

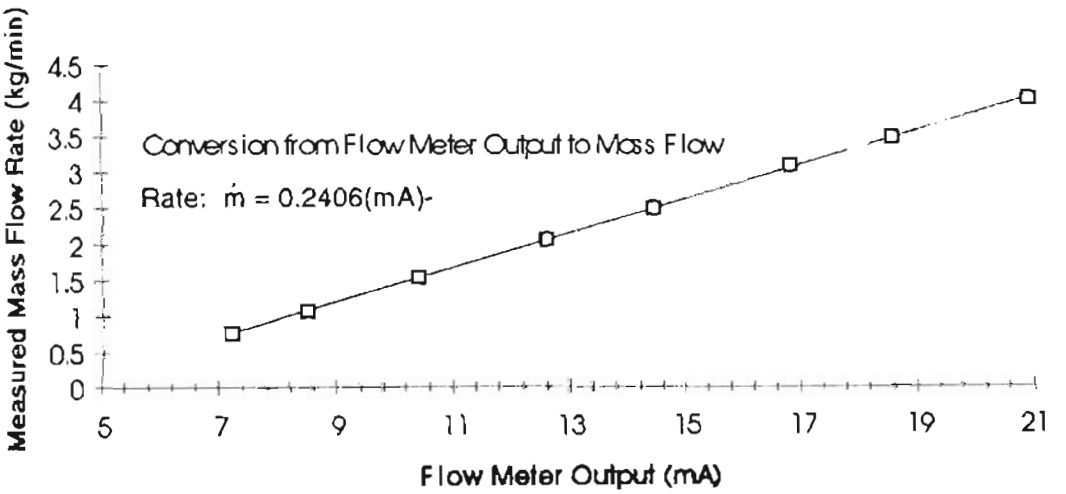

Figure 2.14. Mass Flow Meter Calibration Curve.

mercury U-tube manometer and compressed air. The test configuration consisted of an input of compressed air into the calibration system, which then branched off to the manometer and the pressure transducer, this system is seen in Figure 2.15. However this method only completed the 0-50 psi range of the transducer.

For the upper end of the scale, a dead-weight tester was used. The dead-weight tester, shown in Figure 2.16, is set up for calibration of the pressure gage G. The chamber and cylinder of the tester are filled with a clean oil by first moving the plunger to its most forward position and then slowly withdrawing it while the oil is poured in through the opening for the piston. The gage to be tested is installed and the piston inserted in the cylinder. The pressure exerted on the fluid by the piston is now transmitted to the gage when the valve is opened. This pressure may be varied by adding weights to the piston or by using different piston-cylinder combinations of varying areas. The viscous friction between the piston and the cylinder in the axial direction may be substantially reduced by rotating the piston-weight assembly while the measurement is taken. As the pressure is increased, it may be necessary to advance the plunger to account for the compression of the oil and any entrapped gases in the apparatus. High-pressure

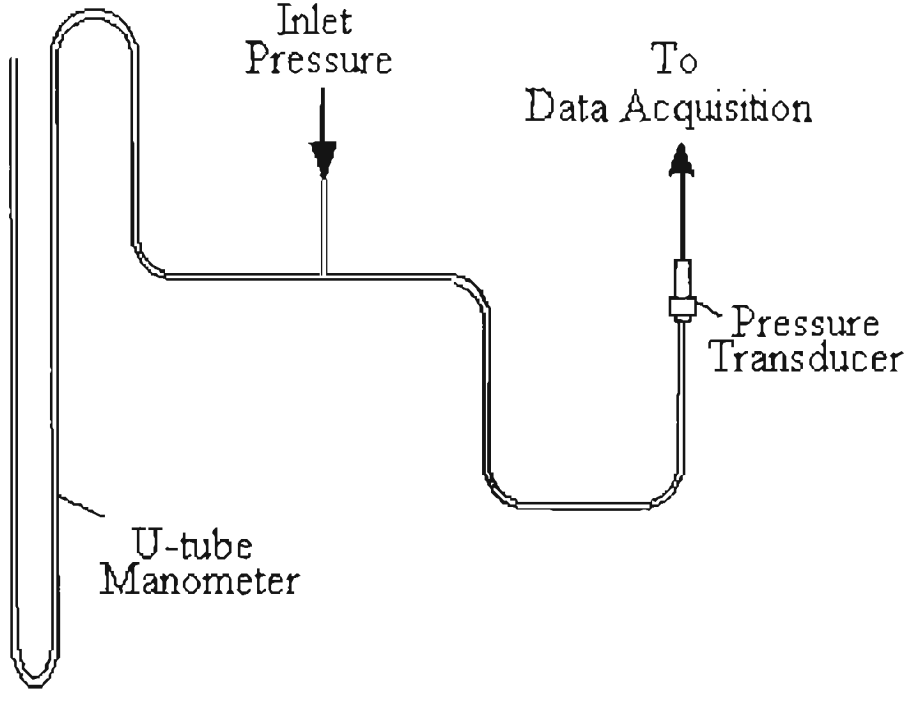

Figure 2.15. Schematic of the Pressure Transducer Calibration.

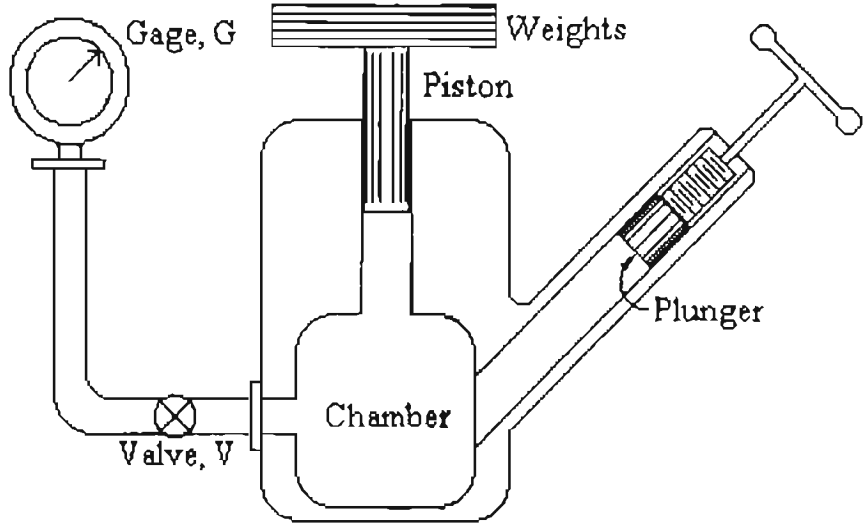

Figure 2.16. Schematic of a Dead-Weight Tester.

dead-weight testers have a special lever system which is used to apply large forces to the piston.

The result of this calibration is shown in Figure 2.17, as a plot of the output of the transducer in Volts versus the measured pressure in pounds per square inch.

An error analysis was performed for the pressure transducer. The accuracy of dead-weight testers are limited by two factors: (1) the friction between the cylinder and the piston and (2) the uncertainty in the area of the piston. The friction is reduced by rotation of the piston and use of long enough surfaces to ensure negligible flow of oil through the annular space between the piston and the cylinder. The area upon which the weight acts is not the area of the piston nor the area of the cylinder; it is some effective area between these two which depends on the clearance spacing and the viscosity of the oil. The smaller the clearance, the more closely the effective area will approximate the cross-sectional area of the piston. The percent error due to the clearance varies according to the following equation:

$$\%\,error \propto \frac{(\rho \Delta p)^{1/2} b^3}{\mu d l} \qquad (2.6)$$

Where the density (ρ) and the viscosity (μ) refer to the oil, the diameter (d) and length (l) refer to the piston, b is the clearance spacing, and the pressure differential (Δp) is the difference of pressure across the cylinder. Therefore, to obtain the error associated with the dead-weight tester, the same uncertainty approach described earlier is used. The result of this analysis is that the maximum percent error for the dead-weight tester is approximately 0.5%, and occurs at a pressure differential of 100 psi. This translates to a maximum uncertainty of 0.5 psi.

For the manometer, the final data consisted of multiplying the measured change in mercury heights by a constant resulting from the change in units. Therefore, this error is straightforward and no complicated error analysis needs to be performed. However, a least squares analysis is still required for the transducer output.

- For the pressures using the manometer:

  The manometer is calibrated in increments of 0.1 inch of mercury. Therefore, the uncertainty of the reading is one half the smallest increment, or 0.05 inch of mercury. However, when using an U-tube manometer, a reading must be taken on both sides; therefore, the total uncertainty is sum of the individual

uncertainties, or 0.1 in. of mercury. Converting this into psi yields an uncertainty of 0.049 psi.

- For pressures using the pressure transducer:

  Because the differential pressure is measured by a pressure transducer whose output consists of an electrical signal, voltage, to the Fluke, some error will occur as this signal fluctuates. Therefore, for the error analysis on the pressure transducer itself, we must look at the fluctuations and perform a least squares analysis for each pressure measurement. This least squares analysis is the same used for the mass flow meter calibration and can be seen in Equation (2.5). The maximum error for the fluctuations occurs for the pressure measurement of 26.4 psi. The corresponding least squares analysis yields an error of 0.125 psi. Furthermore, the minimum error for the pressure transducer occurs for the pressure measurement of 8.6 psi. The corresponding least squares analysis yields an error of 0.095 psi.

Combining these uncertainties yield the following: for pressures below 50 psi (manometer calibrated), the differential pressure has a maximum uncertainty of 0.174 psi and for pressures above 50 psi (dead-weight calibrated), the

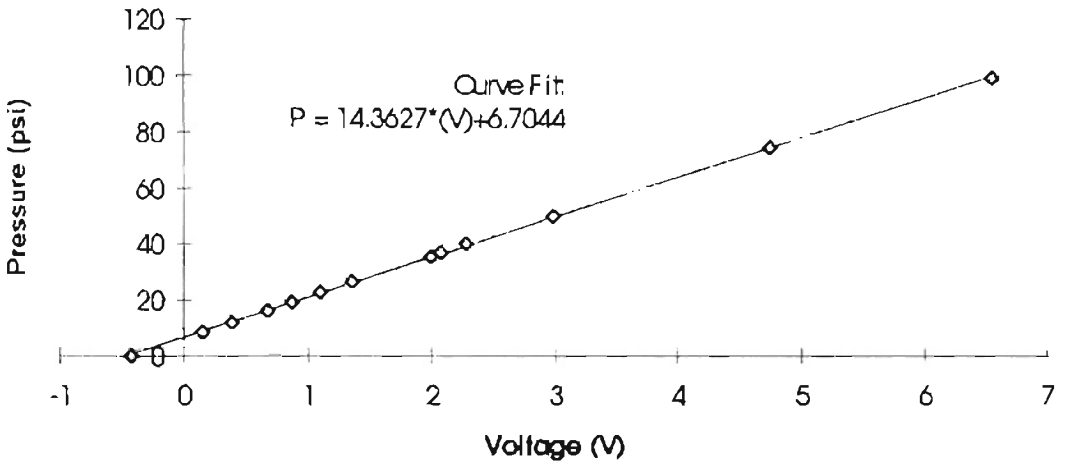

Figure 2.17. Differential Pressure Transducer Calibration Curve.

differential pressure has a maximum uncertainty of 0.625 psi.

2.3 Experimental Procedures

The system warm up, data collection, and shut off procedures were conceived with consideration for accuracy, repeatability, safety, and ease of performance. Furthermore, because the experimentation on the High Flux Heat Exchanger consisted of three distinct categories, the experimental procedure was designed to overlap the different tests.

2.3.1 Warm Up

Before each data collection experiment occurred a quick check of all apparatus and equipment was performed to ensure no leaks nor failed components were present in the system. These checks included the following:

1. First, switch the Fluke data logger on, and select the proper data acquisition program needed for the current experiments.
2. After initiating flow through the test loop, set the flow rate to its maximum, 4.0 kg/min, and check for PAO leaks around the filter, reservoir, and the inlet and outlet of the HFHE.

3. Start the pump on the cold temperature bath (do not start the cooling cycle), then check for coolant leaks at the inlet/outlet to the in-loop heat exchanger and the inlet/outlet of the cold temperature bath.
4. Set the Set Point temperature of the cold temperature bath to cool the test loop to 20°C (at the maximum flow rate and zero heat load, this equates to approximately 18.5°C for the cold temperature bath) and initiate the cooling cycle. If the test-loop temperature measurement (at the inlet of the HFHE) does not measure approximately 20°C, then the thermocouple probes should be recalibrated.
5. Once the test-loop temperature has steadied at 20°C, then check the pressure drop across the HFHE. This pressure drop should be approximately 47 psi. If the measurement from the differential pressure transducer does not match this value, the transducer should be recalibrated.
6. Finally, if a substantial pressure drop occurs across the filter, the filter should be changed.

2.3.2 Operational Procedure

The operating procedures for the three distinct sets of experiments are similar, but retain significant difference to present three distinct sets of operational standards. The first to be presented is the operational procedure for the hydraulic tests.

1. Set the Fluke data logger to the hydraulic test data acquisition program. This program consists of recording the incoming data on the inlet coolant temperature and outlet coolant temperature of the HFHE, the mass flow rate, and the pressure drop across the HFHE.
2. After the test-loop checks have been made, select a coolant temperature and set a corresponding Set Point temperature on the cold temperature bath. The corresponding Set Point temperature will vary depending on the coolant temperature and the room temperature (e.g. If the coolant temperature is set for 50°C and room temperature is 25°C, the Set Point temperature will be greater than 50°C). Retain the maximum mass flow rate of 4.0 kg/min, for all coolant temperatures above 0°C. However, if the selected coolant temperature is below 0°C, then reduce the mass flow rate to 3.0 kg/min.

3. Allow the inlet coolant temperature to reach thermal equilibrium. Thermal equilibrium is defined in this report as when the measured temperature does not increase or decrease more than 0.1°C in a time span of two minutes. The ±0.1°C in temperature allows for the uncertainty of the thermocouples. The time span of two minutes allows for both the thermal lag between the inlet coolant temperature and the HFHE surface, in addition to the maximum time needed for the data collection.
4. Initiate the data acquisition program, allowing fifteen data points to be recorded.
5. After stopping the data acquisition program, decrease the mass flow rate by 0.25 kg/min.
6. Repeat steps 3 through 5 until the minimum mass flow rate, 1.0 kg/min, has been reached.
7. Once the entire flow spectrum has been completed, select a new coolant temperature and repeat the procedure. (Periodically, after the entire flow spectrum has been completed, perform the hydraulic tests in reverse, starting with the minimum flow rate and increasing to the maximum flow rate, to determine any hysteresis in the data collection.)

8. Repeat the above steps until the entire temperature spectrum has been completed.

The second set of experiments consisted of the thermal performance of the HFHE in steady-state operation. To complete this set of experiments the following procedure was followed:

1. Select the individual CHIC of the HFHE to be tested, and perform the thermocouple set up and amplifier set up described in section 2.1.12.
2. Set the Fluke data logger to the steady state thermal test program. This program records the inlet coolant temperature and outlet coolant temperature, the pressure drop across the HFHE, the mass flow rate, the surface thermocouples, the heater thermocouple, the amplifier thermocouples, and the voltage and amperage of the mica heater. The program also calculates the power supplied by the mica heater through the use of the measured voltage and amperage.
3. Set the Set Point temperature to maintain a test-loop temperature of 20°C and a power load of 40 W.
4. Allow for thermal equilibrium of the test-loop temperature. This temperature will be slightly lower than 20°C at zero heat load.

5. Switch on the heater and set the heat load to 40 W. This must be done by monitoring the voltage and amperage from the data logger, and self calculating the power.
6. Allow for thermal equilibrium of the embedded thermocouple (thermocouple measuring the surface temperature of the HFHE beneath the heat flux amplifier). From Flynn [11], this temperature should be approximately 60°C.
7. Once this check has been made, the power to the mica heater is switched off. Then, select a coolant temperature and set a corresponding Set Point temperature on the cold temperature bath. Retain the maximum mass flow rate of 4.0 kg/min, for all coolant temperatures above 0°C. However, if the selected coolant temperature is below 0°C, then reduce the mass flow rate to 3.0 kg/min.
8. Allow thermal equilibrium of the inlet coolant temperature to be reached. Then switch on the power to the mica heater, and set the heat load to 20 W.
9. Allow thermal equilibrium of the heater thermocouple. The heater thermocouple was chosen because the heater has the greatest temperature of

all the components involved in the heat removal, the HFHE, the amplifier, and the mica heater.

10. Initiate the data acquisition program, allowing fifteen data points to be recorded. After stopping the data acquisition program, decrease the mass flow rate by 0.25 kg/min.
11. Once again allow for the thermal equilibrium of the heater temperature, and repeat step 10 until the minimum mass flow rate has been achieved.
12. After the entire spectrum of flow rates has been completed, increase the power setting by 20 W. (Periodically, after the entire spectrum of flow rates has been completed, perform the procedure in reverse, starting with the minimum mass flow rate and increasing to the maximum mass flow rate to check for hysteresis in the data collection.)
13. Repeat steps 9 through 12 until the entire spectrum of heat loads has been completed. Then select a new coolant temperature and repeat the data collection procedure.
14. After the entire spectrum of coolant temperatures has been completed, select a new individual CHIC and perform the entire procedure again until all the required CHICs have been completed.

The final set of experiments consists of the thermal performance of the HFHE in a transient state of operation. To complete this set of experiments, the following procedure was followed:

1. Select the individual CHIC to be evaluated, and set up the thermocouples and the ceramic heater as described in section 2.1.12
2. Set the Fluke data logger to the transient state thermal test program. This program records the imbedded thermocouple temperature, the inlet temperature, and the voltage and the amperage of the mica heater. The acquisition program only records this data to optimize the number of data points collected in the transient time span.
3. Follow the procedure steps 3 through 7 from the steady-state test procedure.
4. While allowing for thermal equilibrium of the coolant temperature, turn on the power to the heater and set the Variac to create 10 W of power. Then turn off the power to the heater while retaining the settings for the 10 W of power.
5. After attaining thermal equilibrium for the coolant temperature, start the data acquisition program. Then turn on the power to the heater and record data points for thirty seconds, then turn

off the power to the heater and record data points for thirty seconds. Repeat the data collection process a sufficient enough times to achieve satisfactory accuracy. This number of repititions was assumed to be three.

6. Stop the data acquisition program, and lower the mass flow rate by 0.5 kg/min.
7. Repeat steps 5 and 6 until the entire mass flow rate spectrum has been completed. Then increase the power setting by 10 W, and follow steps 5 and 6. Repeat this step until the entire power spectrum has been completed.
8. After the power spectrum has been completed, select a new coolant temperature and repeat the entire procedure.

2.3.3 Shut Down

For proper safety, the following procedure should be completed at the end of each set of experiments.

1. Turn off the power to the mica heater, and allow the temperature of the embedded thermocouple to reach room temperature.
2. Then turn off the motor/pump, the cold temperature bath, and the Fluke data logger.

3. Finally, inspect the test section apparatus and ensure that no leaks have become evident.

2.4 Problems

It was discovered that due to the large spectrum of coolant temperatures, sufficient thermal expansion occurs in the rubber hoses inside of the cold temperature bath and in the vinyl tubing connecting the cold temperature bath and the in-loop heat exchanger to cause significant leakage at the fittings. Therefore, after each cycle of coolant temperatures, the fittings inside of the cold temperature bath and the tubing connecting the cold temperature bath and the in-loop heat exchanger were tightened.

Another problem during experimentation occurred at the check on the embedded thermocouple temperature during steady state tests. It was determined if the surface temperature is greater than the referenced value the following must be checked. First, the amplifier is not making significant contact with the CHIC surface due to a lack of contact pressure. This can be checked by slightly tightening the nuts on the securing plate. If the embedded thermocouple temperature decreases, then the contact pressure is not sufficient.

Second, if the amplifier is not making significant contact with the CHIC surface, the reason is due to the

improper alignment between the footprint of the CHIC and the footprint of the amplifier. To check this, remove the insulation and securing plate. Then ease the amplifier off the HFHE and check the footprint in the thermal grease. If the footprint does not overlay the footprint of the CHIC, then the contact between the HFHE and the amplifier is not sufficient.

The third problem that may arise is a non-uniform heat removal by the amplifier. This can be checked by evaluating the amplifier thermocouples. If the thermocouple readings on each plane of the amplifier are not uniform, then the amplifier needs to be replaced.

Finally, a lack of proper impingement on the target plate due to clogged passages of the CHIC passages by particulates in the fluid. This is assumed if no other cause is ascertained. To overcome this problem, the HFHE will need to be removed from the test loop and soaked in a solvent, and rinsed out by compressed air.

2.5 Data Reduction Procedures

A computer program called LAB was the major data reduction tool. A listing of the computer program LAB is given in Appendix D. The program's input is the data output file from the Fluke data logger and the number of inputs

(e.g. for the hydraulic tests, the number of inputs is four: inlet and outlet temperatures, mass flow rate, and pressure drop across the HFHE). The program averages each input and arranges the file in order to create a summary file that includes each flow rate, heat load, and coolant temperature for each CHIC tested (a sample output file is also given in Appendix D). The output file is then in a form to derive the final presentation of the data collected. This derivation of the data is presented in the results and discussion chapter.

Chapter III

RESULTS AND DISCUSSION

3.1 Hydraulic Results

The hydraulic tests consisted of pressure drop measurements across the HFHE for ranges of flow rate and inlet coolant temperature of 1.0 kg/min to 4.0 kg/min by 0.25 increments and -10°C to 50°C by increments of 10°C, respectively. In addition, because of the emphasis on low temperature measurements for system start up the -15°C was also included. The actual pressure taps are immediately before and after the inlet and outlet of the HFHE. Therefore, the pressure drop measured is the actual pressure drop. The results of these tests are in the form of a family of curves of pressure drops across the range of flow rates and coolant temperatures. and the corresponding curve fit equation as a function of flow rate and viscosity and as a function of flow rate and coolant temperature. Figure 3.1 shows the family of curves for the hydraulic performance of the High Flux Heat Exchanger.

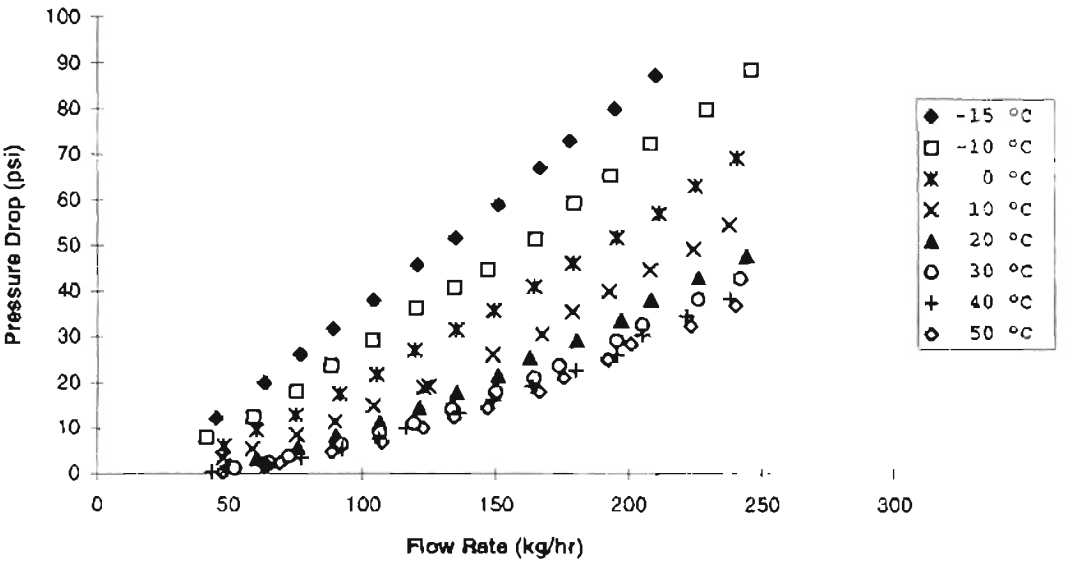

Figure 3.1. Pressure Drop Measurements.

3.1.1 Analytical Hydraulic Model

The next step in the analysis of the hydraulic performance for the HFHE is to determine the equation governing the pressure drop. This is done by the following procedure.

First, beginning with the energy equation [12] for a control volume in a pipe for laminar flow and assuming steady state conditions the following equation for the conservation of energy is developed:

$$\dot{W}_{mech} = \int_{A_e} \rho_e \left(h + \frac{V^2}{2} + gz \right)_e dQ_e - \int_{A_i} \rho_i \left(h + \frac{V^2}{2} + gz \right)_i dQ_i - \dot{W}_{s_\tau} - {}_i\dot{Q}_e \quad (3.1)$$

If the fluid properties vary at most in one direction, and if the control volume has a number of inlet and exit stations through which the fluid flows, then the energy equation can be divided by the mass flow rate and the viscous work term, $\dot{W}_{\tau}$, and the heat transfer term, ${}_i\dot{Q}_e$, can be combined into a total friction loss term, h_f. This new equation can be seen as Equation (3.2).

$$w_{mech} = \sum_e \left(\frac{p}{\gamma} + \frac{V^2}{2g} + z \right)_e - \sum_i \left(\frac{p}{\gamma} + \frac{V^2}{2g} + z \right)_i + h_f \quad (3.2)$$

However, if the entire HFHE is considered the control volume, only one inlet and one exit station occurs. Also, the friction head loss, h_f, can be expressed by a viscous-frictional loss term and a dynamic loss term. Therefore, the energy equation can be expressed in its final form.

$$\left(\frac{p}{\gamma}+z+\frac{V^2}{2g}\right)_1+\left({}_1w_2\right)_{mech}=\left(\frac{p}{\gamma}+z+\frac{V^2}{2g}\right)_2+f\frac{L}{D}\frac{V^2}{2g}+\sum k_i\frac{V^2}{2g} \qquad (3.3)$$

Now applying this form of the energy equation to the HFHE in the test loop, the following modifications can be made. First, for the HFHE, the mechanical work term is negligble, no pumps or turbines exist in the control volume. Next, the HFHE is located in the horizontal plane, therefore the change of potential energy across the HFHE, z_1-z_2, can be neglected. In addition, because the hydraulic tests were performed for an isothermal condition, the density of the PAO can be considered a constant across the HFHE. Applying a constant density with the fact that the cross-sectional area of the inlet equals the cross-sectional area of the outlet, from conservation of mass, translates to the velocity entering the HFHE being equal to the velocity exiting the HFHE. Therefore the change in kinetic energy, $(V^2/2)_1-(V^2/2)_2$, across the control volume can also be

neglected. Finally, both the viscous-friction term and the dynamic term can be modeled by a summation of the individual viscous-friction terms and dynamic terms associated with the individual plates in each CHIC. Therefore, the equivalent tube-orifice model can be expressed as:

$$\Delta p = \sum_{i=1}^{n} k_i \frac{V_i^2 \rho}{2 g_c} + \sum_{i=1}^{n} f_i \frac{L_i}{D_i} \frac{\rho V_i^2}{2 g_c} \qquad (3.4)$$

Now assuming that the flow is predominately laminar flow, the friction factor can be expressed as a function of only the Reynolds number. This friction factor is expressed as:

$$f = \frac{C}{\mathrm{Re}} = \frac{C \mu}{\rho V D} \qquad (3.5)$$

Substituting Equation (3.5) and the expression that the velocity is equal to the volumetric flow rate divided by the cross-sectional area, V=Q/A, yields the following equation for the pressure drop across the HFHE:

$$\Delta p = \sum_{i=1}^{n} \rho Q^2 \left(\frac{k_i}{2 A_i^2 g_c} \right) + \sum_{i=1}^{n} \mu Q \left(\frac{C L_i}{2 g_c A_i D_i^2} \right) \qquad (3.6)$$

The terms in the parentheses represent the minor loss coefficient, the cross-sectional area of the individual tubes, the gravitational constant, the length of the individual tubes, the diameter of the individual tubes, and the constant relating the Reynolds number and the friction factor. All of these are independent of the flow rate and the coolant temperature. Therefore, Equation (3.6) can be simplified as the pressure drop across the HFHE is equivalent to the viscous-frictional head loss, μQ, plus the dynamic head loss, ρQ^2.

$$\Delta p = C_2 \rho Q^2 + C_1 \mu Q \tag{3.7}$$

However, the flow rate measured was in terms of the mass flow rate instead of the volumetric flow rate. Therefore, using the expression that the volumetric flow rate is equivalent to the mass flow rate divided by the density of the fluid, $Q = \dot{m}/\rho$, the final equation for the pressure drop across the HFHE is:

$$\Delta p = \frac{\left(C_1 \mu \dot{m} + C_2 \dot{m}^2\right)}{\rho} \tag{3.8}$$

Because the pressure drops are dependent on the viscosity, density, and flow rate, this set of curves are indicative to the inert properties of the coolant PAO. Therefore, to complete the modeling of the hydraulic performance of the HFHE, equations for the density and the viscosity of the coolant must be developed as functions of the fluid temperature. These equations were developed by Ghajar, et al. [13], and shown below. First, the viscosity of the PAO follows the following equation, in which the viscosity is in terms of m^2/s and the temperature is in terms of K:

$$\nu = \left(10^{\left(\frac{10^{9.67}}{T^{3.923}} \right)} - 0.70 \right) \times 10^{-6} \qquad (3.9)$$

From this equation, it can be seen that the viscosity increases exponentially below 291.7 K or 18.5 °C. This exponential increase can be seen in Figure 3.1. In addition, the density of the coolant fluid PAO, in kg/m^3, is given as a function of the coolant temperature, in K, by the following equation:

$$\rho = 1.36 \times 10^3 - 4.56T + 0.0157T^2 - 0.280 \times 10^{-4} T^3 + 0.174 \times 10^{-7} T^4 \qquad (3.10)$$

Now substituting the expressions for the density and viscosity into Equation (3.8), and realizing that the kinematic viscosity is equal to the absolute viscosity divided by the density, $\nu = \mu/\rho$, the final equation for the pressure drop across the HFHE, psi, in terms of the mass flow rate, kg/hr, and inlet coolant temperature, K, is expressed as the following:

$$\Delta p = C_1\left[\left(10^{\left(\frac{10^{9.67}}{T_f^{3.923}}\right)} - 0.70\right)\times 10^{-6}\right]\dot{m} + C_2\frac{\dot{m}^2}{\left(1.36\times 10^3 - 4.56T_f + 0.0157T_f^{\,2} - 0.28\times 10^{-4}T_f^{\,3} + 0.174\times 10^{-7}T_f^{\,4}\right)} \quad (3.11)$$

3.1.2 Overall Hydraulic Performance

Combining the experimental and analytical models for the pressure drop across the HFHE, the constants for Equation (3.11) can be derived from a curve fit. These constants for C_1 and C_2 were determined to be 7354.83 and 0.428, respectively, for all of the inlet coolant temperatures. These constants yield an equation that fits the experimental data at each discrete temperature with a standard deviation of 1.813 psi and a maximum error of 3.5 psi at a coolant temperature of -15°C and flow rate of 180 kg/hr. This model, as shown in Figures 3.2 and 3.3, fits

the data well, especially at medium and high flows. However, the form of the equation of this model is constrained to pass through the origin. This constraint may affect the fit at the low flow conditions. Evaluation of the hydraulic performance shows at normal flow, 200 kg/hr, and an inlet temperature of -10°C, the pressure losses are 28% dynamic and 72% viscous-frictional. For the same flow at an inlet temperature of 50°C the losses are 78% dynamic and 22% viscous-frictional. At reduced flow, 100 kg/hr, and an inlet temperature of -10°C, the pressure losses are 16% dynamic and 84% viscous-frictional. For the same flow rate and at an inlet temperature of 50°C the losses are 64% dynamic and 36% viscous-frictional.

3.1.3 HFHE Flow Regime

For the development of the hydraulic performance equation, shown in section 3.1.1, the assumption of a laminar flow regime was made. Therefore, a check on this assumption is necessary. For this check, the following procedure was performed, starting with the Reynolds number equation.

$$\mathrm{Re} = \frac{VD}{\nu} \tag{3.12}$$

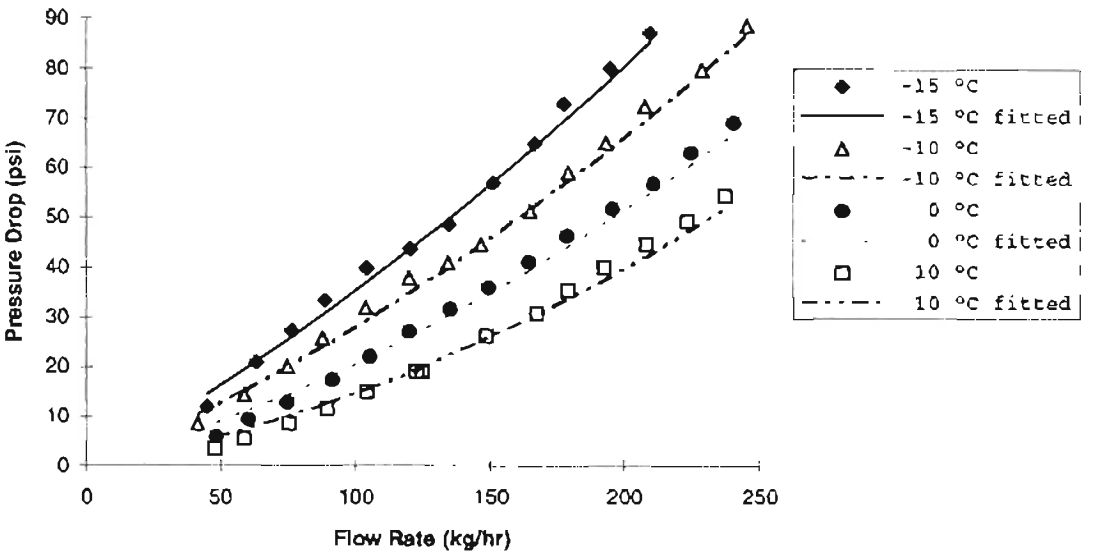

Figure 3.2 Curve Fit for the Pressure Drop (-15°C to 10°C).

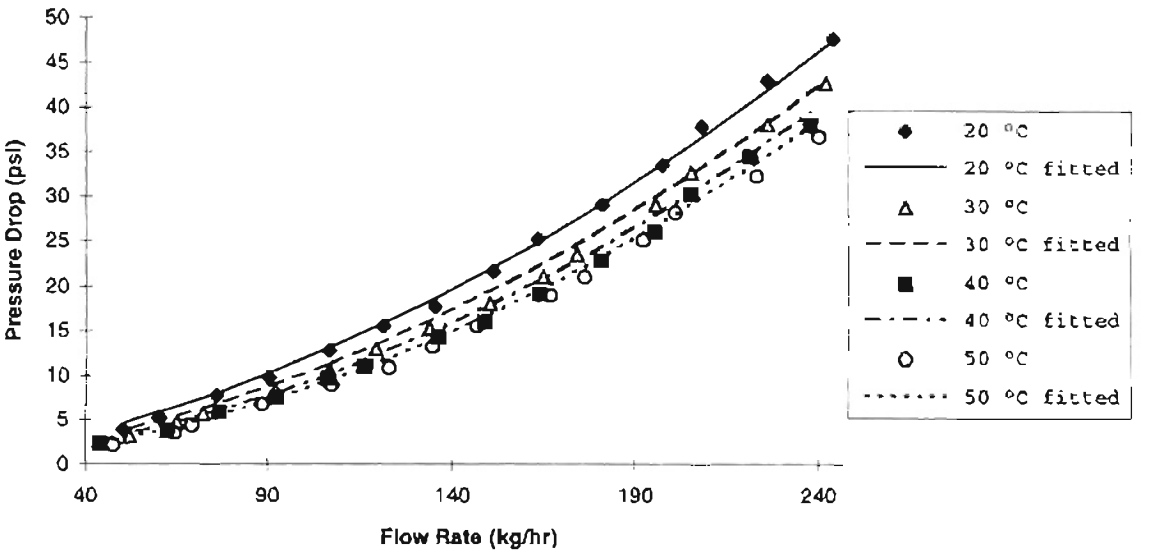

Figure 3.3. Curve Fit for the Pressure Drop (20°C to 50°C).

Now rearranging this equation in terms of the mass flow rate yields the following:

$$\mathrm{Re} = \frac{4\dot{m}}{\pi D \rho \nu} \tag{3.13}$$

Now substituting Equations (3.9) and (3.10) for the density and the viscosity yields an equation for the Reynolds number in terms of the mass flow rate, diameter of the tubing, and the coolant temperature.

$$\mathrm{Re} = \frac{4\dot{m}}{\pi D\left(1.36\times10^{3} - 4.56T_f + 0.0157T_f^{\,2} - 0.28\times10^{-4}T_f^{\,3} + 0.174\times10^{-7}T_f^{\,4}\right)} \times \frac{1}{\left[\left(10^{\left(\frac{10^{0.67}}{T_f^{3.923}}\right)} - 0.70\right)\times10^{-6}\right]} \tag{3.14}$$

Now examining this equation for the outlet and inlet of the HFHE yields that the maximum Reynolds number, occurring at the extreme temperature of 50°C, flow rate of 4.0 kg/min, and pipe diameter of 1.27 cm (0.5 inch), corresponding to the inlet and outlet of the HFHE, is 2176. The Reynolds number occurring at the extreme temperature of -10°C, flow rate of 1.0 kg/min, and pipe diameter of 1.27 cm (0.5 inch)

is about 50. Therefore, the Reynolds number over the entire flow rate range, 1.0 kg/min to 4.0 kg/min, and coolant temperature range, -10°C to 40°C, is laminar.

Furthermore, although the individual tubes in the HFHE are much smaller than the inlet/outlet pipe, the flow rate through each CHIC is only 1/20 the flow rate through the inlet/outlet pipe. In addition, the individual jets diameter are on the order of 0.018 cm (0.007 in). However, each CHIC contains sixty jets, three rows of twenty. Therefore the mass flow rate of the individual jet is 1/1200 of the total mass flow rate through the HFHE. At the maximum Reynolds number case, a coolant temperature of 50°C and a mass flow rate of 4.0 kg/min, the Reynolds number through the individual jets translates to about 130. Therefore, once again the assumption of laminar flow through the individual jets of the HFHE is valid.

Some turbulence does occur through the abrupt turning of the flow through the CHICs; however, the increased pressure drop due to this turbulence is modeled in the dynamic pressure loss term. Therefore, the assumption that the flow is predominately laminar throughout the entire HFHE is valid.

3.1.4 Hydraulic Performance Comparison

Because the Compact High Intensity Cooler was designed in 1983, previous examinations have been performed on the hydraulic performance that have led to an analytic model predicting the pressure drop through the CHIC. In addition, the predictions have been extrapolated to encompass various geometric arrangements of the CHICs, such as the High Flux Heat Exchanger. These predictions can be seen in Flynn, et al. [4] and in Figure 3.4. If the predicted pressure drop seen in Figure 3.4 is compared to the experimental pressure drop seen in Figure 3.1, one can see the experimental pressure drops at high flow rates are 50 to 100% higher than the predicted pressure drops. However, the predicted pressure drops follow a model that assumes ideal bend, split, merge, and area transition losses. However, the actual geometry tested will have more losses. In addition, assumed flow channels and orifices for the prediction model are as designed; however, some flow blockage or deformation of passages from fabrication may occur. Finally, most of the predicted pressure drop in a CHIC is spent in the viscosity over the range of expected operating temperatures. The impingement pressure drops are more predictable. Therefore, the predictions of this HFHE design will have more impingement jets; however, in the HFHE design, the

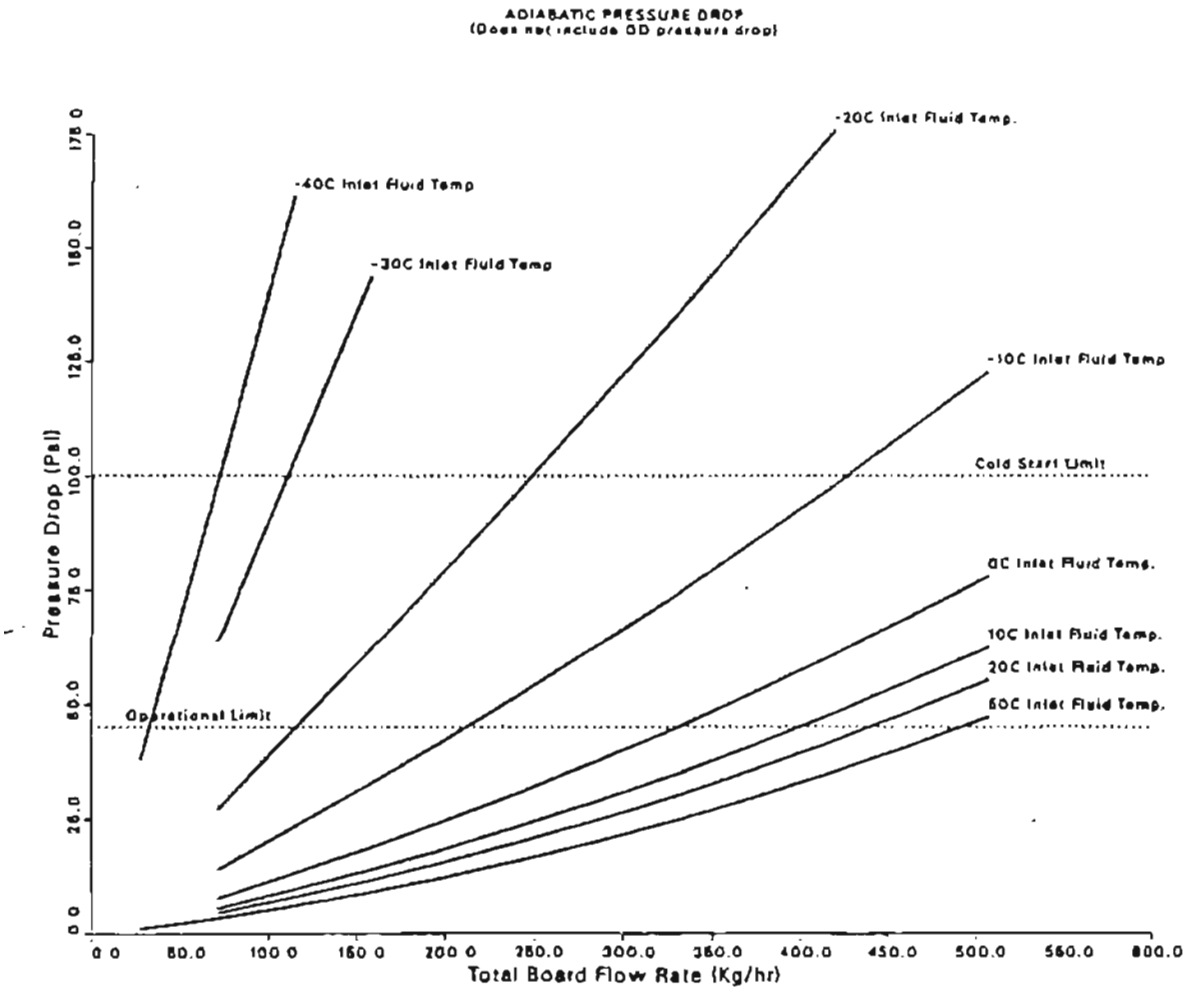

Figure 3.4. Predicted Hydraulic Performance of the HFHE [4].

majority of the pressure losses are line-type frictional losses that occur outside of the orifice plate losses. This is because the HFHE was designed to operate with PAO. All of these factors contribute somewhat to the poor correlation between the previously hydraulic predictions and the experimental analysis.

However, the largest contributor is that in the predictions for the pressure drop across the HFHE seen in Figure 3.4, the flow regime is assumed to be turbulent flow. However, as described earlier, the flow regime for this experimentation is laminar. The effect of this invalid assumption can be shown in the calculation of the constants for Equation (3.11). Upon examination of Equation (3.4), shown below with the velocity replaced with the mass flow rate, the only variable that is dependent on the assumption of laminar flow is the friction factor.

$$\Delta p = \sum_{i=1}^{n} \frac{k_i \dot{m}^2}{2 \rho g_c A_i^2} + \sum_{i=1}^{n} f_i \frac{L_i \dot{m}^2}{2 D_i \rho g_c A_i^2} \qquad (3.15)$$

The minor loss coefficient, k_i, the length of the tubes, L_i, the diameter of the tubes, D_i, and the cross sectional area of the tubes, A_i, are inherent properties of the HFHE and are independent of the flow. The density, ρ, is dependent

on only the coolant temperature. Therefore, the density is independent of the flow.

Finally, the gravitational constant, g_c, is a universal constant and is independent of all the input parameters. Therefore, a comparison between the friction factor for laminar flow and the friction factor for turbulent flow through the HFHE is presented. For the majority of the actual flow regime representing the experimentation with the coolant PAO, the Reynolds number is below 1000 (see section 3.1.3). Using the Moody Chart in [12], this yields a friction factor of over 0.06. However, for the previous predictions of the HFHE, the friction factor for a relatively smooth pipe (such as drawn tubing) is less than 0.03. Therefore, the friction factor is at least 2 times greater for the laminar flow than turbulent flow. Hence, the viscous-frictional term for laminar flow will be twice that of the turbulent flow. This indicates that for laminar flow, the pressure drop across the HFHE should be larger than the predictions for the pressure drop across the HFHE for turbulent flow.

This realization is consistent with the results obtained from this thesis and not consistent with the results obtained by McDonnell Douglas' report [4].

3.2 Thermal Steady-state Performance

The thermal tests include the same flow rate range as the hydraulic tests, but the range of inlet coolant temperatures was reduced to -10°C to 40°C. This reduction is due to the fact that the cold temperature bath used to keep the temperature of PAO constant, must actually cool the PAO below -10°C to remove the power that is added in the thermal tests. In addition, heat loads were applied to the HFHE ranging from 20 W to 100 W by an increment of 20 W.

3.2.1 Radial Heat Loss

Because the HFHE consists of twenty parallel CHICs, an assumption that all CHICs are identically independent is made. Therefore, the thermal tests consisted of applying a heat load to only one of the CHICs in the HFHE at a time. To check the assumption, numerous CHICs were tested to indicate conformity. However, because of the layout of the CHICs in the HFHE, each CHIC is surrounded by channels of PAO. This results in radial heat loss due to conduction heat transfer when only one CHIC is tested at a time. Therefore, the actual heat flux absorbed by the CHIC is less than the heat load applied. So, a two-dimensional heat transfer model was constructed by taking temperature measurements surrounding the testing CHIC, shown in

Figure 2.8. The temperature was then plotted and an exponential decaying curve was fitted. This curve fit followed the following equation:

$$T_s = \theta_1 + \theta_2 e^{\theta_3 \xi} \qquad (3.16)$$

Where the variable ξ is a dummy variable representing the distance from the edge of the CHIC in the x or y direction, in cm, and the surface temperature is given in °C.
A typical curve for the surface temperature profile is shown in Figures 3.5 and 3.6 for the heat loss in the x-direction and the heat loss in the y-direction, respectively. The coordinate system for the HFHE can be seen in Figure 3.7. The constants θ are determined by the curve fit and are dependent on the heat load, fluid temperature, flow rate, and CHIC location. The equation is then differentiated and evaluated at the ξ value representing the symmetry line, shown in Figure 3.7. From this temperature gradient, the heat conducted across the line of symmetry in the x and y direction can be approximated from the following equations, respectively:

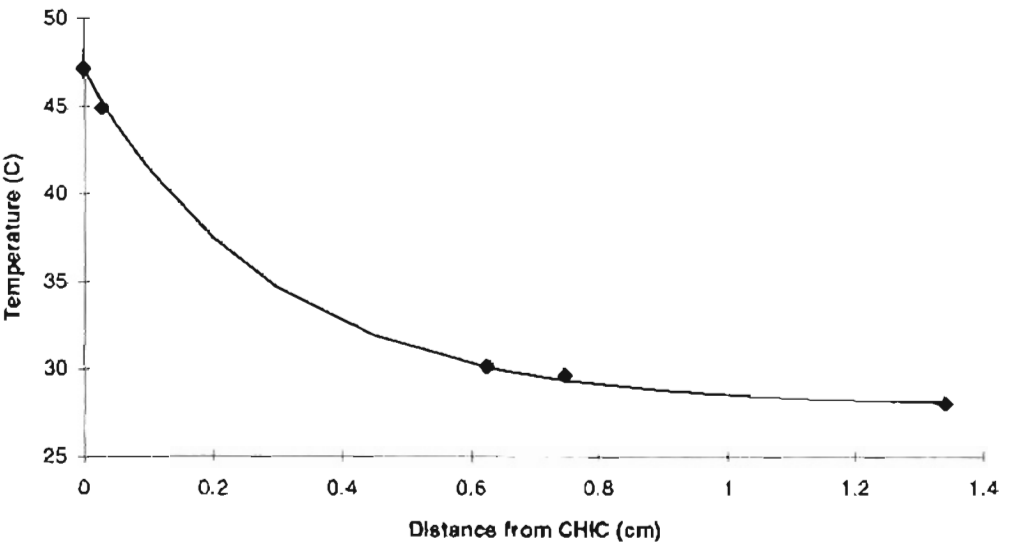

Figure 3.5. X-Directional Temperature Profile.

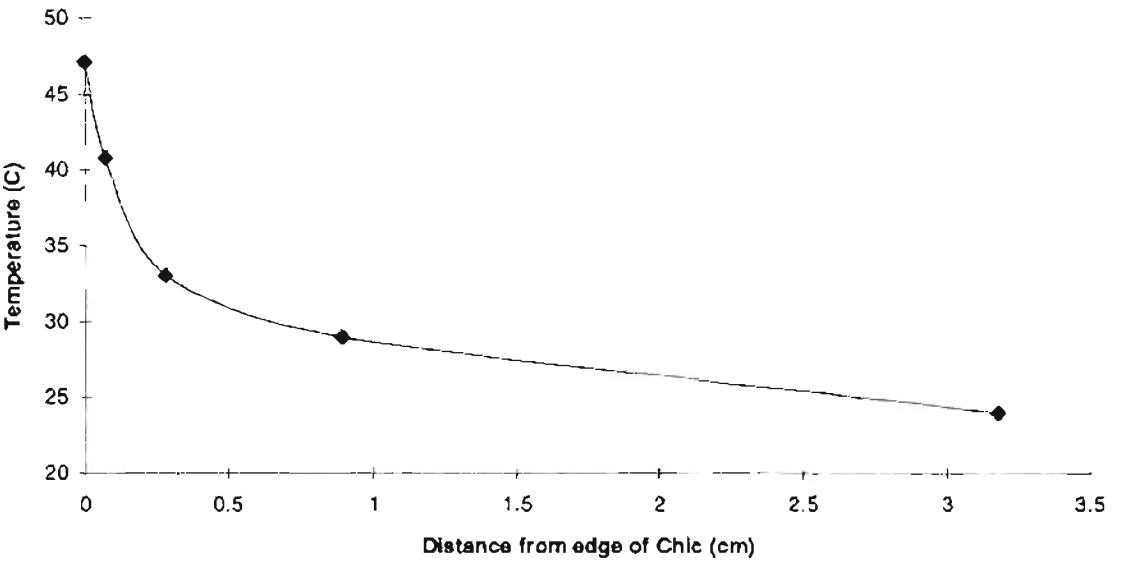

Figure 3.6. Y-Directional Temperature Profile.

$$\dot{Q}_{+/-x} = \pi k r_x t \frac{dT_s}{dx}$$
$$\dot{Q}_{+/-y} = \pi k r_y t \frac{dT_s}{dy} \qquad (3.17)$$

This process is a double sided heat transfer model. Therefore, the total heat loss in the radial direction due to conduction heat transfer for a CHIC surrounded by four CHICs would be the sum of the total heat loss in the x-direction and the y-direction.

However, if the CHIC being tested was surrounded only by two CHICs (the four corner CHICs), the total heat loss would be one half the sum of the total heat loss in the x-direction and the y-direction. In addition, if the CHIC was surrounded by three CHICs (edge CHICs excluding the corner CHICs), then the total heat loss would be the sum of the heat loss in the direction of the two similar CHICs and one half the heat loss in the direction of the third CHIC.

Once the location of the CHICs were accounted for in the total heat loss in the radial direction, it was determined that the individual CHICs tested behaved in similar fashion. This validated the identically independent assumption. The next step in the evaluation of the thermal performance was to develop an analytic equation for the

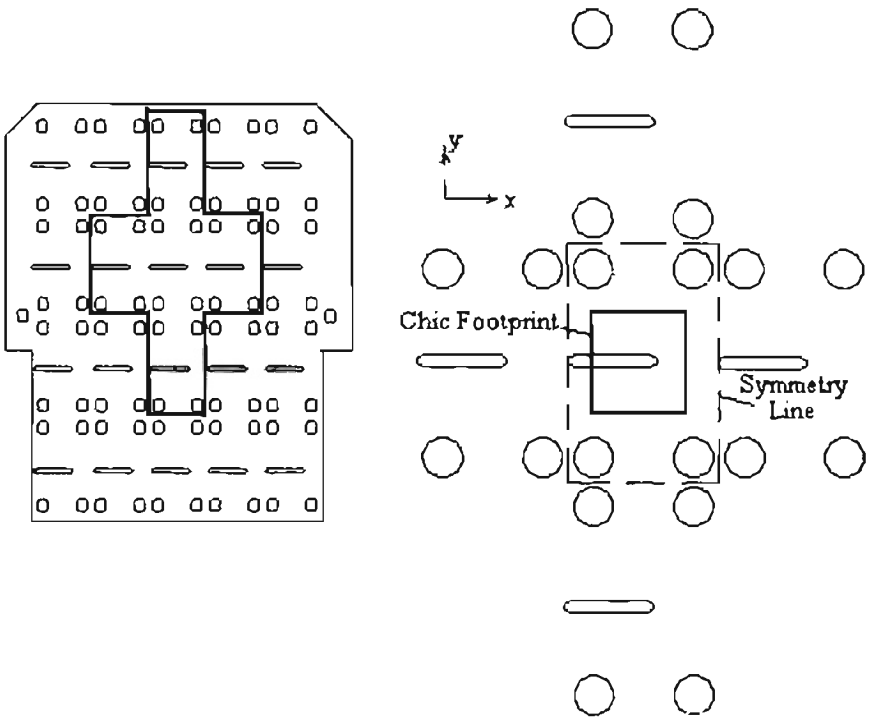

Figure 3.7. Line of Symmetry.

radial heat loss due to conduction heat transfer. In theory, the radial heat loss should be a function of the flow rate only. However, if the energy balance is inspected, it can be shown that the direct path through the CHIC is capable of more heat transfer than the radial path. Therefore, as the heat load is increased, a greater percentage must be transferred directly into the CHIC. This generalization can also be made for the fluid temperature. The affect of the fluid temperature is felt more by the direct route than the radial route. Therefore, as the fluid temperature decreases, a greater percentage of the heat transfer will travel directly into the CHIC. Hence, the actual radial heat loss due to conduction is a function of the flow rate, inlet temperature, and the applied heat load. This is validated by the fact that the largest heat loss occurs at an inlet temperature of 40°C, a flow rate of 60 kg/hr, and a heat load of 20 W. The experimental data was fitted with a curve that was expressed as Equation (3.18). The mass flow rate is expressed in terms of kg/hr and the coolant temperature is expressed in K.

$$\frac{\dot{Q}_{loss}}{\dot{Q}_{applied}} = \phi_1 + \left(\phi_2 + \phi_3 e^{(\phi_4 T)}\right) e^{\left[\left(\phi_5 + \phi_6 e^{(\phi_7 T)}\right)\dot{m}\right]} \qquad (3.18)$$

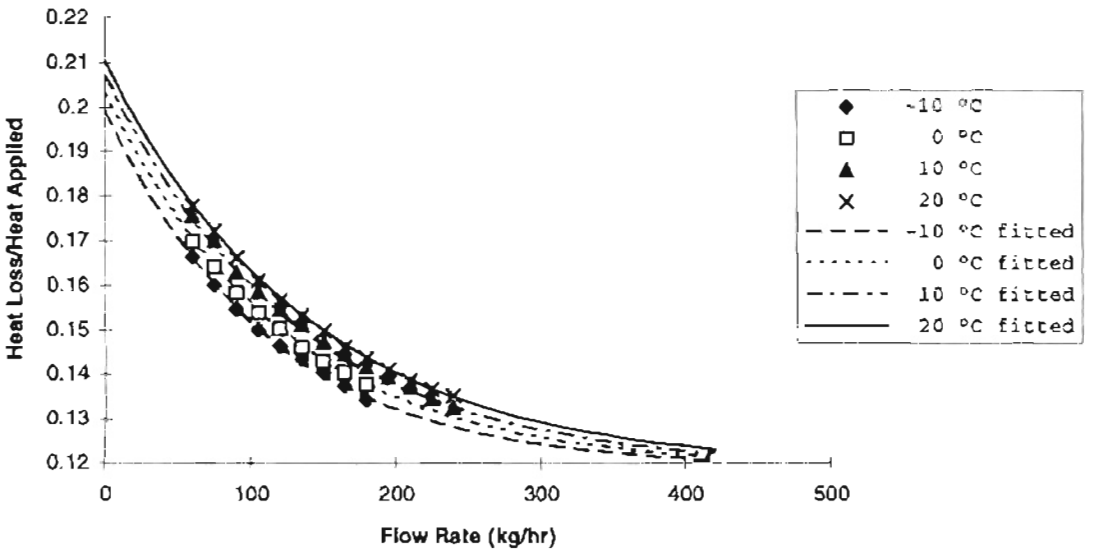

Figure 3.8. Radial Heat Loss Due to Conduction Heat Transfer for an Applied Heat Load of 100 W.

The constants ϕ_n are dependent on the applied heat load. For a heat load of 100 W the constants are as follows: ϕ_1 (0.11858), ϕ_2 (0.11897), ϕ_3 (-0.7860), ϕ_4 (-0.011485), ϕ_5 (-0.0046646), ϕ_6 (-0.37727), and ϕ_7 (-0.017087). The curve fit for the 100 W case is shown in Figure 3.8. This curve fit produces equations that have a standard deviation of 0.000525 and a maximum error of 0.001536. The error analysis for this equation can be seen in Appendix E.

3.2.2 Wall Temperature

The next step in the thermal performance analysis is to develop a thermal resistance equation for the HFHE. To accomplish this, an analytical model must be developed for the wall temperature of the HFHE. This wall temperature theoretically should be a linear function of the heat flux, W/cm^2 as shown below with the wall and fluid temperatures in °C or K:

$$T_w - T_f = \psi \dot{Q} \tag{3.19}$$

However, the flow rate influences the efficiency of the jet impingement heat exchanger. Therefore, the wall temperature should be a linear function of the heat flux, but the

constant, ψ, will be exponentially dependent on the flow rate. To curve fit the experimental data, the heat load used in Equation (3.19) must be the net heat load. This is because the wall temperature data was generated by applying a heat load to only one CHIC. However, when a heat load is applied to all twenty CHICs simultaneously, the radial heat loss will be negligible. Thus the net heat load will be approximately the applied heat load. Therefore, the equation for the wall temperature is shown in Equation (3.20) with the wall and fluid temperatures in °C or K:

$$T_w - T_f = \lambda_0 + \left(\lambda_1 + \lambda_2 e^{(\lambda_3 \dot{m})}\right)\dot{Q} \qquad (3.20)$$

The constants λ_n are independent of the flow rate, heat load, and fluid temperature and have the following values: λ_0 (2.25), λ_1 (0.19779), λ_2 (0.19968), and λ_3 (-0.013115). In addition, the mass flow rate is in kg/hr, and the heat load is in W/cm^2. This curve fit, shown in Figure 3.9, produces a standard deviation of 0.275°C and a maximum error of 0.707°C. This error analysis can be also be seen in Appendix E.

3.2.3 Thermal Resistance

The last step in the procedure for determining the

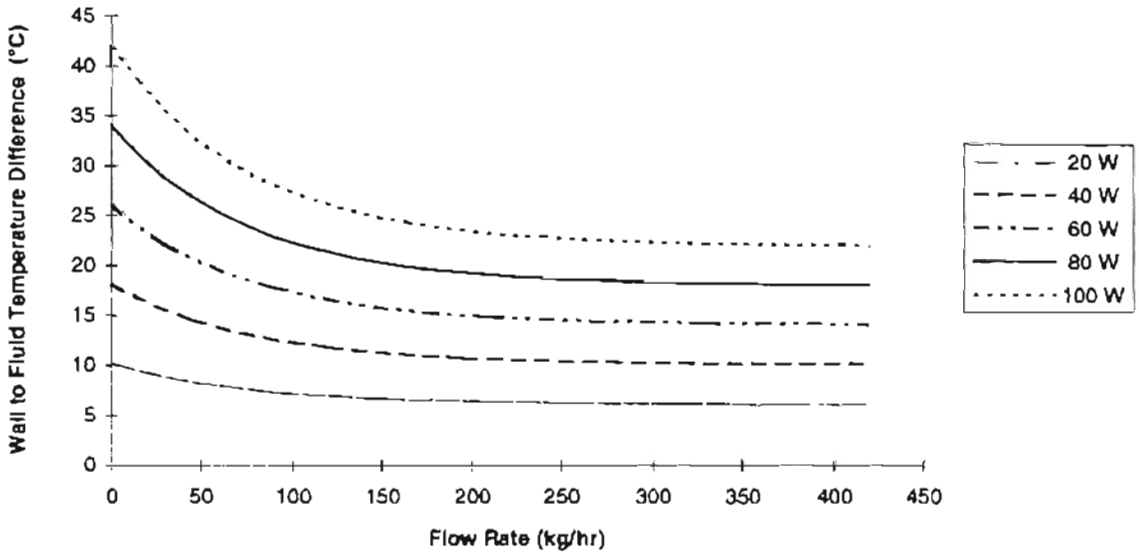

Figure 3.9. Wall Temperature as a Function of the Flow Rate.

properties of the HFHE is the thermal resistance. This thermal resistance of the HFHE, °C/(W/cm^2), can be obtained by the following equation:

$$R_{wf} = \frac{T_w - T_f}{\dot{Q}} \tag{3.21}$$

This equation can be also expressed in terms of the mass flow rate, kg/hr, and the heat load, W/cm^2, by substituting Equation (3.20) into Equation (3.21). This expression is shown in Equation (3.22). In addition the thermal resistance for the HFHE is shown as the mass flow rate and heat load vary in Figure 3.10.

$$R_{wf} = \frac{2.25 + \left(0.20 + 0.20e^{(-0.013\dot{m})}\right)\dot{Q}}{\dot{Q}} \tag{3.22}$$

3.2.4 Thermal Performance

Once the thermal resistance is calculated, the maximum heat flux capable for the HFHE as a function of the inlet temperature and the flow rate can be calculated using the following equation:

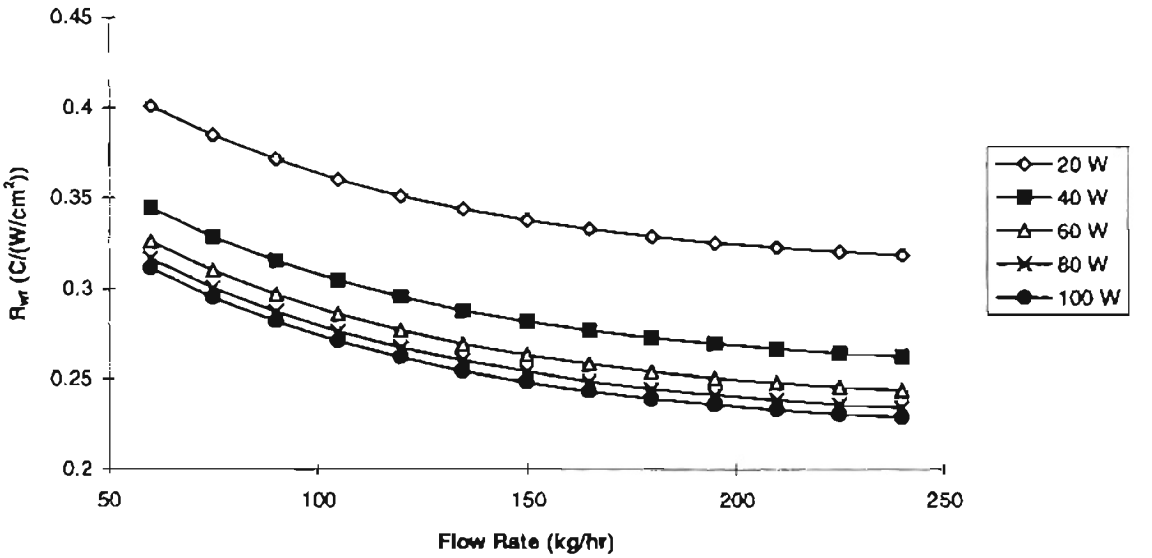

Figure 3.10. Thermal Resistance of the HFHE.

$$\dot{Q} = \frac{T_j - T_f}{R_{jc} + R_{cw} + R_{wf}} \qquad (3.23)$$

The junction temperature, T_j, was designated by the design requirements of the HFHE to be 90° C. The thermal resistance, R_{jc}, from the junction to the case interface and the thermal resistance, R_{cw}, from the case interface to the wall of the HFHE are dependent on the material consistency. The location of these thermal resistances and the junction temperature are shown in Figure 3.11. McDonnell Douglas [4] assumed the values of these thermal resistances both to be 0.2 °C/(W/cm^2). Therefore, Equation (3.23) reduces to a function of the fluid temperature, mass flow rate, and the heat load. Therefore, if Equation (3.22) is substituted into Equation (3.23), and the resulting equation is solved for the ***minimum*** mass flow rate required, $\dot{m}$(kg/hr), for removal of a given applied heat load in terms of the applied heat load, $\dot{Q}$(W/cm^2), fluid temperature, T_f(K), thermal resistances from the junction to the case and the case to the wall, R_{jc} and R_{cw} (°C/(W/cm^2)), and junction temperature, T_j(K), the following equation is generated:

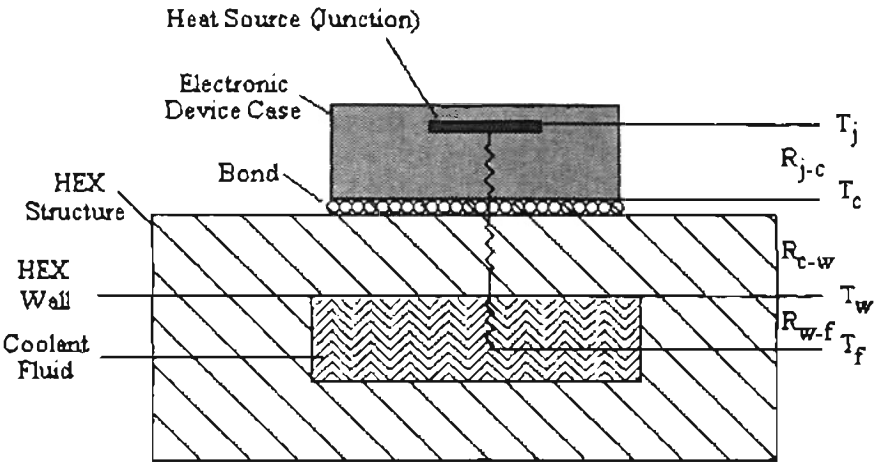

Figure 3.11. Thermal Resistance and Junction Temperature Placement.

$$\dot{m} = -76.24 \ln\left[5.01\left(\frac{-R_{cw}\dot{Q} - R_{jc}\dot{Q} - 2.25 - 0.20\dot{Q} + T_j - T_f}{\dot{Q}}\right)\right] \qquad (3.24)$$

$$IF\ \dot{m}_{measured} \le 0.0:\quad THEN\ \dot{m}_{actual} = 0.0$$
$$ELSE\ \dot{m}_{actual} = \dot{m}_{measured}$$

A logical expression must be inserted into Equation (3.24) because the equation itself does not discern positive and negative values of the mass flow rate. This logical expression can be added into any control device or computer program and does not invalidate the equation for the mass flow rate. The meaning of this logical expression can be explained as follows. The equation will produce a heat flux capability for the HFHE at zero mass flow rate. The reason for this error is that the equation assumes a constant coolant temperature. However, when zero flow occurs in the HFHE and a heat load is supplied, the coolant temperature increases, thereby invalidating Equation (3.24). Therefore, an asymptote must be manually added to the thermal performance curves at zero flow rate. This manual addition is the logical expression. The logical expression itself indicates that any negative values for the flow rate resulting from the input parameters in Equation (3.24) in

actuality mean that any positive non-zero flow through the HFHE is sufficient to remove the input heat flux. Furthermore, a positive value for the mass flow rate resulting from the input parameters in Equation (3.24) reflects the actual ***minimum*** mass flow rate necessary to remove the given heat flux.

3.2.5 Design Heat Load Performance

Now if the heat load is held constant, and the values for the thermal resistance, 0.2 °C/(W/cm^2) and the junction temperature, 90°C, are assumed to be the values described above, then the flow rate can be calculated as a function of the fluid temperature. Because the HFHE was designed to remove 100 W per CHIC, the applied heat load, $\dot{Q}$, was given the value of 100 W. Therefore, the optimum performance curve can be constructed using the flow rates generated by Equation (3.24) over the possible range of coolant temperatures. This performance curve for the heat load of 100 W per CHIC is shown in Figure 3.12. As seen in this figure, the flow rate necessary to generate a maximum cooling rate of 100 W per CHIC remains small until the coolant temperature approaches a value of 28°C (301 K). At this temperature the minimum flow rate necessary for a

cooling rate of 100 W per CHIC increases to infinity. This was reflected in the experimental data. For the value of 0.2 °C/(W/cm^2), for the thermal resistance, R_{jc} and R_{cw}, a heat load of 100 W per CHIC, and a junction temperature of 90°C, the corresponding wall temperature of the HFHE must be 50°C.

During experimentation, at coolant temperatures of 30°C and above, the wall temperature exceeded 50°C over the entire range of flow rates. For a coolant of 40°C, the required 50°C wall temperature, for the removal of 100 W per CHIC, was exceeded at 60 W per CHIC. Furthermore, for a coolant of 30°C, the required 50°C wall temperature was exceeded at 80 W and flow rates less than 3.5 kg/hr. However, the maximum possible coolant temperature can be increased from 28°C by decreasing the thermal resistances of R_{jc} and R_{cw}. If the thermal resistances were reduced from 0.2 to 0.15 °C/(W/cm^2), the corresponding maximum possible coolant temperature is increased from 28°C to 38°C. In addition, if the thermal resistances were increased from 0.2 to 0.25 °C/(W/cm^2), the corresponding maximum possible coolant temperature decreases from 28°C to 18°C. The affect of the thermal resistance values between the junction and

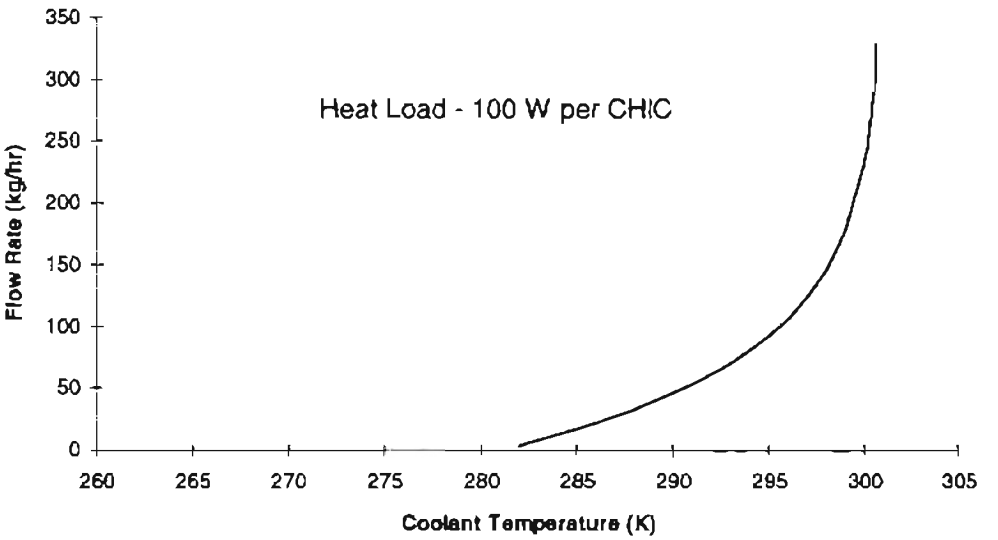

Figure 3.12. Design Specification Thermal Performance Curve for the Minimum Cooling Rate of 100 W per CHIC (R_{cw} and R_{jc}, 0.20 °C/(W/cm^2), and T_j, 90°C).

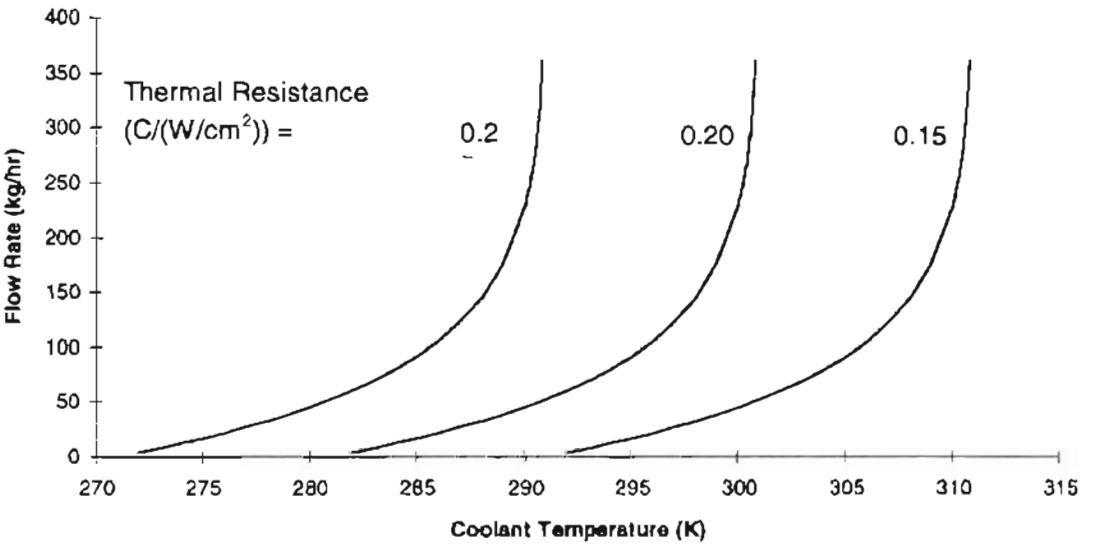

Figure 3.13. Thermal Performance as a Function of the Thermal Resistances.

the case and between the case and the wall of the HFHE on the performance curves are shown in Figure 3.13.

3.2.6 Overall Steady-State Performance

This optimum performance for the HFHE of 100 Watts per CHIC is based on possible future needs in electronic cooling. However, current cooling demands do not reach this high heat flux. Therefore, a complete range of heat loads were examined for the HFHE. So, using Equation (3.24) with the constants for the thermal resistances, R_{wc} and R_{jc}, of 0.2 °C/(W/cm^2), and a constant junction temperature of 90°C, a family of performance curves can be constructed by varying the coolant temperature and heat load. As a note, in previous sections it has been stated that for a junction temperature of 90°C, the corresponding wall temperature, for thermal resistance values of 0.2 °C/(W/cm^2), is 50°C. However, this wall temperature corresponds to a heat load of 100 Watts per CHIC. Tables 3.1 to 3.3 show the corresponding wall temperature for the spectrum of heat ranges considered.

Figures 3.14 through 3.16 show the family of curves for the corresponding thermal resistances, R_{wc} and R_{jc}, and heat loads shown in Tables 3.1 through 3.3.

Table 3.1. Correlation Between the Wall and Junction Temperature for Thermal Resistances of 0.15 °C/(W/cm²).

Heat Load (W/cm^2)	R_{wc} ($°C/(W/cm^2)$)	R_{jc} ($°C/(W/cm^2)$)	T_j (°C)	T_w (°C)
20	0.15	0.15	90	84
40	0.15	0.15	90	78
60	0.15	0.15	90	72
80	0.15	0.15	90	66
100	0.15	0.15	90	60

Table 3.2. Correlation Between the Wall and Junction Temperature for Thermal Resistances of 0.20 °C/(W/cm²).

Heat Load (W/cm^2)	R_{wc} ($°C/(W/cm^2)$)	R_{jc} ($°C/(W/cm^2)$)	T_j (°C)	T_w (°C)
20	0.2	0.2	90	82
40	0.2	0.2	90	74
60	0.2	0.2	90	66
80	0.2	0.2	90	58
100	0.2	0.2	90	50

Table 3.3. Correlation Between the Wall and Junction Temperature for Thermal Resistances of 0.25 °C/(W/cm²).

Heat Load (W/cm^2)	R_{wc} ($°C/(W/cm^2)$)	R_{jc} ($°C/(W/cm^2)$)	T_j (°C)	T_w (°C)
20	0.25	0.25	90	80
40	0.25	0.25	90	70
60	0.25	0.25	90	60
80	0.25	0.25	90	50
100	0.25	0.25	90	40

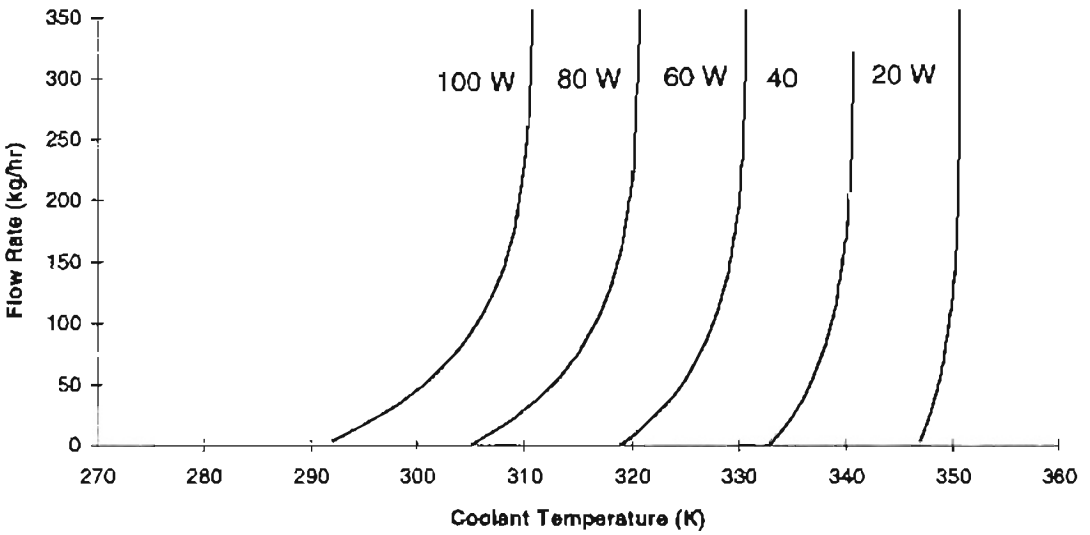

Figure 3.14. Thermal Performance as a Function of the Heat Load with Thermal Resistances of 0.15 °C/(W/cm²).

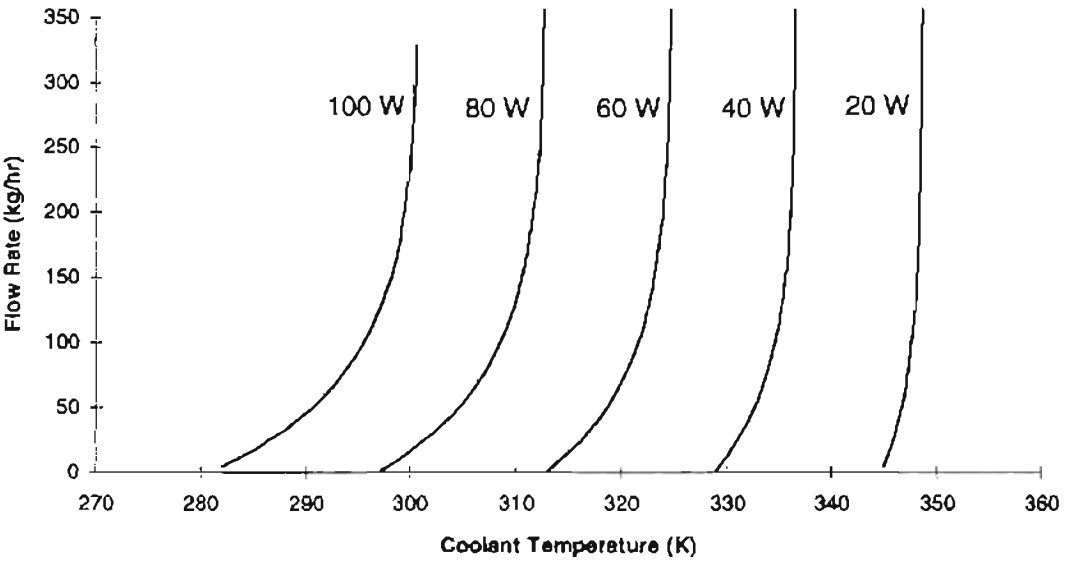

Figure 3.15. Thermal Performance as a Function of the Heat Load with Thermal Resistances of 0.2 °C/(W/cm²).

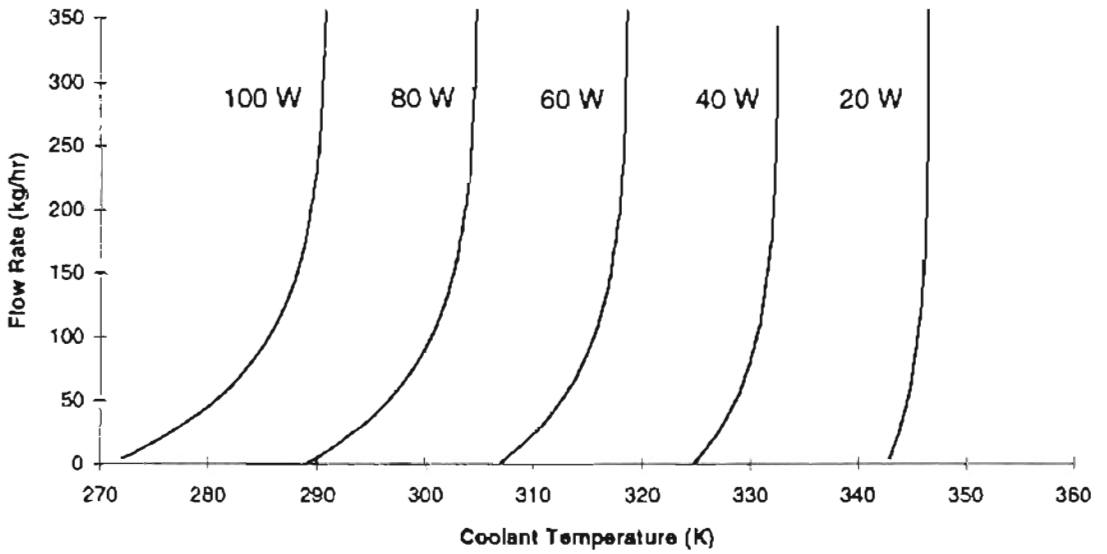

Figure 3.16. Thermal Performance as a Function of the Heat Load with Thermal Resistances of 0.25 °C/(W/cm^2).

These curves represent the minimum mass flow rate necessary to remove the inputted heat flux for an inputted coolant temperature. In addition, Figures 3.14 through 3.16, are for the required junction temperature of 90°C. As these plots show, for the lower heat loads (less than 20 W), the necessary mass flow rate is independent of the coolant temperature. For example, if the coolant temperature is below 348 K (75°C), then any flow rate through the HFHE is sufficient to remove a heat flux of 20 W/cm^2. However, as the heat load is increased, the necessary mass flow rate becomes dependent on the coolant temperature. For example, to remove a heat flux of 100 W/cm^2 with thermal resistances of 0.20 $°C/(W/cm^2)$, the minimum necessary mass flow rate is 150 kg/hr at a coolant temperature of 298 K (25°C). However, if the coolant temperature is reduced to 290 K (17°C), then the minimum necessary mass flow rate through the HFHE reduces to 50 kg/hr. Furthermore, if the coolant temperature is reduced below 281 K (8°C), then any mass flow rate through the HFHE will remove 100 W/cm^2.

3.2.7 Maximum Heat Flux Capability

The heat flux capability of the HFHE may be estimated by extrapolating the results from Equation (3.11) using the operating conditions specified by the Air Force. These operating conditions include a coolant temperature of 0°C and a pressure drop across the HFHE of 311 kPa (45 psi). Therefore, solving Equation (3.11) for the mass flow rate and substituting the operating condition values for the coolant temperature and the pressure drop across the HFHE yields a mass flow rate of 182 kg/hr. Using this value in the HFHE thermal resistance equation, Equation (3.22), the thermal resistance is then solved as a function of the heat flux. This equation can then be substituted into Equation (3.23), and solved for the heat flux, shown as Equation (3.25).

$$\dot{Q} = \frac{T_j - T_f - 2.25}{-\left(R_{cw} + R_{jc}\right) - 0.20 - 0.20e^{(-0.013\dot{m})}} \qquad (3.25)$$

The operating conditions for the HFHE are as follows: a junction temperature, T_j, of 363 K (90°C), a coolant temperature, T_f, of 273 K (0°C), thermal resistances, R_{cw} and R_{jc}, of 0.20 °C/(W/cm^2), and a mass flow rate, $\dot{m}$, of 182 kg/hr. With these inputs, the maximum heat flux capability of the HFHE is calculated to be 142.4 W/cm^2. However, this

maximum heat flux capability is not an absolute. The maximum heat flux is dependent on the operating coolant temperature and thermal resistances between the case and the junction and between the case and the wall. Therefore, the variation in the heat flux capability for the HFHE is shown in Table 3.4. As a note, for each new coolant temperature, the mass flow rate must be recalculated for the total pressure drop to remain constant at 45 psi (311 kPa). As can be seen, although a higher mass flow rate is possible at the higher coolant temperatures, the coolant temperature remains as the driving factor in the heat flux capability.

As can be seen from Table 3.4, if the refrigeration cycle for the avionic electronic system is capable of coolant temperature below 293 K (20°C) or if the thermal resistance between the junction and the wall of the HFHE can be maintained below 0.2 °C/(W/cm^2), then the HFHE's cooling capacity is well above the required 100 W/cm^2.

3.2.8 Steady-State Comparison

In the only previous study of the thermal performance, McDonnell Douglas [4] presented the thermal performance through plots of the thermal resistance for the HFHE and a maximum heat flux capability. Therefore, the final presentation of the thermal performance curves in this

Table 3.4 Maximum Heat Flux Capability.

Pressure Drop		Mass Flow Rate	Junction Temperature	Coolant Temperature	Thermal Resistance (junction to case)	Thermal Resistance (case to wall)	Maximum Heat Flux Capability
kPa	(psi)	kg/hr	K	K	°C/(W/cm^2)	°C/(W/cm^2)	W/cm^2
311	45	181.68	363	273	0.20	0.20	142.40
311	45	181.68	363	273	0.25	0.25	122.52
311	45	181.68	363	273	0.15	0.15	169.99
311	45	220.47	363	293	0.20	0.20	111.27
311	45	220.47	363	293	0.25	0.25	95.57
311	45	220.47	363	293	0.15	0.15	133.14

report are unique. Furthermore, it is impossible to compare the thermal resistance of the HFHE presented by McDonnell Douglas and the thermal resistance of the HFHE presented in this report. This is because the thermal resistance presented by McDonnell Douglas is only dependent on the flow rate. This conclusion for the thermal resistance was reached because McDonnell Douglas [4] performed a shotgun test matrix. This analysis with the shotgun approach is shown in Figure 3.17. This figure shows the correlation between conduction heat loss and the flow rate. For this correlation, McDonnell Douglas presents a linear curve dependent on only the flow rate. The data used in this analysis is shown in Table 3.5. In this table, McDonnell Douglas' CHIC site D corresponds to CHIC B, see Figure 1.1, evaluated in this report.

Furthermore, in this table, McDonnell Douglas used the volumetric flow rate for the variance in the flow rate. However, the volumetric flow rate does not reflect the change in density with the coolant temperature. Therefore, comparisons between the different temperatures cannot be made at the same volumetric flow rate. Therefore, the volumetric flow rate used by McDonnell Douglas has been converted into the mass flow rate used in this report. As stated previously, Figure 3.17 indicates a linear function

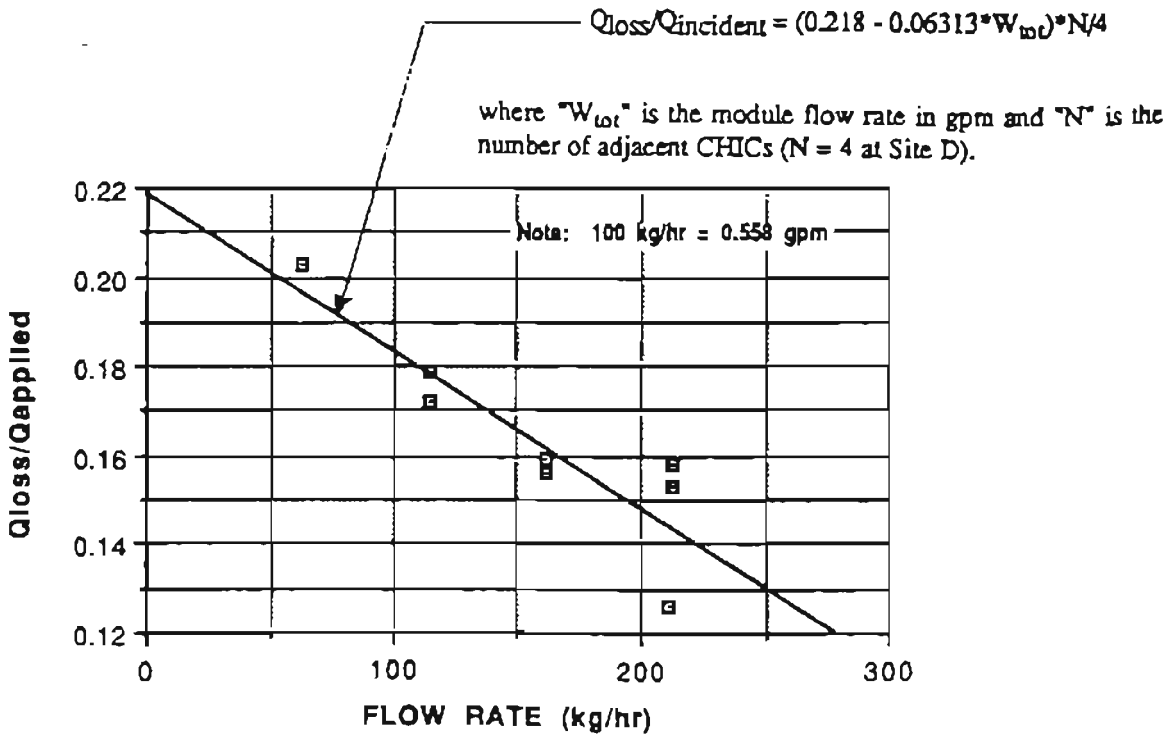

Figure 3.17. Correlation Between Conduction Heat Loss and Flow Rate [12].

Table 3.5. McDonnell Douglas' Approach for the Radial Heat Loss.

Test I.D.	CHIC Site	Coolant Temperature	Coolant Flow Rate		Amplifier Heat Flux
		°C	gpm	kg/min	W
86	D	18.80	1.18	3.56	118.94
83	D	20.24	1.19	3.58	101.00
81	D	20.25	1.19	3.58	82.13
78	D	20.25	0.90	2.71	79.41
80	D	20.53	0.90	2.71	79.92
76	D	19.87	0.64	1.93	76.83
60	D	20.01	0.64	1.93	45.47
74	D	20.36	0.35	1.05	78.73

dependent on only the flow rate; however, as shown in Figure 3.7, the heat loss due to conduction is also dependent on the coolant temperature. Moreover, as shown in Appendix F, the heat loss due to conduction is dependent on the coolant flow rate, the coolant temperature, and the heat load and this dependency is not a linear relationship.

In the shotgun test matrix used by McDonnell Douglas, only four flow rates were examined: 0.3 gal/min, 0.6 gal/min, 0.9 gal/min, and 1.2 gal/min. In addition, only two heat loads, 50 W/cm^2 and 100 W/cm^2, and four coolant temperatures, 10°C, 20°C, 30°C, and 40°C, were examined. However, in contrast to the research performed at Oklahoma State University, McDonnell Douglas did not fully represent the heat loads nor the coolant temperatures with all of the flow rates. Therefore, the interpretation of their results did not indicate a dependency of the thermal resistance on the heat load. Any variation in the thermal resistance with the heat load was explained due to the curve fit error.

Because all of the thermal performance characteristics of the HFHE, the radial heat loss due to conduction, the thermal resistance, and the temperature difference between the wall and the fluid temperatures, were considered as functions of only the flow rate by McDonnell Douglas, comparisons between their thermal results and the thermal

performance results presented in this thesis are impratical. Furthermore, McDonnell Douglas did not formulate any thermal performance curves or a thermal performance equation as seen in sections 3.2.4 through 3.2.6. Therefore, the only true comparison that can be made is the maximum heat flux capability of the HFHE. This "maximum" heat flux capability represents the operating conditions of the HFHE: a coolant temperature of 0°C, a pressure drop of 311 kPa (45 psi), and wall-to-case and case-to-junction thermal resistances of 0.2 °C/(W/cm^2). With these conditions McDonnell Douglas [4] derived a maximum heat flux of 134 W/cm^2. This compares to the maximum heat flux derived in section 3.2.6 of 142 W/cm^2. This translates to a 5.6% difference.

However, this relatively close comparison is misleading. For these operating conditions, McDonnell Douglas reported a correlation of a mass flow rate of 329 kg/hr and a wall-to-fluid thermal resistance of 0.270 °C/(W/cm^2). However, for the operating conditions of a pressure drop of 45 psi (311 kPa), a coolant temperature of 0°C, and an applied heat load of 100 W/cm^2, this report has a correlation of a mass flow rate of 182 kg/hr and a wall-to-fluid thermal resistance of 0.232 °C/(W/cm^2). These diversities can be explained by revisiting the previous sections of this report. First, the thermal resistance

performance results presented in this thesis are impratical. Furthermore, McDonnell Douglas did not formulate any thermal performance curves or a thermal performance equation as seen in sections 3.2.4 through 3.2.6. Therefore, the only true comparison that can be made is the maximum heat flux capability of the HFHE. This "maximum" heat flux capability represents the operating conditions of the HFHE: a coolant temperature of 0°C, a pressure drop of 311 kPa (45 psi), and wall-to-case and case-to-junction thermal resistances of 0.2 °C/(W/cm^2). With these conditions McDonnell Douglas [4] derived a maximum heat flux of 134 W/cm^2. This compares to the maximum heat flux derived in section 3.2.6 of 142 W/cm^2. This translates to a 5.6% difference.

However, this relatively close comparison is misleading. For these operating conditions, McDonnell Douglas reported a correlation of a mass flow rate of 329 kg/hr and a wall-to-fluid thermal resistance of 0.270 °C/(W/cm^2). However, for the operating conditions of a pressure drop of 45 psi (311 kPa), a coolant temperature of 0°C, and an applied heat load of 100 W/cm^2, this report has a correlation of a mass flow rate of 182 kg/hr and a wall-to-fluid thermal resistance of 0.232 °C/(W/cm^2). These diversities can be explained by revisiting the previous sections of this report. First, the thermal resistance

calculated by McDonnell Douglas is based on a linear function dependent on only the mass flow rate. However, as expained earlier in this section, the thermal resistance is not a linear function, nor is it solely dependent on the mass flow rate. Moreover, the thermal resistance is a function of the flow rate, coolant temperature, and heat load of the HFHE. Finally, the corresponding mass flow rate for the operating pressure of 311 kPa (45 psi), relates to the hydraulic performance curves obtained in section one of this chapter. McDonnell Douglas proclaims that for a mass flow rate of 329 kg/hr and a coolant temperature of 0°C, the pressure drop across the HFHE is 311 kPa (45 psi). However, as stated in Flynn et al. [4], this pressure drop across the HFHE is lower than the predicted value by Sundstrand. However, as explained in section 3.1.4, for a laminar flow regime the pressure drop across the HFHE should be greater than the pressure drop for a turbulent flow regime that is used as the analytical model used for Sundstrand's predictions. This concept is consistent with the results that at a flow rate of 182 kg/hr and a coolant temperature of 0°C, the pressure drop across the HFHE is 311 kPa (45 psi). McDonnell Douglas' hydraulic results used for their maximum heat flux calculation are not consistent with this concept.

3.3 Transient Thermal Performance

While the in-flight performance was modeled with steady state heat loads, the start-up and shut-down performance for the HFHE was modeled with transient heat loads. This performance is presented in the thesis by analyzing the thermal lag of the HFHE as a function of the coolant temperature, mass flow rate, and heat load. Furthermore, the thermal lag is performed by analyzing the HFHE wall temperature.

For the transient tests, the coolant temperature range was reduced to 0°C to 30°C, but still with increments of 10°C. This reduction is valid because the criterion used for analyzing the transient thermal performance, this being the wall temperature of the HFHE, is independent of the coolant temperature. However, as the coolant temperature increases so does the initial wall temperature before a heat load is applied. Therefore, for comparison between different coolant temperatures, the wall temperature must be modified. This modification consists of taking the difference between the wall temperature and the coolant temperature. This is shown in Figures 3.18 and 3.19, for the start-up model and the shut-down model, respectively. Finally, Figures 3.18 and 3.19 are for a mass flow rate of

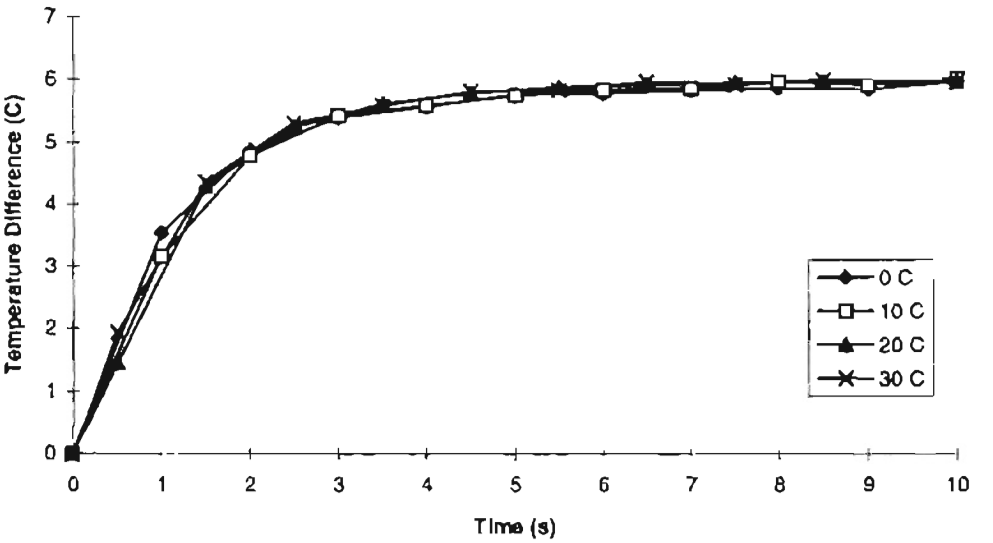

Figure 3.18. Thermal Lag of the HFHE During Startup as a Function of Coolant Temperature (2.5 kg/min, 20 W).

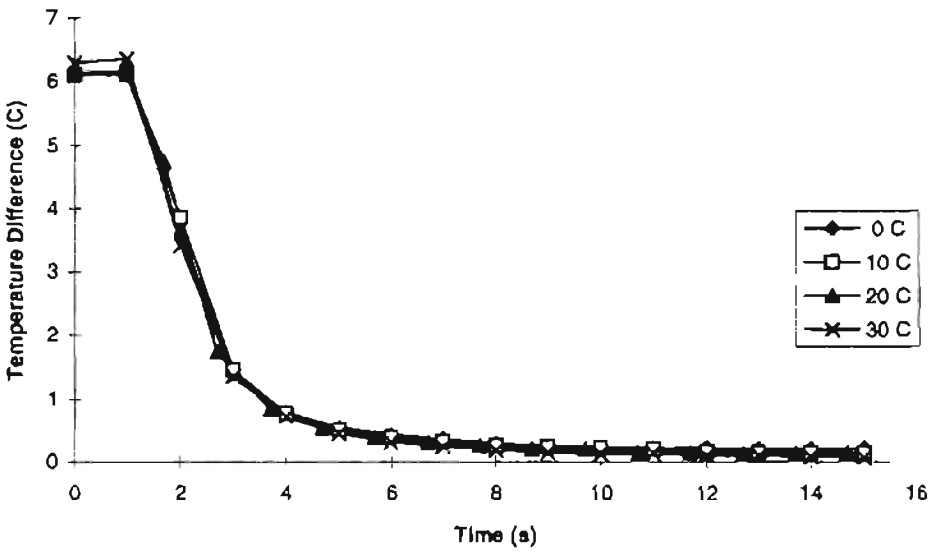

Figure 3.19. Thermal Lag of the HFHE during Shutdown as a Function of Coolant Temperature (2.5 kg/min, 20 W).

2.5 kg/min, and a heat load of 20 W. In addition, the flow rate data points were the same as the flow rate data points for the last three CHICs (for example: 1.0, 1.5, 2.0, 2.5, and 3.0 kg/min for a coolant temperature of 0°C), and the heat load range was reduced to 10 W to 50 W by an increment of 10 W. This reduction of the heat load was due to the upper thermal restrictions of the MiniSystems ceramic heater. The results of the transient tests are presented into two main categories, the start-up and the shut-down models.

3.3.1 Performance During Start-Up

The emphasis of this study on the start-up performance of the HFHE regards the relationship of the thermal lag and the dependent parameters: the mass flow rate, the coolant temperature, and the heat load. However, as Figures 3.18 and 3.19 show, the thermal lag is independent of the coolant temperature. As stated in Chapter II, the start-up performance was obtained by a thermal pulse for thirty seconds, or until thermal equilibrium has been reached. This pulse provides an instantaneous heat flux for the required test load. The thermal lag was then taken as the amount of time necessary for the wall temperatures to reach thermal equilibrium. Figures 3.20 through 3.24 show the

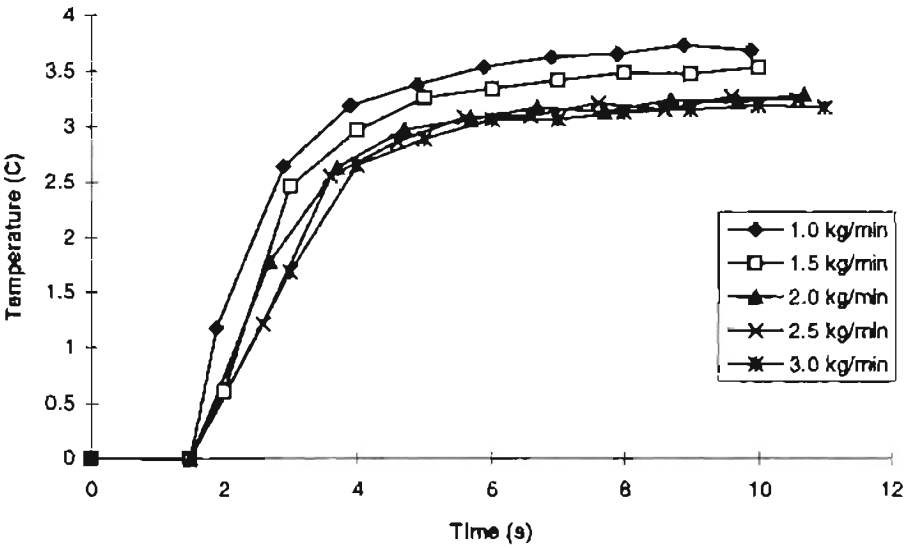

Figure 3.20. Thermal Lag during Startup for a Heat Load of 10 W and Coolant Temperature of 0°C.

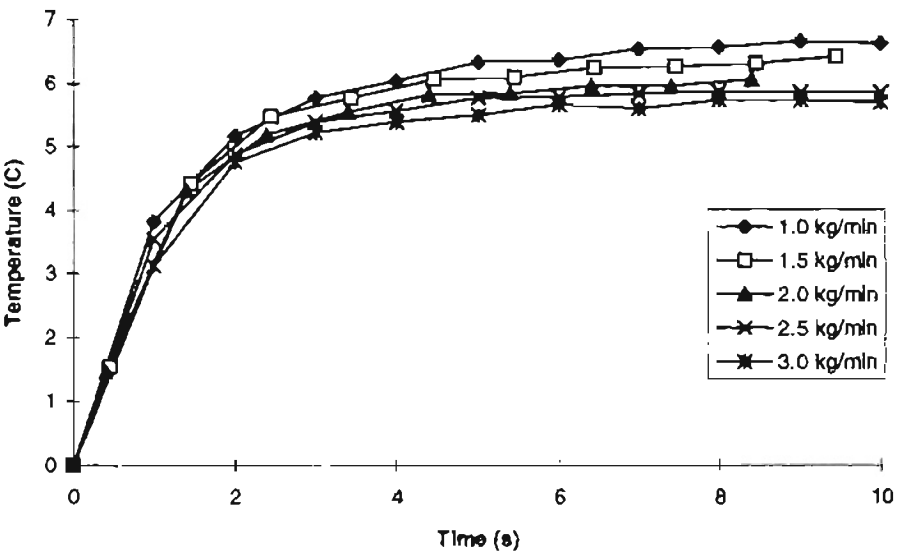

Figure 3.21. Thermal Lag during Startup for a Heat Load of 20 W and Coolant Temperature of 0°C.

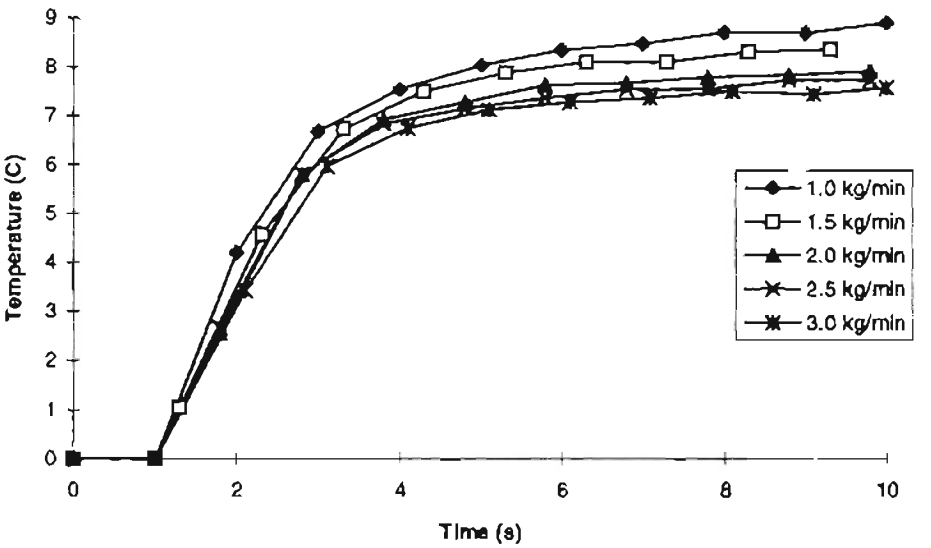

Figure 3.22. Thermal Lag during Startup for a Heat Load of 30 W and Coolant Temperature of 0°C.

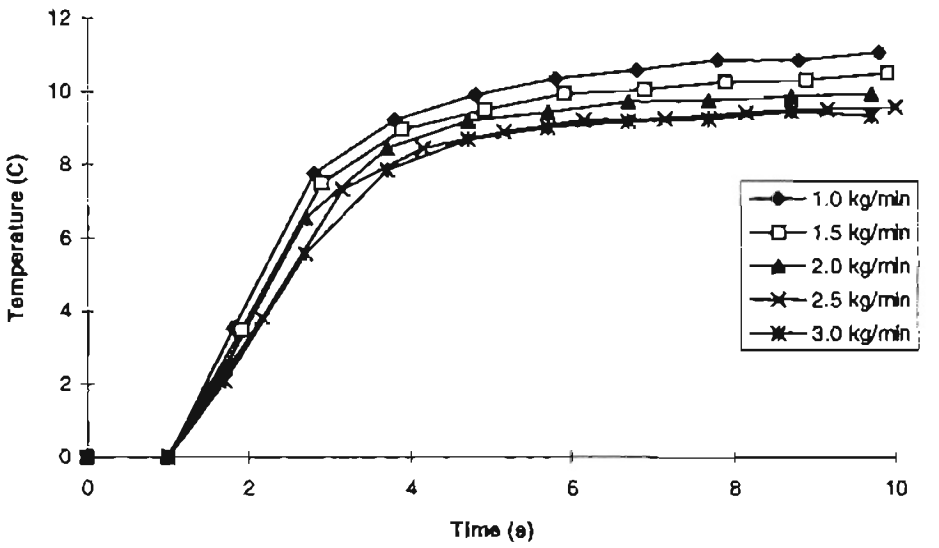

Figure 3.23. Thermal Lag during Startup for a Heat Load of 40 W and Coolant Temperature of 0°C.

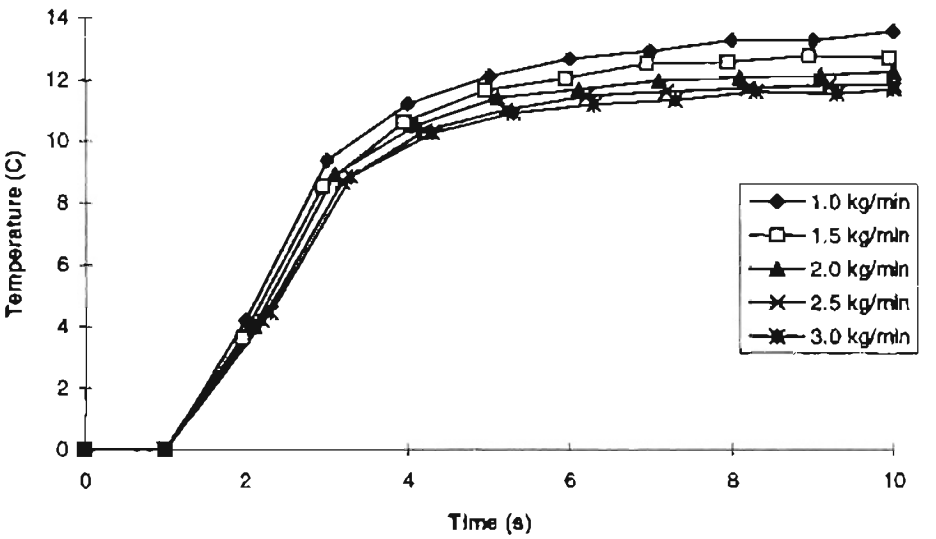

Figure 3.24. Thermal Lag during Startup for a Heat Load of 50 W and Coolant Temperature of 0°C.

thermal lag as a function of the mass flow rate. For each of these figures, the coolant temperature was 0°C.

As seen in the above figures, the time for the wall temperature to reach 90% of the thermal equilibrium temperature varies with both the mass flow rate and the heat load. The dependence of the lag time on these parameters are summarized in Table 3.6. As this table indicates, the trends are as follows: as the flow rate is increased, the thermal lag is decreased and as the heat load is increased, the thermal lag is increased. The minimum thermal lag is approximately 2.6 seconds and occurs at a flow rate of 3.0 kg/min and a heat load of 10 W. The maximum thermal lag is approximately 4.25 seconds and occurs at a flow rate of 1.0 kg/min and a heat load of 50 W. However, these results were expected, for as the flow rate is decreased and the heat load is increased, the temperature differential between the coolant temperature and the wall temperature, for steady-state conditions, increases. Therefore, for a constant coolant temperature, the wall temperature increases as the flow rate is decreased and the heat load is increased. Hence, the time to reach the elevated temperatures should increase as shown. The thermal performance during startup is also presented as a function of the heat load in Figures 3.25 through 3.29.

Table 3.6. Thermal Lag as a Function of the Heat Load a nd Mass Flow Rate for a Coolant Temperature of 0°C

Flow Rate	1.0 kg/min	1.5 kg/min	2.0 kg/min	2.5 kg/min	3.0 kg/min
Heat Load	Thermal Lag Time				
10 W	3.65 s	3.25 s	3.05 s	2.75 s	2.60 s
20 W	4.00 s	3.40 s	3.20 s	3.00 s	2.85 s
30 W	4.10 s	3.55 s	3.35 s	3.25 s	3.15 s
40 W	4.20 s	3.80 s	3.50 s	3.35 s	3.25 s
50 W	4.25 s	3.90 s	3.65 s	3.50 s	3.40 s

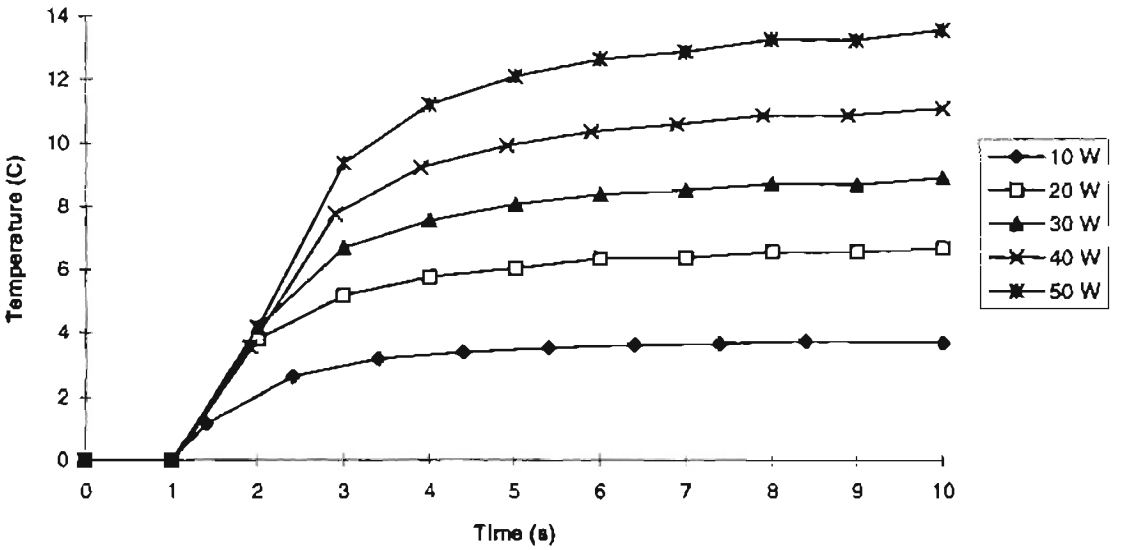

Figure 3.25. Thermal Lag during Startup for a Flow Rate of 1.0 kg/min and Coolant Temperature of 0°C.

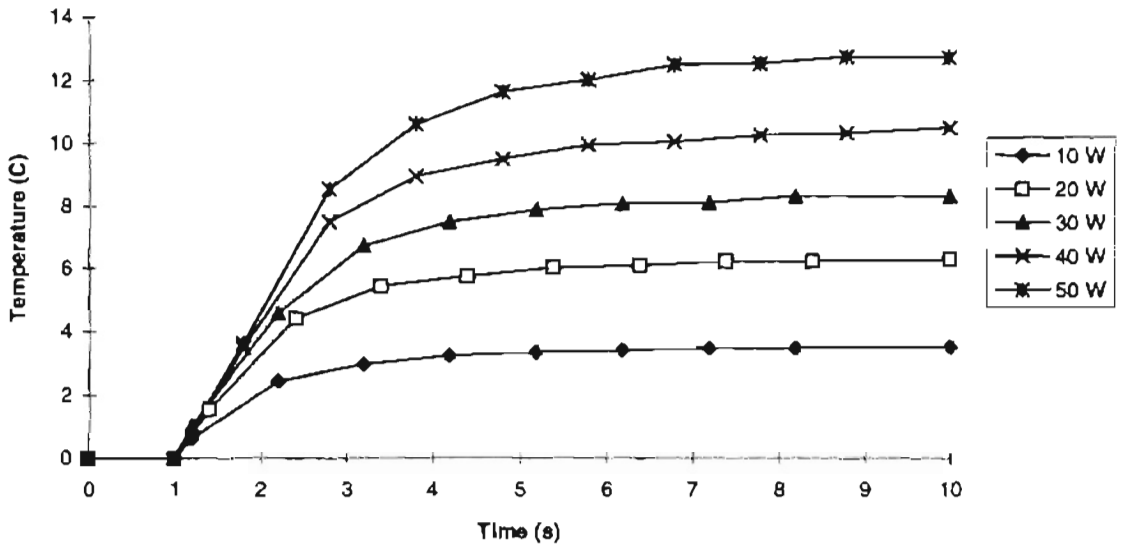

Figure 3.26. Thermal Lag during Startup for a Flow Rate of 1.5 kg/min and Coolant Temperature of 0°C.

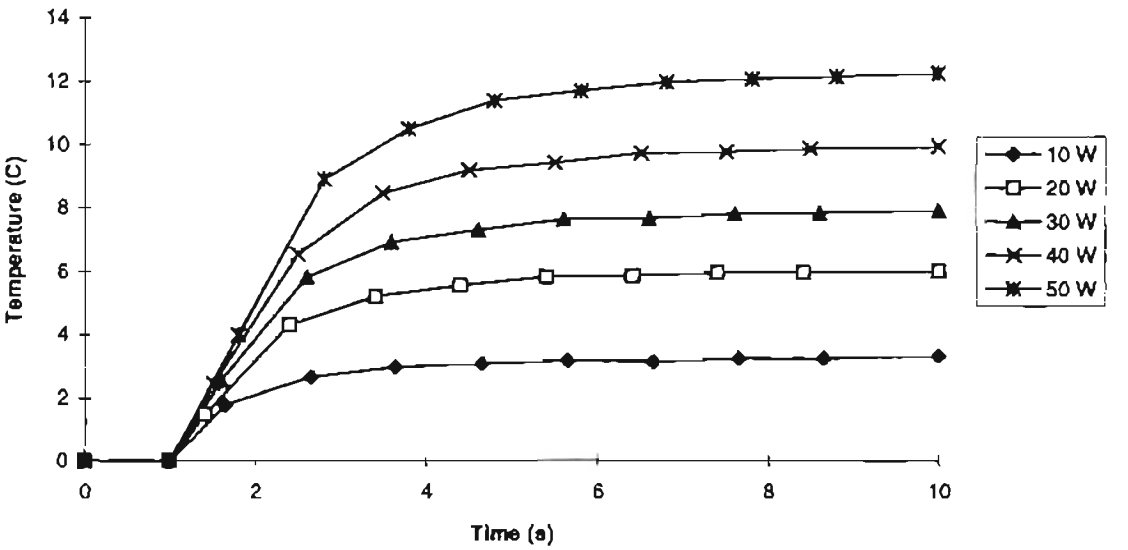

Figure 3.27. Thermal Lag during Startup for a Flow Rate of 2.0 kg/min and Coolant Temperature of 0°C.

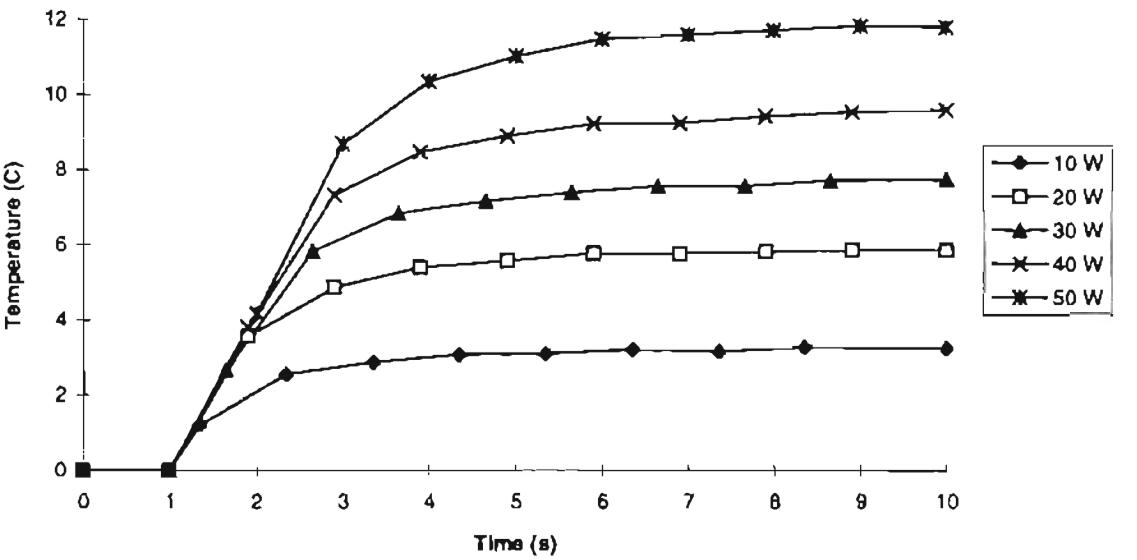

Figure 3.28. Thermal Lag during Startup for a Flow Rate of 2.5 kg/min and Coolant Temperature of 0°C.

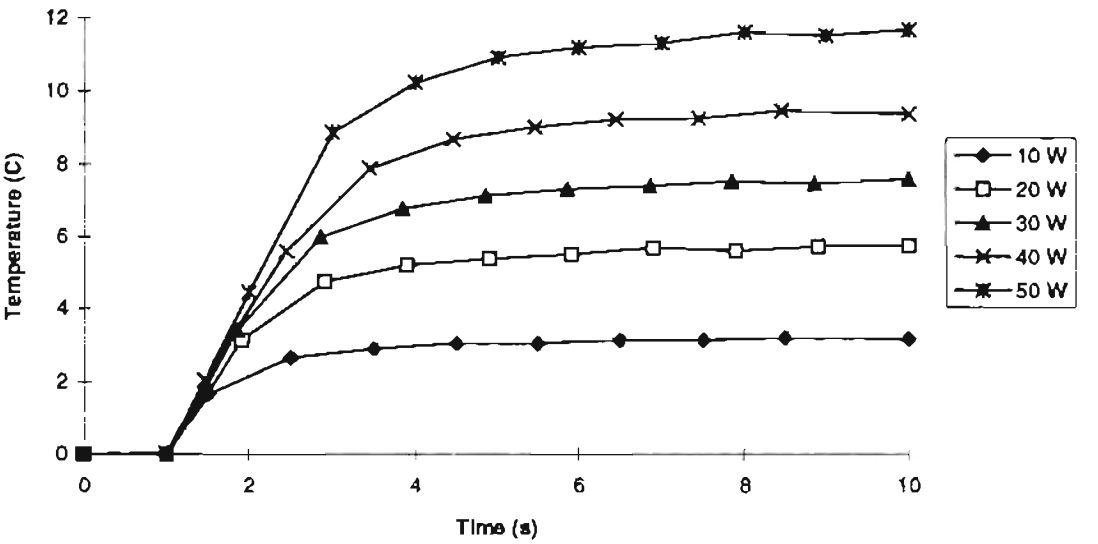

Figure 3.29. Thermal Lag during Startup for a Flow Rate of 3.0 kg/min and Coolant Temperature of 0°C.

3.3.2 Performance During Shutdown

The modeling of the thermal performance during the shutdown stage was accomplished by allowing the wall temperature to reach thermal steady-state at a given heat load, then turning off the power to the MiniSystems ceramic heater. This provides an abrupt end to the heat load pulse. The ranges for the shutdown modeling are retained from the startup modeling, and the time interval is thirty seconds, or until the wall temperature reaches thermal equilibrium. In addition, the presentation of the results for this modeling is retained from the modeling of the startup. The thermal lag is presented as functions of both the mass flow rate and the heat load. However, for this thesis the presentation of these results are condensed to only the extreme cases of the heat loads and mass flow rate, for a coolant temperature of 0°C. This condensed version can be seen in Figures 3.30 and 3.31 for the thermal lag as a function of the flow rate, and in Figures 3.32 and 3.33 for the thermal lag as a function of the heat load. As before, the trend for the thermal lag is as follows: the thermal lag time increases as the flow rate decreases and the heat load increases. The entire spectrum for the thermal lag times are presented in Table 3.7.

3.3.2 Performance During Shutdown

The modeling of the thermal performance during the shutdown stage was accomplished by allowing the wall temperature to reach thermal steady-state at a given heat load, then turning off the power to the MiniSystems ceramic heater. This provides an abrupt end to the heat load pulse. The ranges for the shutdown modeling are retained from the startup modeling, and the time interval is thirty seconds, or until the wall temperature reaches thermal equilibrium. In addition, the presentation of the results for this modeling is retained from the modeling of the startup. The thermal lag is presented as functions of both the mass flow rate and the heat load. However, for this thesis the presentation of these results are condensed to only the extreme cases of the heat loads and mass flow rate, for a coolant temperature of 0°C. This condensed version can be seen in Figures 3.30 and 3.31 for the thermal lag as a function of the flow rate, and in Figures 3.32 and 3.33 for the thermal lag as a function of the heat load. As before, the trend for the thermal lag is as follows: the thermal lag time increases as the flow rate decreases and the heat load increases. The entire spectrum for the thermal lag times are presented in Table 3.7.

Table 3.7. Thermal Lag Times During Shutdown for a Coolant Temperature of 0°C.

Flow Rate	1.0 kg/min	1.5 kg/min	2.0 kg/min	2.5 kg/min	3.0 kg/min
Heat Load	Thermal Lag Time				
10 W	3.90 s	3.80 s	3.70 s	3.65 s	3.60 s
20 W	4.20 s	4.00 s	3.90 s	3.80 s	3.75 s
30 W	4.50 s	4.20 s	4.05 s	3.95 s	3.90 s
40 W	4.60 s	4.40 s	4.20 s	4.10 s	4.00 s
50 W	4.70 s	4.50 s	4.35 s	4.25 s	4.20 s

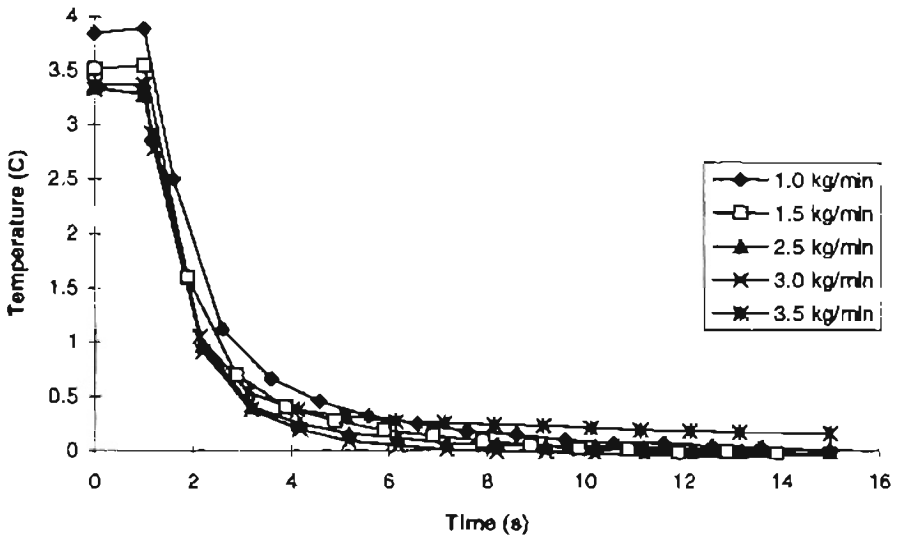

Figure 3.30. Thermal Lag during Shutdown for a Heat Load of 10 W and Coolant Temperature of 0°C.

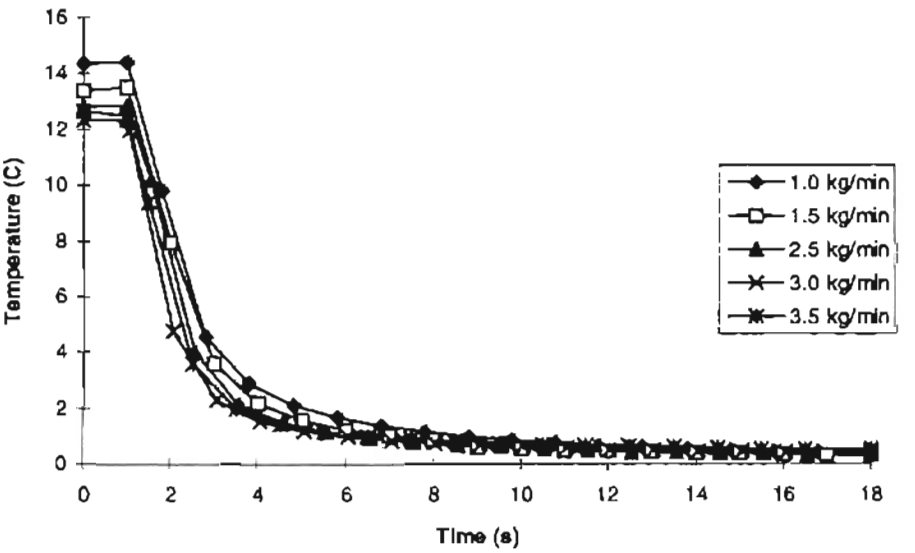

Figure 3.31. Thermal Lag during Shutdown for a Heat Load of 20 W and Coolant Temperature of 0°C.

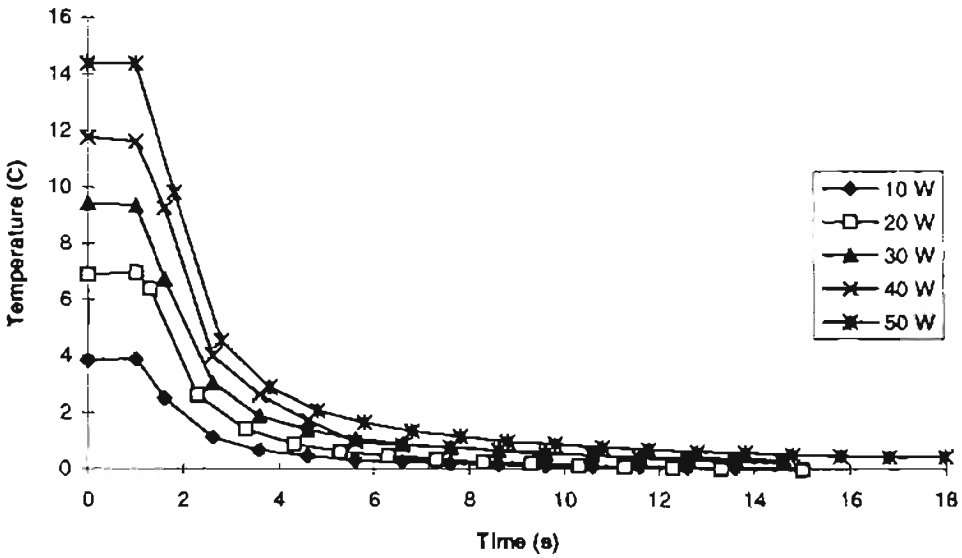

Figure 3.32. Thermal Lag during Shutdown for a Flow Rate of 1.0 kg/min and Coolant Temperature of 0°C.

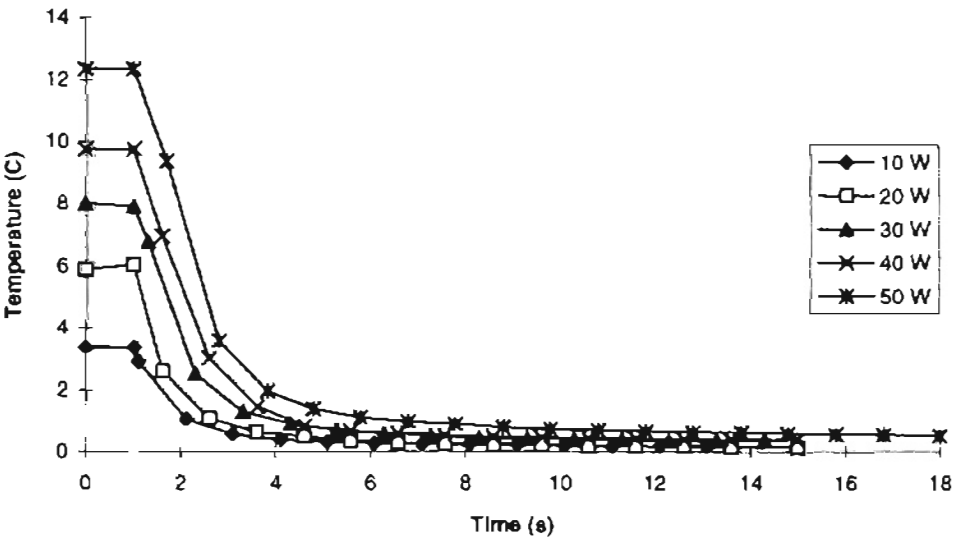

Figure 3.33. Thermal Lag during Shutdown for a Flow Rate of 3.0 kg/min and Coolant Temperature of 0°C.

3.3.3 Maximum Thermal Lag Times

As seen in Table 3.6, the maximum thermal lag time during startup approaches 4.5 seconds. In addition as seen in Table 3.7, the maximum thermal lag time during shutdown approaches 5.0 seconds. If these values were extrapolated to a heat load of 100 W and allowing for a margin of error, the maximum thermal lag time for the startup is approximately 6.0 seconds. In addition, the maximum thermal lag time during shutdown for a heat load of 100 W is approximately 7.0 seconds

3.3.4 Transient Performance Comparison

As the steady-state thermal tests, the only prior analysis of the transient thermal performance of the HFHE was conducted by McDonnell Douglas. For this analysis, three types of transient tests were conducted: a slow ramp to steady-state conditions, full transient testing using a slow ramp, and full transient testing using a fast ramp. However, as stated in the report by Flynn, et al. [4], none of these tests represent a transient load of any specific device. Furthermore, the results presented by McDonnell Douglas focus on both the wall temperature and the heater temperature. However, the heater temperature is dependent on the thermal resistance between the wall and the junction

(in this case, the thermal resistance of the thermal grease between the heater and the HFHE and the thermal resistance of the heater itself). Therefore, the only temperature worth noting is the wall temperature of the HFHE, as presented in this thesis. Furthermore, the abrupt pulsing of the heat load used in this thesis does reflect an actual physical characteristic. This pulsing represents the startup and shutdown of the electronic devices being cooled by the HFHE. Furthermore, the pulsing allows for all of the transient tests to approach a steady-state condition. This follows the reasoning that at startup or shutdown the electronic devices will run or remain off for a considerable length of time producing a steady-state situation. The conclusion made by McDonnell Douglas about the transient tests that "the wall temperature under the condition of increasing heat flux should always be lower than that expected under steady-state conditions" is valid. However, the addition that the wall temperature under the increasing heat flux approaches the steady-state condition should be made.

For both McDonnell Douglas and this thesis, a note should be made that the maximum thermal lag time will vary depending on the thermal resistance of the thermal grease and heat source. Because McDonnell Douglas and this

research used MiniSystems ceramic heaters, the thermal resistance of the heat source should be similar. This allows for comparison between the results.

CHAPTER IV

SUMMARY AND CONCLUSIONS

4.1 Conclusions

The goals of this thesis as set forth in Chapter 1 were successfully achieved. Construction of a versatile setup was completed, the hydraulic, steady-state thermal, and transient thermal performance of the High Flux Heat Exchanger were studied, a complete data base for all types of performance was assimilated, and performance curves encompassing all of the tests were developed. In this chapter, the accomplishment of the primary objectives set forth in Chapter I will be presented.

4.1.1 Experimental Apparatus

Although most of the components in the test loop have been on loan from Wright Laboratories, the setup design itself can be used for future testing of new heat exchangers that meet the SEM-E configuration. Furthermore, the experimental procedure outlined in Chapter II represents a

solid foundation for future experimentation on any high flux heat exchanger.

4.1.2 Hydraulic Performance

The primary objective for the hydraulic performance was stated as follows: to investigate the influence of the coolant flow rate and temperature on the pressure drop across the inlet and the outlet of the HFHE. In addition, this investigation should result in a hydraulic performance equation and corresponding performance curve with the flow rate and temperature as the dependent variables.

The investigation of the pressure drop across the inlet and outlet of the HFHE was completed for a coolant temperature range of -15°C to 50°C. Furthermore, for each coolant temperature, the investigation covered a flow rate range of 60 kg/hr to 240 kg/hr. This analysis culminated in the development of the hydraulic performance equation. The model for the hydraulic performance equates the pressure drop across the HFHE to the sum of the viscous-frictional losses and the dynamic losses. The following performance equation consists of the mass flow rate, kg/hr, and the coolant temperature, K, as the inputs and yield the pressure drop in psi. The constants C_1, viscous-frictional losses,

and C_2, dynamic losses, have values of 7354.83 and 0.428, respectively. The corresponding curve for this equation can be seen in section 3.1.2.

$$\Delta p = C_1\left[\left(10^{\left(\frac{10^{9.67}}{T^{3.933}}\right)} - 0.70\right)\times 10^{-6}\right]\dot{m} + C_2\frac{\dot{m}^2}{\left(1.36\times 10^3 - 4.56T + 0.0157T^2 - 0.28\times 10^{-4}T^3 + 0.174\times 10^{-7}T^4\right)} \quad (3.11)$$

4.1.2 Steady-State Thermal Performance

The objectives set forth in Chapter I for the steady-state thermal tests was to investigate the influence of the coolant flow rate and temperature on the heat flux removal capabilities of the HFHE for steady-state heat loads. This investigation should result in a thermal performance curve and correlating equation for the necessary coolant flow rate with respect to the coolant temperature to achieve a given amount of heat flux removal (e.g. one performance curve for 100 Watts of heat flux removal, one performance curve for 80 Watts of heat flux removal, etc.). However, to accomplish this investigation, several thermal characteristics of the HFHE were necessary. The characteristics included the conducted radial heat loss, the wall temperature at the

surface of each CHIC, and the thermal resistance of the HFHE.

The simplification of applying a heat load to one CHIC at a time is valid under the assumption that all twenty CHICs perform identically and independently. However, this simplification causes an error in the net heat flux measurement through the CHIC. This error occurs as a portion of the heat flux is removed radially by the surrounding CHICs. Therefore an analytical expression was developed for the radial heat loss due to conduction. This heat loss is presented as a ratio of the heat loss per heat load and is equivalent to an exponential decay, dependent on the coolant temperature, the heat load applied, and the mass flow rate. The equation for the heat loss, at a constant heat flux is given by the following equation. The coefficients for this equation are shown in Appendix F, for each heat load examined.

$$\frac{\dot{Q}_{loss}}{\dot{Q}_{applied}} = \phi_1 + \left(\phi_2 + \phi_3 e^{(\phi_4 T)}\right) e^{\left(\left(\phi_5 + \phi_6 e^{(\phi_7 T)}\right)\dot{m}\right)} \qquad (3.18)$$

The next thermal characteristic of the HFHE is the wall temperature at the surface of the individual CHIC. This equation is derived by the use of the measured wall

temperature and the net heat flux through the HFHE derived from Equation (3.18). However, for the use of the wall temperature equation under normal heat load conditions (heat loads applied to all 20 CHICs at once), the applied heat load is used. This is due to the fact that the applied heat load is equivalent to the net heat load under normal heat load conditions. The wall temperature, °C, is equivalent to the sum of the fluid temperature, °C, and an exponential decay that is a function of the mass flow rate, kg/hr, and the applied heat load, W, shown in Equation (3.20).

$$T_w - T_f = \lambda_0 + \left(\lambda_1 + \lambda_2 e^{(\lambda_3 \dot{m})}\right)\dot{Q} \qquad (3.20)$$

For this equation the coefficients are as follows: λ_0 (2.25), λ_1 (0.19779), λ_2 (0.19968), and λ_3 (-0.013115). These coefficients are valid for all of the mass flow rates, coolant temperatures, and applied heat loads. The last thermal characteristic of the HFHE is its thermal resistance. This equation is developed by equating the thermal resistance, °C/(W/cm^2), to the difference between the wall temperature, °C, and the coolant temperature, °C, divided by the applied heat load, W.

$$R_{wf} = \frac{2.25 + \left(0.20 + 0.20e^{(-0.013\dot{m})}\right)\dot{Q}}{\dot{Q}} \qquad (3.22)$$

Using the thermal resistance equation, the steady-state thermal performance equation was developed. This equation indicates that the mass flow rate, $\dot{m}$ (kg/hr), is a logarithmic function of the wall-to-case thermal resistance, R_{cw} (°C/(W/cm^2)), case-to-junction thermal resistance, R_{jc} (°C/(W/cm^2)), applied heat load, $\dot{Q}$ (W), junction temperature, T_j (K), and coolant temperature, T_f (K).

$$\dot{m} = -76.24 \ln\left[5.01\left(\frac{-R_{cw}\dot{Q} - R_{jc}\dot{Q} - 2.25 - 0.20\dot{Q} + T_j - T_f}{\dot{Q}}\right)\right] \qquad (3.24)$$

This equation represents the *minimum* mass flow rate required to remove the given applied heat load. However, because this equation does not register the impossibility of negative flow rates, the following logical statement must be included.

$$IF\ \dot{m}_{measured} \le 0.0:\quad THEN\ \dot{m}_{actual} = 0.0$$
$$ELSE\ \dot{m}_{actual} = \dot{m}_{measured}$$

The steady-state thermal test investigation was completed with the presentation of the steady-state performance curves, shown in section 3.2.6.

4.1.4 Transient Thermal Performance

The third objective of this research was to investigate the influence of the coolant flow rate and temperature on the heat flux removal capabilities of the HFHE for transient heat loads. This investigation should result in graphical presentation of the thermal lag of the HFHE. This presentation was for the startup and shutdown conditions of the HFHE. Through this investigation, it was determined that the thermal lag of the HFHE was dependent on the heat load applied and the mass flow rate. However, the thermal lag of the HFHE is independent of the coolant temperature. Moreover, as the figures in section 3.3 indicate, the thermal lag increases as the mass flow rate decreases and the applied heat load increases.

4.1.5 Overall Performance

The last objective of this research was to develop a guideline for the overall performance of the HFHE. This consisted of a performance chart and correlating equation

combining the hydraulic performance and the steady-state performance curves. The completion of this objective can be seen in Figures 4.1 and 4.2. However, another prime directive of the overall performance not included in this objective is the determination of the input parameter that drives the HFHE performance.

As seen in Figure 3.12, the critical parameter for the performance of the HFHE is the coolant temperature. If the coolant temperature is kept below 20°C, then the corresponding minimum flow rate for a cooling rate of 100 W per CHIC can be kept under 70 kg/hr. To further show the importance of the coolant temperature on the performance of the HFHE, Equation (3.24), the mass flow rate as a function of the coolant temperature for an applied heat load of 100 W per CHIC, was substituted into Equation (3.11), the pressure drop as a function of the flow rate and the coolant temperature. The result is an equation for the pressure drop as a function of the coolant temperature for an applied heat load of 100 W per CHIC. This result is shown in Figure 4.1, and, as expressed earlier, if the coolant temperature can be kept below 20°C, then the minimum pressure drop across the HFHE needed for a cooling rate of 100 W per CHIC is 7.2 psi. However, the pressure drop in this equation is the dynamic pressure drop only. As expressed in the

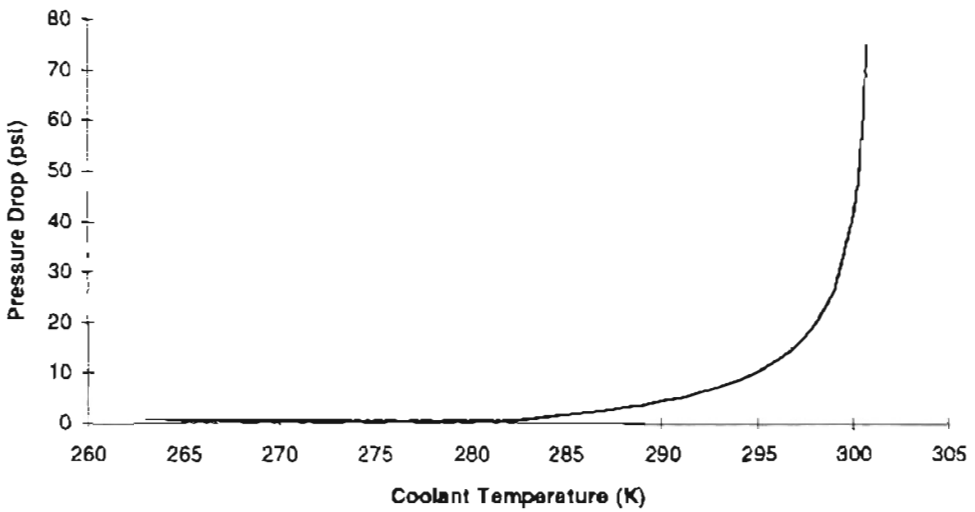

Figure 4.1. Dynamic Hydraulic Performance Curve for the Minimum Cooling Rate of 100 W per CHIC.

hydraulic section of this report, as the fluid temperature decreases below 18°C, the viscosity of the fluid begins to increase exponentially. Therefore, as the coolant flow rate reaches extremely low values, <0.5 kg/hr, the Reynolds' number approaches zero. This caused the friction factor, which is inversely proportional to the flow rate, to become very large. Therefore, the pressure drop needed to initiate the flow through the HFHE will be substantially larger than the dynamic pressure drop across the HFHE when the coolant temperature is below 0°C. Hence, it is critical that the inlet temperature remain between 0°C and 20°C. In a practical sense, this can be accomplished by placing a temperature sensor in the actual electronic coolant loop. This sensor should trigger a secondary refrigeration/heater unit to maintain the coolant temperature between 0°C and 20°C. In addition, a control device should be included in the electronic coolant loop to control the flow rate as the coolant temperature varies. Finally, if the above conditions are met, a pump for the electronic coolant loop can be sized by the performance curve pressure and the pressure drop through the rest of the coolant loop.

However, the requirement for 100 W/cm^2 of heat flux removal represents future possibilities for electronic devices. Modern electronic devices operate at lower

temperatures and need lower heat flux removal than future expectations. Therefore, for a complete analysis of the HFHE, the overall performance curves were plotted for the complete range of heat loads, and is shown in Figure 4.2.

The curves represent the minimum pressure drop across the HFHE necessary for the removal of the correlating heat flux. However, these curves represent the dynamic pressure drop. Therefore, the pressure drop needed to initiate the flow might be slightly higher.

4.2 Summation

As alluded in section one of this chapter, the results of this analysis on the HFHE differ from previous experimentation. The results from this analysis are far more detailed and includes wider parameter ranges and more internal data points. In addition, for the final correlations, an increased number of dependent variables have been investigated than the previous documentations. However, the discrepencies are consistent with the factors introduced in Chapter III, a laminar flow regime instead of a turbulent flow regime and McDonnell Douglas' simplifications in the modeling of the thermal resistance of the HFHE. Because of all of these factors, it is believed that these results retained in this independent research contains more accuracy than the aforementioned results.

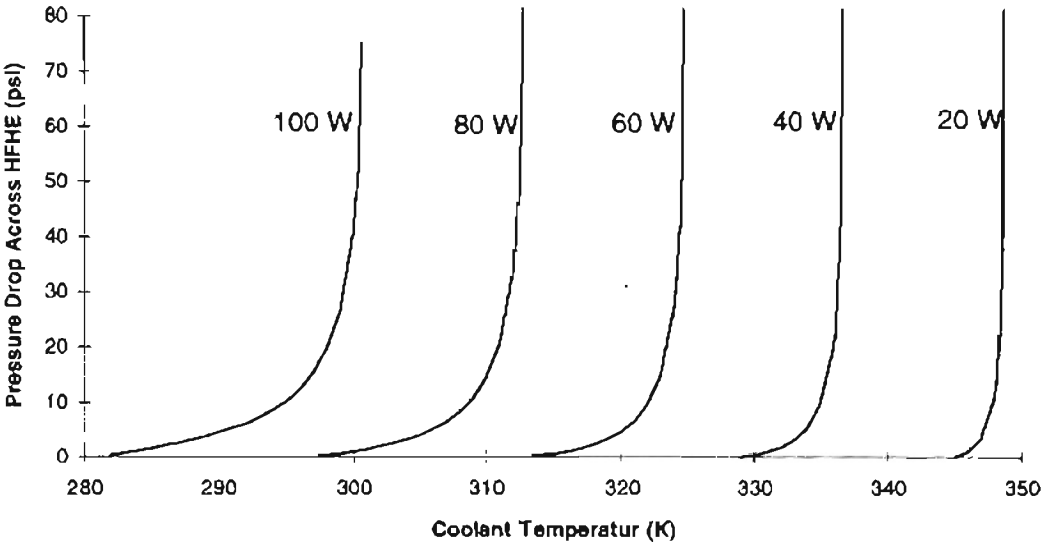

Figure 4.2. Performance Curves with Thermal Resistances of 0.2 °C/(W/cm²).

REFERENCES

1. Mackowski, M. J., "Requirements for High Flux Cooling of Future Avionics Systems," SAE Paper No. 912104, September 1991.

2. Flynn, E. M., "Evaluation of Cooling Concepts for High Power Avionics Applications," SAE Paper No. 921942, October 1992.

3. Bland, T. J., Niggemann, R. E., and Parekh, M. B., "A Compact High Intensity Cooler (CHIC)," SAE Paper No. 831127, July 1983.

4. Flynn, E. M., Downing, R. S., and Nguyen, D. C., "High Flux Heat Exchanger," Wright Laboratory Final Report No. WL-TR-94-2043, February 1994.

5. Bland, T. J., Ciaccio, M. P., Downing, R. S., and Smith, W.G., "The Development of Advanced Cooling Methods for High-Power Electronics," SAE Paper No. 901962, October 1990.

6. Grote, M. G., Hendron, R. E., Kipp, H. W., and Lapinski, J. R., "Test Results of Wafer Thin Coolers at Heat Fluxes from 5 to 125 W/cm^2," SAE Paper No. 880997, July 1988.

7. Flynn, E. M., and Mackowski, M. J., "High Flux Heat Exchanger," Wright Laboratory Interim Report No. WL-TR-93-2027, January 1993.

8. Gschwender, L. J., Snyder, C. E., and Conte, A. A., "Polyalphaolefins as Candidate Replacements for Silicate Ester Dielectric Coolants in Military Applications," Lubrication Engineering Journal, Vol. 41, No. 4, pp. 221-228, April 1985.

9. Zoppoth, R. C., and Dillard, J., "PAO Report: Extended Testing of Polyalphaolefins as a Dielectric/Coolant Fluid," Texas Instruments, Defense Systems and Electronics Group, Dallas, Tx, July 1988.

10. Ghajar, A. J., "Comparison of Hydraulic and Thermal Performances of PAO and Coolanol 25R Liquid Coolants," Final Report, Summer Faculty Research Program, Wright Laboratory, August 1993.

11. Flynn, E.M., Personal Communication, Summer 1994.

12. Granger, R. A., Fluid Mechanics. CBS College Publishing, New York, 1985.

13. Ghajar, A. J., Tang, W. C., and Beam, J. E., "Methodology for Comparison of Hydraulic and Thermal Performance of Alternative Heat Transfer Fluids in Complex Systems," Heat Transfer Engineering, Vol. 16, No. 1, pp. 68-72, 1995.

APPENDICES

APPENDIX A

DATA MEASUREMENTS

Because of fluctuations in the output signals of the data collecting components in the test loop, an average value is used for each individual parameter. However, it must be determined how many measurements to take to get the actual average. If an insufficient number of measurements are taken, then a false reading will occur. However, an overly sufficient number of measurements will create redundancy, take up needed disk space, and prolong the data reduction procedure. Therefore, this appendix will examine the required number of data points for the hydraulic and steady-state thermal tests.

A.1 Hydraulic Tests

To examine the required number of data points needed for sufficient accuracy, 100 data points were recorded for the hydraulic tests at a coolant temperature of 10°C and a mass flow rate of 2.5 kg/min. For the hydraulic tests, the important parameters are the coolant temperature, mass flow

rate, pressure drop across the HFHE, and the density of the coolant. In addition, the room temperature was measured, because of its consistency, to portray the individual output fluctuations of the thermocouples.

For this analysis, a running average was calculated for each parameter. This average was then compared to the prior average to determine the effect of the fluctuated value of the parameter on the running average. A value of 0.0099 was selected, arbitrarily, as the largest difference possible for sufficient accuracy. The individual measurement, the running average, and the average difference can be seen for the coolant temperature and the room temperature in Table A.1 and for the pressure drop across the HFHE and the mass flow rate in Table A.2.

The density of the coolant is not measured directly and is solely dependent on the coolant temperature. Therefore, the number of measurements for a sufficient accuracy for the coolant temperature is also a sufficient number for the accuracy of the density of the coolant. As can be seen, the value of the difference between the averages never exceeds 0.001 after 13 data measurements. Therefore, to provide a small factor of safety, 15 data measurements was concluded to be sufficient for the accuracy of the overall average of the parameters.

Table A.1. Required Measurements for Sufficient Accuracy for the Coolant and Room Temperature.

Channel	50	Coolant	Temperature	51	Room	Temperature
Number of Data Points	Individual Data Point	Running Average	Difference of Averages	Individual Data Point	Running Average	Difference of Averages
	(°C)	(°C)	(°C)	(°C)	(°C)	(°C)
1	9.784	9.784		22.593	22.593	
2	9.686	9.735	-0.049	22.511	22.552	-0.041
3	9.981	9.817	0.082	22.669	22.591	0.039
4	9.706	9.78925	-0.02775	22.413	22.5465	-0.0445
5	9.733	9.778	-0.01125	22.344	22.506	-0.0405
6	9.961	9.8085	0.0305	22.49	22.50333	-0.00267
7	9.965	9.830857	0.022357	22.567	22.51243	0.009095
8	9.828	9.8305	-0.00036	22.418	22.50063	-0.0118
9	9.934	9.842	0.0115	22.468	22.497	-0.00363
10	10.021	9.8599	0.0179	22.652	22.5125	0.0155
11	9.91	9.864455	0.004555	22.338	22.49664	-0.01586
12	10.052	9.880083	0.015629	22.365	22.48567	-0.01097
13	9.782	9.872538	-0.00754	22.312	22.47231	-0.01336
14	9.758	9.864357	-0.00818	22.601	22.4815	0.009192
15	9.879	9.865333	0.000976	22.56	22.48673	0.005233
16	9.848	9.86425	-0.00108	22.564	22.49156	0.004829
17	10.011	9.872882	0.008632	22.626	22.49947	0.007908
18	9.83	9.8705	-0.00238	22.552	22.50239	0.002918
19	9.998	9.877211	0.006711	22.584	22.50668	0.004295
20	10.014	9.88405	0.006839	22.645	22.5136	0.006916
21	9.814	9.880714	-0.00334	22.465	22.51129	-0.00231
22	10.061	9.888909	0.008195	22.618	22.51614	0.004851
23	9.748	9.882783	-0.00613	22.545	22.51739	0.001255
24	9.943	9.885292	0.002509	22.56	22.51917	0.001775
25	9.802	9.88196	-0.00333	22.263	22.50892	-0.01025
26	9.819	9.879538	-0.00242	22.283	22.50023	-0.00869
27	10.019	9.884704	0.005165	22.535	22.50152	0.001288
28	10.034	9.890036	0.005332	22.535	22.50271	0.001196
29	9.873	9.889448	-0.00059	22.577	22.50528	0.002562
30	9.768	9.8854	-0.00405	22.462	22.50383	-0.00144
31	9.677	9.878677	-0.00672	22.256	22.49584	-0.00799
32	9.815	9.876688	-0.00199	22.318	22.49028	-0.00556
33	10.107	9.883667	0.006979	22.59	22.4933	0.003022
34	10.039	9.888235	0.004569	22.368	22.48962	-0.00369
35	9.926	9.889314	0.001079	22.529	22.49074	0.001125
36	9.793	9.886639	-0.00268	22.444	22.48944	-0.0013
37	9.714	9.881973	-0.00467	22.265	22.48338	-0.00607
38	9.867	9.881579	-0.00039	22.327	22.47926	-0.00412
39	10.008	9.884821	0.003242	22.494	22.47964	0.000378
40	9.824	9.8833	-0.00152	22.285	22.47478	-0.00487
41	9.691	9.87861	-0.00469	22.242	22.4691	-0.00568
42	10.013	9.88181	0.0032	22.499	22.46981	0.000712

Table A.1. (cont.)

Channel	50	Coolant	Temperature	51	Room	Temperature
Number of Data Points	Individual Data Point	Running Average	Difference of Averages	Individual Data Point	Running Average	Difference of Averages
	(°C)	(°C)	(°C)	(°C)	(°C)	(°C)
43	9.836	9.880744	-0.00107	22.258	22.46488	-0.00493
44	9.797	9.878841	-0.0019	22.247	22.45993	-0.00495
45	9.817	9.877467	-0.00137	22.266	22.45562	-0.00431
46	10.061	9.881457	0.00399	22.576	22.45824	0.002617
47	10.076	9.885596	0.004139	22.603	22.46132	0.00308
48	9.699	9.881708	-0.00389	22.323	22.45844	-0.00288
49	10.002	9.884163	0.002455	22.461	22.45849	5.23E-05
50	9.917	9.88482	0.000657	22.508	22.45948	0.00099
51	9.959	9.886275	0.001455	22.446	22.45922	-0.00026
52	9.762	9.883885	-0.00239	22.255	22.45529	-0.00393
53	9.747	9.881302	-0.00258	22.255	22.45151	-0.00378
54	9.854	9.880796	-0.00051	22.274	22.44822	-0.00329
55	9.905	9.881236	0.00044	22.336	22.44618	-0.00204
56	10.046	9.884179	0.002942	22.558	22.44818	0.001997
57	9.987	9.885982	0.001804	22.603	22.45089	0.002716
58	9.871	9.885724	-0.00026	22.535	22.45234	0.00145
59	9.976	9.887254	0.00153	22.52	22.45349	0.001147
60	9.775	9.885383	-0.00187	22.367	22.45205	-0.00144
61	9.725	9.882754	-0.00263	22.234	22.44848	-0.00357
62	9.941	9.883694	0.000939	22.386	22.44747	-0.00101
63	10.05	9.886333	0.00264	22.433	22.44724	-0.00023
64	9.866	9.886016	-0.00032	22.299	22.44492	-0.00232
65	9.972	9.887338	0.001323	22.356	22.44355	-0.00137
66	9.733	9.885	-0.00234	22.242	22.4405	-0.00305
67	10.05	9.887463	0.002463	22.406	22.43999	-0.00051
68	9.891	9.887515	5.20E-05	22.437	22.43994	-4.40E-05
69	9.843	9.88687	-0.00065	22.246	22.43713	-0.00281
70	10.06	9.889343	0.002473	22.4	22.4366	-0.00053
71	9.989	9.890746	0.001404	22.533	22.43796	0.001358
72	9.863	9.890361	-0.00039	22.38	22.43715	-0.0008
73	9.743	9.888342	-0.00202	22.266	22.43481	-0.00234
74	9.896	9.888446	0.000103	22.472	22.43531	0.000503
75	9.715	9.886133	-0.00231	22.236	22.43265	-0.00266
76	9.88	9.886053	-8.10E-05	22.358	22.43167	-0.00098
77	10.042	9.888078	0.002025	22.557	22.4333	0.001628
78	10.116	9.891	0.002922	22.584	22.43523	0.001932
79	10.072	9.893291	0.002291	22.512	22.4362	0.000972
80	10.147	9.896462	0.003171	22.542	22.43753	0.001322
81	9.998	9.897716	0.001254	22.527	22.43863	0.001105
82	9.861	9.897268	-0.00045	22.366	22.43774	-0.00089
83	9.738	9.895349	-0.00192	22.201	22.43489	-0.00285
84	9.693	9.89294	-0.00241	22.459	22.43518	0.000287
85	9.85	9.892435	-0.00051	22.313	22.43374	-0.00144

Table A.1. (cont.)

Channel	50	Coolant	Temperature	51	Room	Temperature
Number of Data Points	Individual Data Point	Running Average	Difference of Averages	Individual Data Point	Running Average	Difference of Averages
	(°C)	(°C)	(°C)	(°C)	(°C)	(°C)
86	9.85	9.891942	-0.00049	22.313	22.43234	-0.0014
87	9.728	9.890057	-0.00188	22.248	22.43022	-0.00212
88	9.881	9.889955	-0.0001	22.325	22.42902	-0.0012
89	9.802	9.888966	-0.00099	22.236	22.42685	-0.00217
90	9.802	9.888	-0.00097	22.248	22.42487	-0.00199
91	9.924	9.888396	0.000396	22.34	22.42393	-0.00093
92	9.889	9.888402	6.57E-06	22.52	22.42498	0.001044
93	10.07	9.890355	0.001953	22.596	22.42682	0.001839
94	9.906	9.890521	0.000166	22.44	22.42696	0.00014
95	10.054	9.892242	0.001721	22.554	22.42829	0.001337
96	9.941	9.89275	0.000508	22.616	22.43025	0.001955
97	9.926	9.893093	0.000343	22.589	22.43189	0.001637
98	9.706	9.891184	-0.00191	22.471	22.43229	0.000399
99	10.005	9.892333	0.00115	22.605	22.43403	0.001745
100	9.725	9.89066	-0.00167	22.363	22.43332	-0.00071

Table A.2. Required Measurements for Sufficient Accuracy for the Pressure Drop and Mass Flow Rate.

Channel	55 Pressure Drop			61 Mass Flow Rate		
Number of Data Points	Individual Data Point	Running Average	Difference of Averages	Individual Data Point	Running Average	Difference of Averages
	(psi)	(psi)	(psi)	(kg/min))	(kg/min)	(kg/min)
1	26.073	26.073		2.486	2.486	
2	26.313	26.193	0.12	2.449	2.4675	-0.0185
3	25.932	26.106	-0.087	2.514	2.483	0.0155
4	25.821	26.03475	-0.07125	2.464	2.47825	-0.00475
5	26.036	26.035	0.00025	2.379	2.4584	-0.01985
6	25.991	26.02767	-0.00733	2.534	2.471	0.0126
7	26.222	26.05543	0.027762	2.511	2.476714	0.005714
8	26.111	26.06238	0.006946	2.473	2.47625	-0.00046
9	25.968	26.05189	-0.01049	2.496	2.478444	0.002194
10	25.837	26.0304	-0.02149	2.31	2.4616	-0.01684
11	26.215	26.04718	0.016782	2.559	2.470455	0.008855
12	26.158	26.05642	0.009235	2.537	2.476	0.005545
13	26.628	26.10038	0.043968	2.467	2.475308	-0.00069
14	26.092	26.09979	-0.0006	2.414	2.470929	-0.00438
15	26.023	26.09467	-0.00512	2.472	2.471	7.14E-05
16	25.957	26.08606	-0.0086	2.366	2.464438	-0.00656
17	26.108	26.08735	0.00129	2.563	2.470235	0.005798
18	26.165	26.09167	0.004314	2.515	2.472722	0.002487
19	26.221	26.09848	0.006807	2.452	2.471632	-0.00109
20	26.244	26.11075	0.007013	2.512	2.47365	0.002018
21	26.08	26.10929	-0.00146	2.386	2.469476	-0.00417
22	26.031	26.10573	-0.00356	2.47	2.4695	2.38E-05
23	26.08	26.10461	-0.00112	2.448	2.468565	-0.00093
24	25.892	26.09575	-0.00886	2.444	2.467542	-0.00102
25	26.078	26.05592	0.00092	2.471	2.46768	0.000138
26	26.114	26.05815	0.002234	2.331	2.462423	-0.00526
27	26.139	26.05956	0.00141	2.485	2.463259	0.000836
28	25.188	26.06139	-0.00177	2.343	2.458964	-0.00429
29	26.079	26.05234	0.000952	2.439	2.458276	-0.00069
30	26.209	26.05757	0.005222	2.361	2.455033	-0.00324
31	26.102	26.059	0.001433	2.436	2.454419	-0.00061
32	26.375	26.06825	0.00925	2.439	2.453938	-0.00048
33	25.993	26.07567	-0.00258	2.397	2.452212	-0.00173
34	26.134	26.07738	0.001716	2.407	2.450882	-0.00133
35	26.061	26.07691	-0.00047	2.489	2.451971	0.001089
36	26.255	26.08186	0.004947	2.396	2.450417	-0.00155
37	26.313	26.08811	0.006247	2.555	2.453243	0.002827
38	26.322	26.09426	0.006155	2.426	2.452526	-0.00072
39	26.193	26.09679	0.002532	2.492	2.453538	0.001012
40	26.142	26.09793	0.00113	2.512	2.455	0.001462
41	26.025	26.09615	-0.00178	2.545	2.457195	0.002195
42	26.189	26.09836	0.002211	2.417	2.456238	-0.00096

Table A.2. (cont.)

Channel	55 Pressure Drop			61 Mass Flow Rate		
Number of Data Points	Individual Data Point	Running Average	Difference of Averages	Individual Data Point	Running Average	Difference of Averages
	(psi)	(psi)	(psi)	(kg/min)	(kg/min)	(kg/min)
43	26.212	26.101	0.002643	2.394	2.454791	-0.00145
44	26.309	26.10573	0.004727	2.517	2.456205	0.001414
45	25.888	26.10089	-0.00484	2.466	2.456422	0.000218
46	26.03	26.09935	-0.00154	2.545	2.458348	0.001926
47	26.109	26.09955	0.000205	2.555	2.460404	0.002056
48	26.32	26.10415	0.004593	2.337	2.457833	-0.00257
49	26.213	26.10637	0.002222	2.532	2.459347	0.001514
50	26.201	26.10826	0.001893	2.477	2.4597	0.000353
51	26.008	26.10629	-0.00197	2.53	2.461078	0.001378
52	26.067	26.10554	-0.00076	2.516	2.462135	0.001056
53	26.044	26.10438	-0.00116	2.424	2.461415	-0.00072
54	26.003	26.1025	-0.00188	2.538	2.462833	0.001418
55	26.059	26.10171	-0.00079	2.507	2.463636	0.000803
56	26.265	26.10463	0.002916	2.47	2.46375	0.000114
57	26.316	26.10833	0.003708	2.52	2.464737	0.000987
58	26.148	26.10902	0.000684	2.556	2.46631	0.001574
59	26.106	26.10897	-5.10E-05	2.567	2.468017	0.001707
60	24.608	26.08395	-0.02502	2.45	2.467717	-0.0003
61	26.035	26.08315	-0.0008	2.506	2.468344	0.000628
62	26.185	26.08479	0.001643	2.282	2.465339	-0.00301
63	26.091	26.08489	9.86E-05	2.529	2.466349	0.00101
64	26.305	26.08833	0.003439	2.412	2.4655	-0.00085
65	26.391	26.09298	0.004656	2.449	2.465246	-0.00025
66	25.132	26.07842	-0.01456	2.488	2.465591	0.000345
67	26	26.07725	-0.00117	2.51	2.466254	0.000663
68	26.056	26.07694	-0.00031	2.528	2.467162	0.000908
69	26.14	26.07786	0.000914	2.519	2.467913	0.000751
70	26.003	26.07679	-0.00107	2.488	2.4682	0.000287
71	26.035	26.0762	-0.00059	2.497	2.468606	0.000406
72	25.904	26.07381	-0.00239	2.544	2.469653	0.001047
73	26.203	26.07558	0.00177	2.547	2.470712	0.00106
74	26.176	26.07693	0.001357	2.574	2.472108	0.001396
75	26.411	26.08139	0.004454	2.488	2.47232	0.000212
76	26.301	26.08428	0.00289	2.407	2.471461	-0.00086
77	26.617	26.09119	0.006918	2.361	2.470026	-0.00143
78	25.915	26.08894	-0.00226	2.519	2.470654	0.000628
79	26.187	26.09018	0.001241	2.491	2.470911	0.000258
80	26.124	26.0906	0.000423	2.397	2.469988	-0.00092
81	26.167	26.09154	0.000943	2.442	2.469642	-0.00035
82	26.099	26.09163	9.09E-05	2.384	2.468598	-0.00104
83	26.132	26.09212	0.000486	2.471	2.468627	2.89E-05
84	26.039	26.09149	-0.00063	2.468	2.468619	-7.50E-06
85	26.288	26.0938	0.002312	2.457	2.468482	-0.00014

Table A.2. (cont.)

Channel	55 PressureDrop			61 Mass Flow Rate		
Number of Data Points	Individual Data Point	Running Average	Difference of Averages	Individual Data Point	Running Average	Difference of Averages
	(psi)	(psi)	(psi)	(kg/min)	(kg/min)	(kg/min)
86	26.609	26.09979	0.005991	2.496	2.468802	0.00032
87	25.988	26.09851	-0.00128	2.51	2.469276	0.000474
88	26.105	26.09858	7.38E-05	2.535	2.470023	0.000747
89	26.064	26.09819	-0.00039	2.479	2.470124	0.000101
90	26.132	26.09857	0.000376	2.472	2.470144	2.08E-05
91	26.428	26.10219	0.00362	2.496	2.470429	0.000284
92	25.956	26.1006	-0.00159	2.525	2.471022	0.000593
93	25.915	26.0986	-0.002	2.474	2.471054	3.20E-05
94	26.321	26.10097	0.002366	2.539	2.471777	0.000723
95	26.001	26.09992	-0.00105	2.529	2.472379	0.000602
96	26.106	26.09998	6.34E-05	2.506	2.472729	0.00035
97	26.252	26.10155	0.001567	2.553	2.473557	0.000828
98	26.291	26.10348	0.001933	2.513	2.473959	0.000402
99	26.25	26.10496	0.00148	2.435	2.473566	-0.00039
100	26.005	26.10396	-0.001	2.339	2.47222	-0.00135

A.2 Steady-State Thermal Tests

After the thermal system has reached steady-state, an average may be used to represent each parameter's value. However, even though the system is steady state, some fluctuations may occur in the output of the data collecting apparatus. Therefore, an analysis, similar to that of the hydraulic tests, was performed to calculate the minimum number of measurements needed to reach sufficient accuracy for the parameters' values. However, because the hydraulic tests showed that 15 data measurements were sufficient, only 30 data measurements were included into the thermal analysis (instead of 100 measurements that were used for the hydraulic tests). For the steady state test, the important parameters include: the surface temperatures, the coolant temperature, the mass flow rate, the density of the coolant, and the voltage and current inputted into the system. Instead of including 12 surface temperatures, the embedded temperature was selected to represent all of the surface temperatures. This is valid because all of the surface temperature thermocouples yielded similar fluctuations in their output. Furthermore, the voltage and current were lumped into one category, the power inputted into the system. This is valid because the power consists of the product of the voltage and current outputs and is the actual parameter used in the presentation of the results. Finally,

the density of the coolant was not included into the analysis of the required measurements due to the same reasoning as stated in section A.1.

For the analysis of the required measurements for the steady-state thermal tests, 30 data measurements were taken for CHIC A, see Figure 1.1, at a coolant temperature of 40°C, mass flow rate of 3.75 kg/min, and a heat load of 20 W. The actual analysis for the required measurements is identical to the analysis performed for the hydraulic test. This includes calculating a running average, and the amount each data measurement affects the average. This amount is represented by the difference in the running average to its prior value. Finally, an error value of 0.0099 was selected, arbitrarily, as the maximum difference in the running average for sufficient accuracy in the presentation of the data. This analysis can be seen in Table A.3, for the embedded temperature and the coolant temperature, and in Table A.4, for the mass flow rate and the power input. As seen in these tables, the difference in the averages does not exceed 0.001 after the 13 measurement. Therefore, for sufficient accuracy, including a small safety factor, 15 data measurements was selected for each thermal test run.

Table A.3. Required Measurement for Thermal Accuracy for the Embedded and Coolant Temperature

Channel	11 Embedded Temperature			50 Coolant Temperature		
Data Number	Individual Data Point	Running Average	Difference of Averages	Individual Data Point	Running Average	Difference of Averages
	(°C)	(°C)	(°C)	(°C)	(°C)	(°C)
1	48.745	48.745		39.826	39.826	
2	48.735	48.74	-0.005	39.76	39.793	-0.033
3	48.743	48.741	0.001	39.771	39.78567	-0.00733
4	48.747	48.7425	0.0015	39.791	39.787	0.001333
5	48.755	48.745	0.0025	39.879	39.8054	0.0184
6	48.749	48.74567	0.000667	39.998	39.8375	0.0321
7	48.739	48.74471	-0.00095	39.987	39.85886	0.021357
8	48.738	48.74388	-0.00084	39.969	39.87263	0.013768
9	48.767	48.74644	0.002569	39.815	39.86622	-0.0064
10	48.76784	48.74858	0.002139	39.808	39.8604	-0.00582
11	48.784	48.7518	0.00322	39.812	39.856	-0.0044
12	48.78186	48.75431	0.002505	39.871	39.85725	0.00125
13	48.77864	48.75618	0.001872	40.011	39.86908	0.011827
14	48.876	48.76474	0.008559	39.978	39.87686	0.00778
15	48.77	48.76509	0.000351	40.024	39.89333	0.009333
16	48.76144	48.76486	-0.00023	39.877	39.89231	-0.00102
17	48.76109	48.76464	-0.00022	39.891	39.89224	-7.70E-05
18	48.861	48.76999	0.005353	39.965	39.89628	0.004042
19	48.757	48.76931	-0.00068	40.07	39.90542	0.009143
20	48.75165	48.76843	-0.00088	40.028	39.91155	0.006129
21	48.854	48.7725	0.004075	40.111	39.92105	0.009498
22	48.758	48.77184	-0.00066	40.031	39.93059	0.009543
23	48.75393	48.77106	-0.00078	39.942	39.93109	0.0005
24	48.861	48.77481	0.003747	40.139	39.93975	0.00866
25	48.86178	48.77829	0.003479	40.088	39.94568	0.00593
26	48.85803	48.78136	0.003067	40.014	39.94831	0.00263
27	48.85455	48.78407	0.002711	39.912	39.94696	-0.00135
28	48.799	48.7846	0.000533	39.941	39.94675	-0.00021
29	48.79629	48.785	0.000403	40.055	39.95048	0.00373
30	48.882	48.78824	0.003233	40.104	39.9556	0.00512

Table A.4. Required Measurement for Thermal Accuracy for the Mass Flow Rate and Power Input

Channel	61 Mass Flow Rate			82 Power Input		
Number of Data Points	Individual Data Point	Running Average	Difference of Averages	Individual Data Point	Running Average	Difference of Averages
	(kg/min)	(kg/min)	(kg/min)	(W)	(W)	(W)
1	3.725	3.725		19.522	19.522	
2	3.716	3.7205	-0.0045	19.535	19.5285	0.0065
3	3.8	3.747	0.0265	19.718	19.59167	0.063167
4	3.741	3.7455	-0.0015	19.718	19.62325	0.031583
5	3.77	3.7504	0.0049	19.723	19.6432	0.01995
6	3.693	3.740833	-0.00957	19.723	19.6565	0.0133
7	3.738	3.740429	-0.0004	19.543	19.64029	-0.01621
8	3.728	3.738875	-0.00155	19.543	19.62813	-0.01216
9	3.679	3.732222	-0.00665	19.547	19.61911	-0.00901
10	3.641	3.7231	-0.00912	19.732	19.6304	0.011289
11	3.704	3.721364	-0.00174	19.727	19.63918	0.008782
12	3.791	3.727167	0.005803	19.757	19.649	0.009818
13	3.664	3.722308	-0.00486	19.753	19.657	0.008
14	3.71	3.721429	-0.00088	19.77	19.66507	0.008071
15	3.741	3.722733	0.001305	19.782	19.67287	0.007795
16	3.735	3.7235	0.000767	19.778	19.67944	0.006571
17	3.661	3.719824	-0.00368	19.774	19.685	0.005562
18	3.773	3.722778	0.002954	19.778	19.69017	0.005167
19	3.717	3.722474	-0.0003	19.782	19.695	0.004833
20	3.783	3.7255	0.003026	19.791	19.6998	0.0048
21	3.767	3.727476	0.001976	19.778	19.70352	0.003724
22	3.744	3.728227	0.000751	19.778	19.70691	0.003385
23	3.735	3.728522	0.000294	19.766	19.70948	0.002569
24	3.776	3.7305	0.001978	19.539	19.70238	-0.0071
25	3.742	3.73096	0.00046	19.539	19.69584	-0.00653
26	3.686	3.729231	-0.00173	19.535	19.68965	-0.00619
27	3.715	3.728704	-0.00053	19.535	19.68393	-0.00573
28	3.628	3.725107	-0.0036	19.718	19.68514	0.001217
29	3.776	3.726862	0.001755	19.535	19.67997	-0.00518
30	3.676	3.725167	-0.0017	19.493	19.67373	-0.00623

APPENDIX B

PLATE STACKING FOR THE HFHE

In this appendix, a listing of the individual copper laminates and their corresponding diagrams are presented.

B.1 Stacking Order

The HFHE consists of eight individual laminates. Plate A, the target plate, is the surface that the jets impinge upon. Plate B, the target spacer, provides a y-direction for the jets, see Figure 1.2. Plate C, the orifice plate, and plate C*, the orifice plate flipped over, are for creating the jets. Plate D, the spacer plate, is a plate that lies in between the C plates to provide some depth to the jets. Plate E, the spacer/manifold divider plate, is similar to plate D and provides the same function. However, Plate E does not include a channel opening for the exiting fluid from the HFHE. Plate F, the distributor plate, creates a uniform flow throughout the CHIC, and plate G which is the back cover for the CHIC. This particular stacking represents the number four model of the HFHE

developed by McDonnell Douglas [4]. This stacking differs from the model used by McDonnell Douglas in that it contains an orifice plate that has large openings, 0.010 in, as well as orifice plates that contain the usual small openings, 0.008 in. The large orifice plate, located on the target side of the manifold divider, provides a short circuit flow path. The stacking order can be seen in Table B.1.

B.2 Plate Diagrams

Each laminate consists of copper plates 0.038 or 0.010 cm (0.015 or 0.004 inches) in thickness. These plates were assembled by hydrogen diffusion. This bonding creates one sheet of copper 0.467 cm (0.184 inches) thick. The individual laminates can be seen in Figures B.1 through B.8.

Table B.1. CHIC Plate Stacking Order, Unit #4

Plate Number	Plate Type	Description	Thickness	
			cm	in
1	A	Target Plate	0.038	0.015
2	A	Target Plate	0.038	0.015
3	B	Target Spacer	0.038	0.015
4	C	Orifice	0.010	0.004
5	D	Spacer	0.010	0.004
6	C* big	Orifice (Flipped)	0.010	0.004
7	D	Spacer	0.010	0.004
8	C	Orifice	0.010	0.004
9	E	Spacer/Manifold	0.038	0.004
10	C* small	Orifice (Flipped)	0.010	0.004
11	D	Spacer	0.010	0.004
12	C	Orifice	0.010	0.004
13	D	Spacer	0.010	0.004
14	C* small	Orifice (Flipped)	0.010	0.004
15	D	Spacer	0.010	0.004
16	C	Orifice	0.010	0.004
17	D	Spacer	0.010	0.004
18	C* small	Orifice (Flipped)	0.010	0.004
19	D	Spacer	0.010	0.004
20	C	Orifice	0.010	0.004
21	F	Distributor	0.038	0.015
22	F	Distributor	0.038	0.015
23	F	Distributor	0.038	0.015
24	G	Back Cover	0.038	0.015
25	G	Back Cover	0.038	0.015
		TOTAL	0.467	0.184

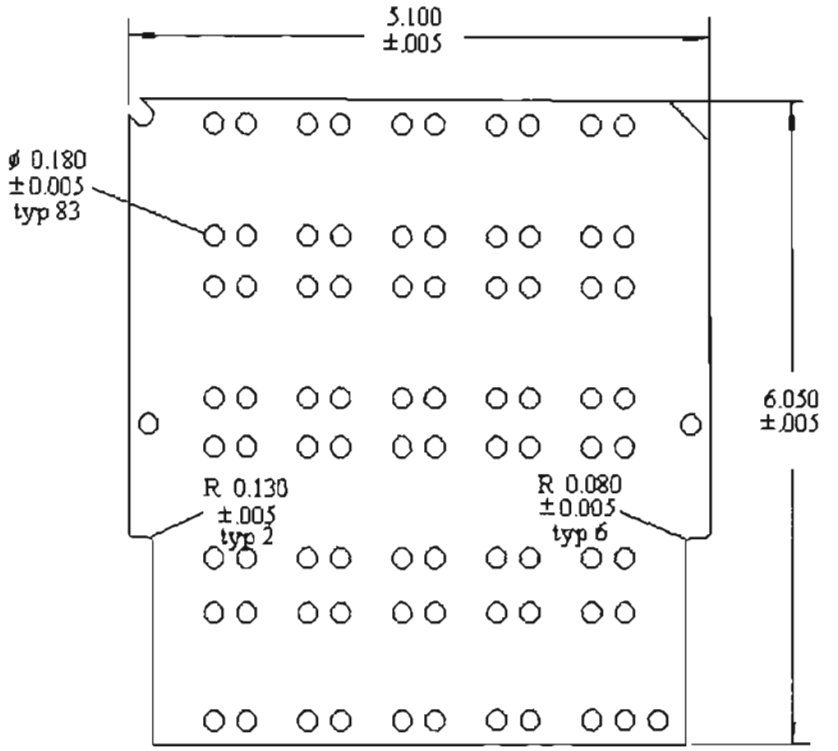

Figure B.1. Plate "A", Target Plate. (units in inches)

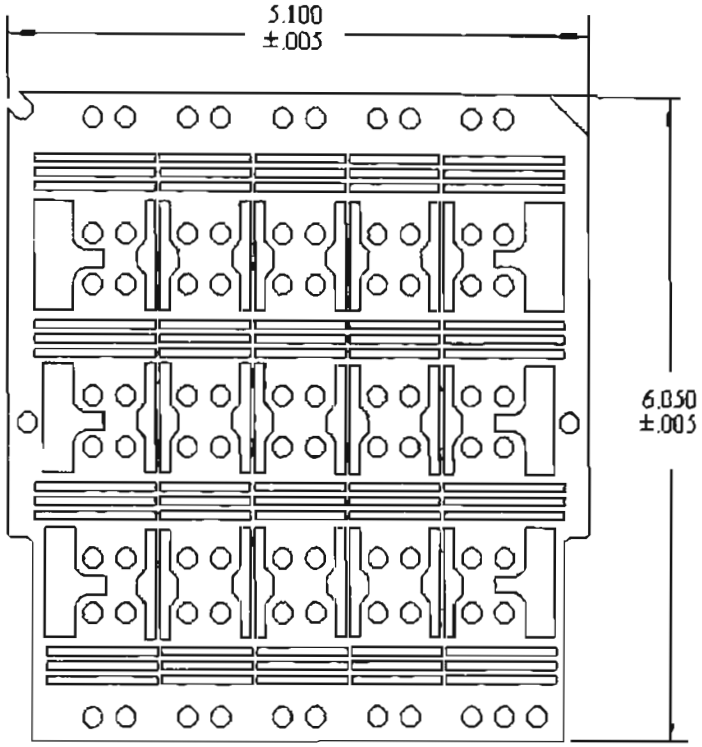

Figure B.2. Plate "B", Target Spacer. (units in inches)

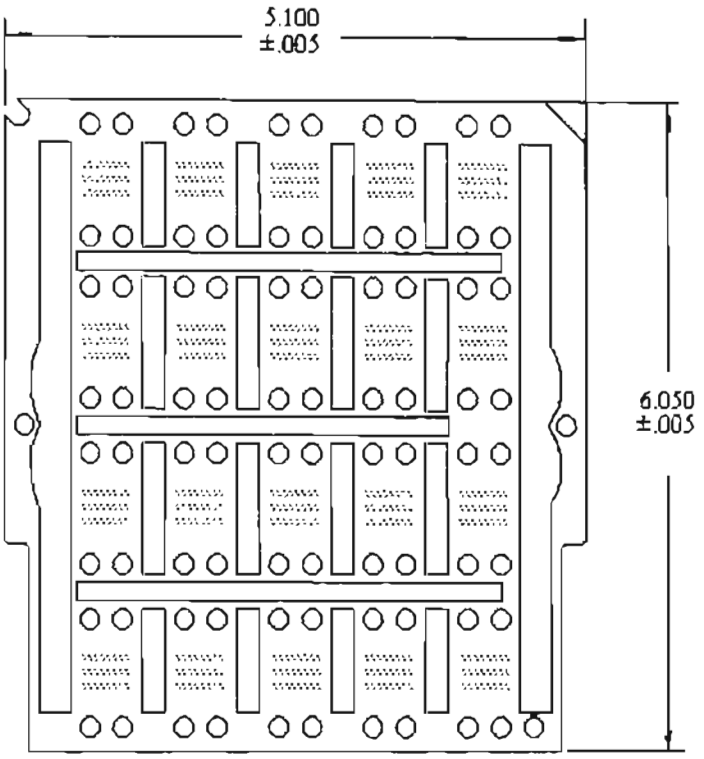

Figure B.3. Plate "C", Orifice Plate. (units in inches)

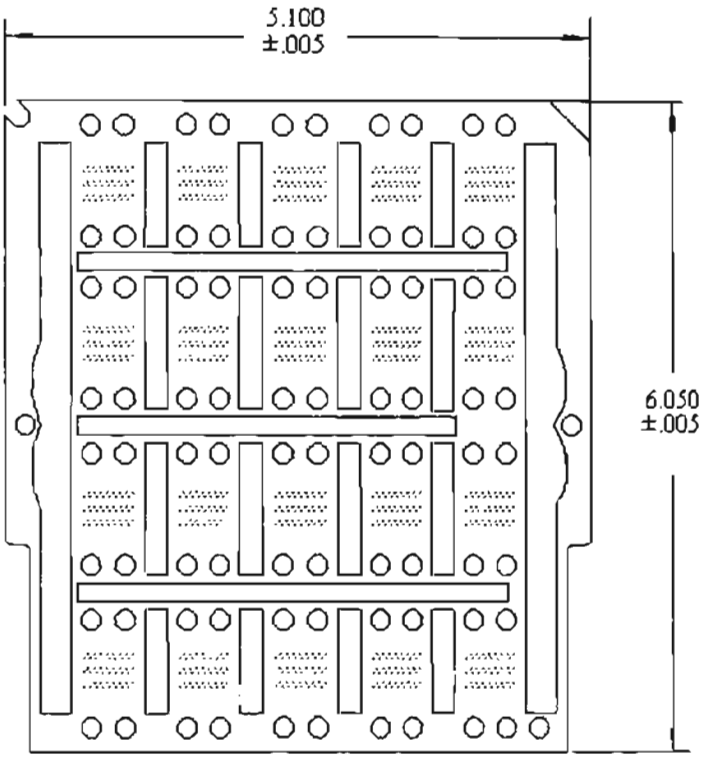

Figure B.4. Plate "C*", Orifice Plate, Orifices Staggered Relative to Plate "C". (units in inches)

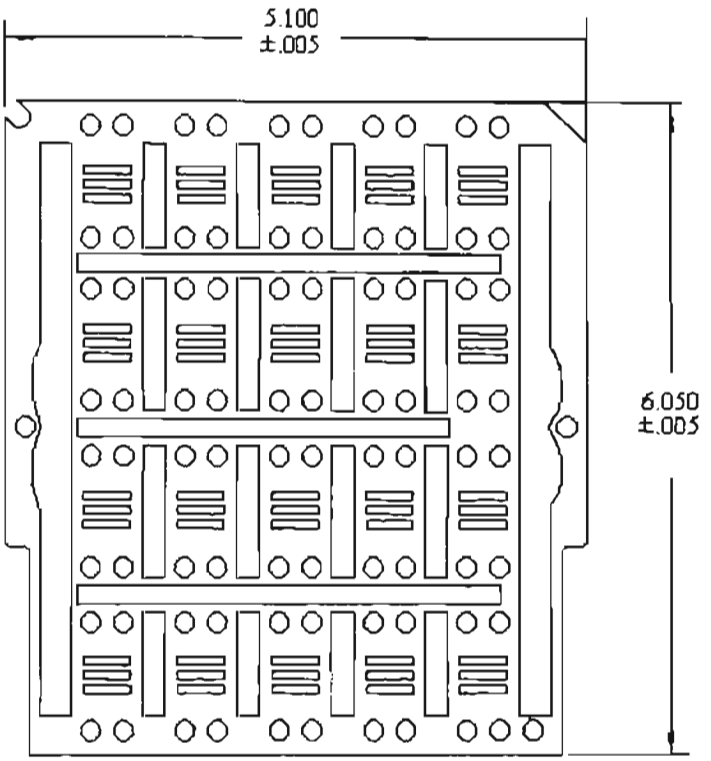

Figure B.5. Plate "D", Spacer Plate. (units in inches)

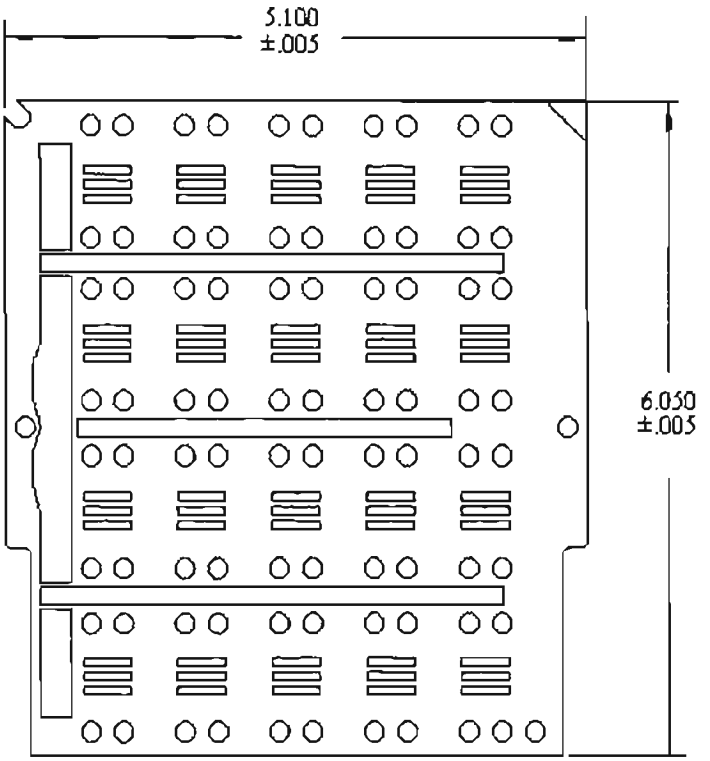

Figure B.6. Plate "E", Spacer/Manifold Divider Plate.
(units in inches)

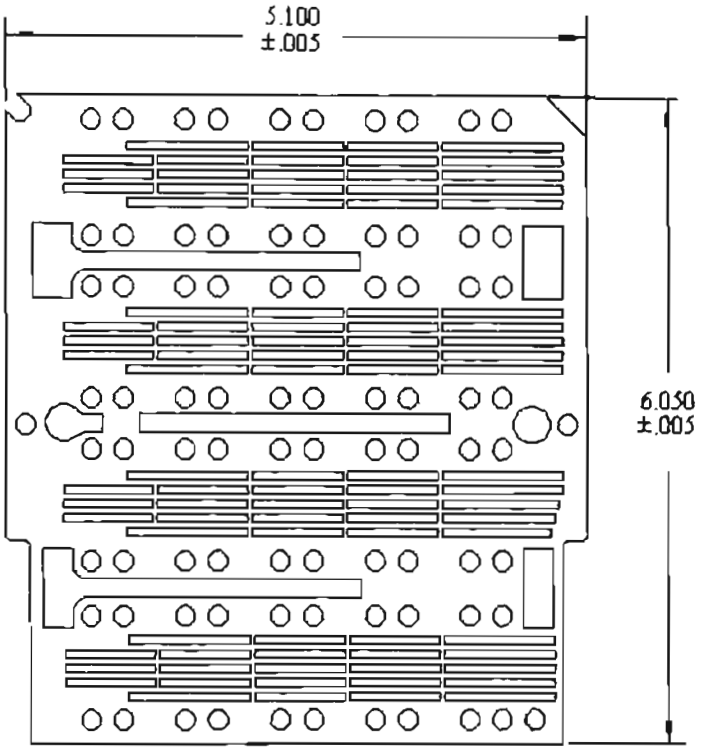

Figure B.7. Plate "F", Distributor Plate. (units in inches)

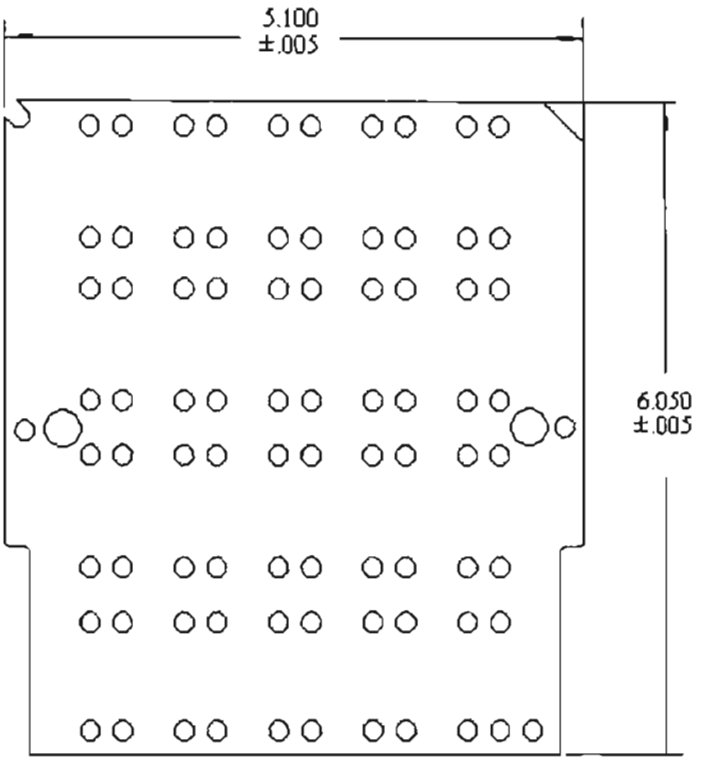

Figure B.8. Plate "G", Back Cover. (units in inches)

APPENDIX C

THERMOCOUPLE CALIBRATION RESULTS

In this appendix, the results of the thermocouple calibration are presented. This presentation includes an example calibration curve, the calibration data, and the curve fit equation. In addition, the curve fit equation includes the standard deviation and maximum error. As explained in Chapter II, the thermocouples were calibrated with the use of the cold temperature bath over the range of -20°C to 60°C at an increment of 10°C. However, due to the limited size of the reservoir of the temperature bath, it was not possible to calibrate all of the thermocouples at the same time. Therefore, the thermocouples were divided into the following sections: the surface thermocouples 0 through 8, the surface thermocouples 11 through 15, and the heat flux amplifier thermocouples. The amplifier thermocouple section also includes the thermocouple probes, which measure the coolant temperature at the inlet and outlet of the HFHE. As can be seen by Tables C.1 and C.2,

the calibration data for each of the thermocouples are very similar.

C.1 Surface Thermocouples 0 - 8

These surface thermocouples are for the temperature profile in the y-direction used in the calculation of the radial heat loss due to conduction. In addition, these thermocouples were used to measure the heater temperature and the wall temperature of the HFHE. An example of the calibration curve for the surface thermocouples is shown in Figure C.1. In addition, the calibration data and the curve fit equations for these thermocouples are shown in Table C.1 and Table C.2, respectively. Furthermore, the maximum error for each thermocouple occurs at 20°C.

C.2 Surface Thermocouples 11-15

These surface thermocouples are for the temperature profile in the x-direction used in the calculation of the radial heat loss due to conduction. An example of the calibration curve for the surface thermocouples is shown in Figure C.2. In addition, the calibration data and the curve fit equations for these thermocouples are shown in Table C.3 and Table C.4, respectively. All of the maximum errors occurred at 10°C or 60°C.

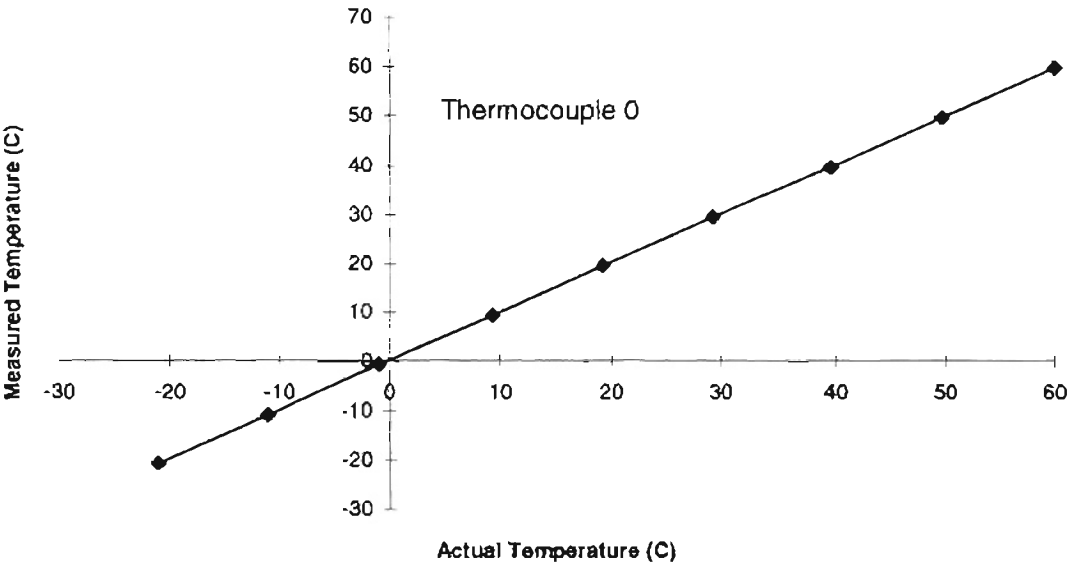

Figure C.1. Example Calibration Curve for the Surface Thermocouple 0.

Table C.1. Calibration Data for the Surface Thermocouples 0-8.

Thermo-couple Number	Surface Temp. (C)	Surface Temp. (C)	Surface Temp. (C)	Surface Temp. (C)	Surface Temp. (C)	Surface Temp. (C)	Surface Temp. (C)	Surface Temp. (C)	Surface Temp. (C)
Actual	-21.020	-11.020	-0.916	9.217	19.230	29.300	39.617	49.680	59.990
0	-20.788	-10.735	-0.631	9.406	19.549	29.546	39.789	49.961	60.099
1	-20.769	-10.706	-0.639	9.449	19.579	29.582	39.822	49.968	60.156
2	-20.680	-10.663	-0.565	9.486	19.637	29.629	39.868	50.032	60.168
3	-20.630	-10.584	-0.503	9.565	19.713	29.705	39.932	50.088	60.228
4	-20.611	-10.553	-0.479	9.599	19.708	29.729	39.954	50.125	60.244
5	-20.518	-10.497	-0.451	9.660	19.776	29.780	40.005	50.170	60.315
6	-20.559	-10.520	-0.444	9.682	19.765	29.797	40.031	50.204	60.340
7	-20.517	-10.487	-0.451	9.700	19.815	29.846	40.058	50.231	60.383
8	-20.438	-10.436	-0.420	9.741	19.859	29.869	40.085	50.255	60.398

Table C.2. Curve Fit Equations for the Surface Thermocouples 0-8.

	Y=mx + b			
Thermcouple Number	Slope (m)	Intercept (b)	Standard Deviation	Maximum Error
0	1.0011	-0.257	0.06	0.101
1	1.0009	-0.2794	0.052	0.103
2	1.0013	-0.3409	0.06	0.109
3	1.0014	-0.4089	0.062	0.117
4	1.0014	-0.4318	0.06	-0.1
5	1.0015	-0.4927	0.056	0.1
6	1.0008	-0.4834	0.055	-0.09
7	1.0006	-0.5121	0.059	0.102
8	1.0012	-0.5615	0.061	0.109

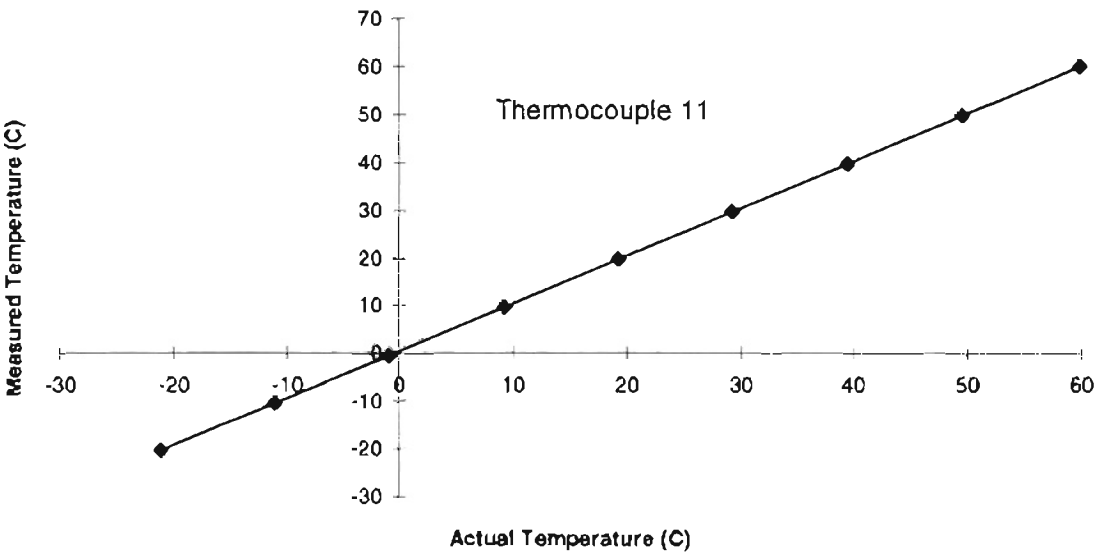

Figure C.2. Calibration Curve for Thermocouple 11.

Table C.3. Calibration Data for the Surface Thermocouples 11-15.

Thermo-couple	Surface Temp.	Surface Temp.	Surface Temp.	Surface Temp.	Surface Temp.	Surface Temp.	Surface Temp.	Surface Temp.	Surface Temp.
Number	(C)	(C)	(C)	(C)	(C)	(C)	(C)	(C)	(C)
Actual	-21.0611	-10.9833	-0.91111	9.21717 2	19.2333 3	29.3055 6	39.4722 2	49.6333 3	59.8944 4
11	-20.1028	-10.1508	-0.45	9.8261	19.8102 7	29.81	39.9555 8	50.0685 6	60.3622
12	-20.2484	-10.3112	-0.41667	9.8037	19.8044 5	29.8424	40.12	50.1444 4	60.3971
13	-20.3948	-10.2855	-0.58333	9.8139	19.8381 8	29.8538	40.0539 2	50.1925 6	60.4822
14	-20.4642	-10.2799	-0.35	9.8632	19.8761 8	29.8843	40.07	50.1854 4	60.4702
15	-20.2952	-10.2002	-0.3148	9.744	19.811	29.388	39.589	49.781	60.069

Table C.4. Curve Fit Equations for the Surface Thermocouples 11-15.

	Y=mx + b			
Thermcouple Number	Slope (m)	Intercept (b)	Standard Deviation	Maximum Error
11	1.005306	-0.69768	0.104541	-0.23896
12	1.002414	-0.64086	0.074716	-0.14742
13	1.00043	-0.58305	0.097719	-0.25552
14	1.000876	-0.62354	0.040109	0.070888
15	1.009418	-0.60484	0.118078	-0.11521

C.3 Amplifier Thermocouples

These surface thermocouples are for the temperature profile of the heat flux amplifier used in the approximation of the wall temperature of the HFHE. In addition, these thermocouples include the two thermocouple probes used to measure the coolant temperature at the inlet and outlet of the HFHE. The number for the thermocouple probes for the inlet and outlet of the HFHE are thermocouple 50 and 51, respectively. An example of the calibration curve for the amplifier thermocouples is shown in Figure C.3. In addition, the calibration data and the curve fit equations for these thermocouples are shown in Table C.5 and Table C.6, respectively. As can be seen from these tables, the maximum error occurs at 20°C for all of the thermocouples except for thermocouples 27 and 45 which contain maximum errors at 50°C.

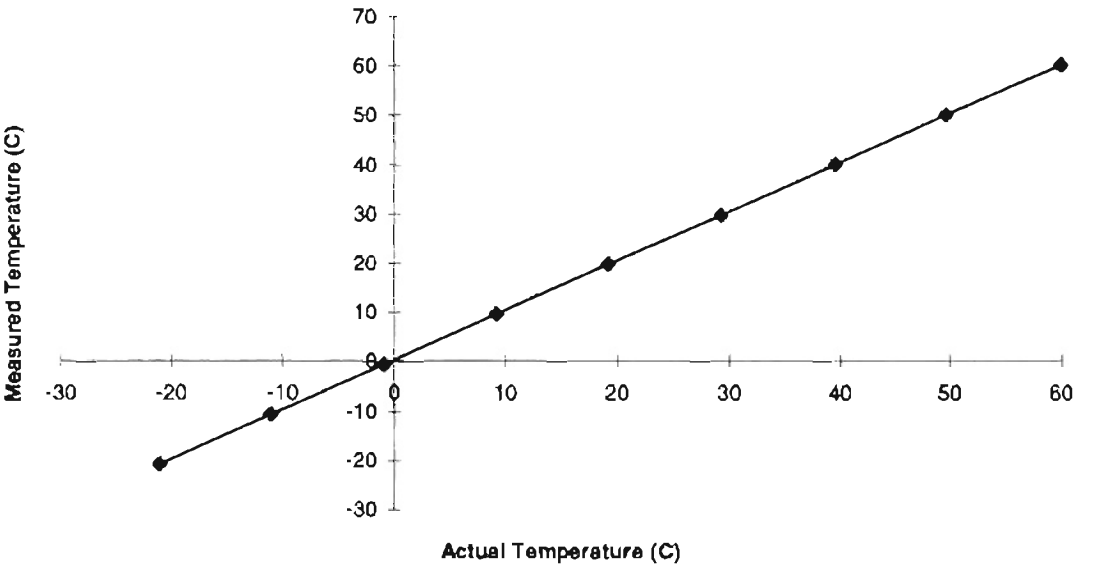

Figure C.3. Calibration Curve for Thermocouple 51.

Table C.5. Calibration Data for the Amplifier Thermocouples

Thermo-couple Number	Surface Temp. (C)	Surface Temp. (C)	Surface Temp. (C)	Surface Temp. (C)	Surface Temp. (C)	Surface Temp. (C)	Surface Temp. (C)	Surface Temp. (C)	Surface Temp. (C)
Actual	-21.02	-11.02	-0.916	9.217	19.23	29.3	39.617	49.68	59.99
22	-20.558	-10.54	-0.544	9.512	19.623	29.59	39.778	49.935	60.087
24	-20.423	-10.43	-0.461	9.624	19.726	29.69	39.867	50.022	60.163
25	-20.446	-10.457	-0.489	9.622	19.739	29.707	39.894	50.052	60.195
27	-20.406	-10.424	-0.465	9.678	19.789	29.764	39.953	50.114	60.259
30	-20.256	-10.299	-0.374	9.829	19.936	29.912	40.096	50.252	60.389
32	-20.277	-10.33	-0.4	9.799	19.915	29.886	40.073	50.231	60.368
33	-20.274	-10.328	-0.394	9.814	19.924	29.894	40.084	50.244	60.381
35	-20.275	-10.322	-0.388	9.814	19.926	29.902	40.087	50.247	60.393
38	-20.327	-10.38	-0.443	9.763	19.871	29.842	40.035	50.198	60.337
40	-20.595	-10.568	-0.554	9.462	19.559	29.535	39.72	49.873	60.036
41	-20.509	-10.488	-0.49	9.542	19.644	29.61	39.79	49.948	60.1
43	-20.388	-10.383	-0.404	9.678	19.774	29.741	39.926	50.078	60.23
45	-20.384	-10.392	-0.419	9.697	19.802	29.778	39.974	50.142	60.3
50	-20.45	-10.49	-0.43	9.862	19.923	29.998	40.202	50.125	60.542
51	-20.686	-10.637	-0.532	9.782	19.909	30.018	40.271	50.488	60.751

Table C.4. Curve Fit Equations for the Amplifier Thermocouples

	Y=mx + b			
Thermcouple Number	Slope (m)	Intercept (b)	Standard Deviation	Maximum Error
22	1.0042	-0.395	0.056	0.098
24	1.0047	-0.5048	0.058	0.102
25	1.0039	-0.4923	0.061	0.11
27	1.0035	-0.5333	0.063	0.11
30	1.0034	-0.6677	0.073	0.122
32	1.0033	-0.6419	0.074	0.125
33	1.0032	-0.6482	0.073	0.125
35	1.0031	-0.6509	0.072	0.123
38	1.0031	-0.5967	0.072	0.122
40	1.0047	-0.3571	0.054	0.08
41	1.0048	-0.4359	0.056	0.089
43	1.0045	-0.5525	0.055	0.097
45	1.0034	-0.5595	0.058	0.097
50	1.0001	-0.5807	0.092	0.104
51	0.994	-0.4675	0.062	0.105

APPENDIX D

DATA REDUCTION PROCESS

In this appendix, a step by step process of the data reduction is presented. This presentation begins with the output data file from the Fluke data logger for the steady-state thermal tests on CHIC B, see Figure 1.1. This output file is then reduced into an intermediate file listed as BT6F12P2 by the data reduction program, LAB. LAB is a self written FORTRAN program specifically for the reduction of the output file of the Fluke data logger. In addition, the data reduction program inputs the averaged value for all of the parameters into a summary file. Each summary file contains the output information over the entire ranges of flow rates and heat loads for a given coolant temperature. An example summary file is given for the coolant temperature of 30°C. Finally, in this appendix, the self-constructed data reduction program, LAB, is presented by its' source code.

D.1 Fluke Output Data File

The following data file is an example of the output file from the Fluke data logger. This particular output file is for a coolant temperature of 30°C, flow rate of 3.75 kg/min, and a heat load of 40 W.

```
Data File BT6F12P2
**************************************************************
BEGIN SCAN GROUP 1    12 JUL 95  14:49:53
HYD. TESTS

C    1 BORDER BARRIER    35.171 C
C    2 BORDER BARRIER    34.246 C
C    3 BORDER BARRIER    33.586 C
C    4 BORDER BARRIER    32.658 C
C    5 BORDER BARRIER    30.796 C
C    6 BORDER BARRIER    39.496 C
C    7 BORDER BARRIER    30.867 C
C    8 BORDER BARRIER    30.879 C
C   11 BARRIER HTR       31.006 C
C   12 BARRIER HTR       35.423 C
C   13 BARRIER HTR       33.978 C
C   14 BARRIER HTR       33.433 C
C   15 BARRIER HTR       32.292 C
C   22 AMPLIFIER         50.832 C
C   24 AMPLIFIER         51.308 C
C   27 AMPLIFIER         50.274 C
C   30 AMPLIFIER         53.598 C
C   38 AMPLIFIER         55.690 C
C   40 AMPLIFIER         54.435 C
C   41 AMPLIFIER         55.297 C
C   45 AMPLIFIER         65.143 C
C   50 HFHE TC IN        29.912 C
C   52 TEMP OUT          30.273 C
C   55 PRESSURE IN       41.744 PSIG
C   61 PAO FLOWRATE       3.687 KG/MIN
C   62 PAO DENSITY       0.7854 KG/L
C   80 VAC IN             28.30 VAC IN
C   81 AMP IN             1.413 AMP
C   82 WATTS IN          39.994 W

END SCAN GROUP 1      12 JUL 95  14:49:56


BEGIN SCAN GROUP 1    12 JUL 95  14:50:03
```

```
HYD. TESTS

C    1 BORDER BARRIER    35.034 C
C    2 BORDER BARRIER    34.206 C
C    3 BORDER BARRIER    33.564 C
C    4 BORDER BARRIER    32.621 C
C    5 BORDER BARRIER    30.745 C
C    6 BORDER BARRIER    39.445 C
C    7 BORDER BARRIER    30.813 C
C    8 BORDER BARRIER    30.827 C
C   11 BARRIER HTR       30.984 C
C   12 BARRIER HTR       35.328 C
C   13 BARRIER HTR       33.941 C
C   14 BARRIER HTR       33.394 C
C   15 BARRIER HTR       32.267 C
C   22 AMPLIFIER         50.667 C
C   24 AMPLIFIER         51.225 C
C   27 AMPLIFIER         50.166 C
C   30 AMPLIFIER         53.777 C
C   38 AMPLIFIER         55.950 C
C   40 AMPLIFIER         54.427 C
C   41 AMPLIFIER         55.277 C
C   45 AMPLIFIER         64.938 C
C   50 HFHE TC IN        30.040 C
C   52 TEMP OUT          30.499 C
C   55 PRESSURE IN       41.857 PSIG
C   61 PAO FLOWRATE       3.755 KG/MIN
C   62 PAO DENSITY       0.7853 KG/L
C   80 VAC IN             28.32 VAC IN
C   81 AMP IN             1.413 AMP
C   82 WATTS IN          40.028 W

END SCAN GROUP 1     12 JUL 95  14:50:06


BEGIN SCAN GROUP 1   12 JUL 95  14:50:13
HYD. TESTS

C    1 BORDER BARRIER    35.010 C
C    2 BORDER BARRIER    34.196 C
C    3 BORDER BARRIER    33.595 C
C    4 BORDER BARRIER    32.611 C
C    5 BORDER BARRIER    30.749 C
C    6 BORDER BARRIER    39.450 C
C    7 BORDER BARRIER    30.832 C
C    8 BORDER BARRIER    30.817 C
C   11 BARRIER HTR       30.989 C
C   12 BARRIER HTR       35.277 C
C   13 BARRIER HTR       33.946 C
C   14 BARRIER HTR       33.386 C
```

```
C  15 BARRIER HTR       32.260 C
C  22 AMPLIFIER         50.659 C
C  24 AMPLIFIER         51.214 C
C  27 AMPLIFIER         50.061 C
C  30 AMPLIFIER         53.616 C
C  38 AMPLIFIER         55.708 C
C  40 AMPLIFIER         54.459 C
C  41 AMPLIFIER         55.428 C
C  45 AMPLIFIER         64.969 C
C  50 HFHE TC IN        29.783 C
C  52 TEMP OUT          30.385 C
C  55 PRESSURE IN       41.613 PSIG
C  61 PAO FLOWRATE       3.701 KG/MIN
C  62 PAO DENSITY       0.7855 KG/L
C  80 VAC IN             28.34 VAC IN
C  81 AMP IN             1.413 AMP
C  82 WATTS IN          40.047 W

END SCAN GROUP 1     12 JUL 95  14:50:16


BEGIN SCAN GROUP 1   12 JUL 95  14:50:23
HYD. TESTS

C   1 BORDER BARRIER   35.136 C
C   2 BORDER BARRIER   34.210 C
C   3 BORDER BARRIER   33.539 C
C   4 BORDER BARRIER   32.611 C
C   5 BORDER BARRIER   30.719 C
C   6 BORDER BARRIER   39.421 C
C   7 BORDER BARRIER   30.805 C
C   8 BORDER BARRIER   30.805 C
C  11 BARRIER HTR      30.944 C
C  12 BARRIER HTR      35.362 C
C  13 BARRIER HTR      33.919 C
C  14 BARRIER HTR      33.357 C
C  15 BARRIER HTR      32.216 C
C  22 AMPLIFIER        50.729 C
C  24 AMPLIFIER        51.247 C
C  27 AMPLIFIER        50.267 C
C  30 AMPLIFIER        53.578 C
C  38 AMPLIFIER        55.777 C
C  40 AMPLIFIER        54.381 C
C  41 AMPLIFIER        55.110 C
C  45 AMPLIFIER        64.984 C
C  50 HFHE TC IN       30.071 C
C  52 TEMP OUT         30.348 C
C  55 PRESSURE IN      41.755 PSIG
C  61 PAO FLOWRATE      3.746 KG/MIN
C  62 PAO DENSITY      0.7852 KG/L
```

```
C  80 VAC IN             28.32 VAC IN
C  81 AMP IN              1.413 AMP
C  82 WATTS IN           40.028 W

END SCAN GROUP 1      12 JUL 95  14:50:26


BEGIN SCAN GROUP 1    12 JUL 95  14:50:33
HYD. TESTS

C   1 BORDER BARRIER    34.876 C
C   2 BORDER BARRIER    34.132 C
C   3 BORDER BARRIER    33.573 C
C   4 BORDER BARRIER    32.545 C
C   5 BORDER BARRIER    30.668 C
C   6 BORDER BARRIER    39.370 C
C   7 BORDER BARRIER    30.739 C
C   8 BORDER BARRIER    30.753 C
C  11 BARRIER HTR       30.907 C
C  12 BARRIER HTR       35.296 C
C  13 BARRIER HTR       33.882 C
C  14 BARRIER HTR       33.320 C
C  15 BARRIER HTR       32.193 C
C  22 AMPLIFIER         50.679 C
C  24 AMPLIFIER         51.169 C
C  27 AMPLIFIER         50.012 C
C  30 AMPLIFIER         53.636 C
C  38 AMPLIFIER         55.702 C
C  40 AMPLIFIER         54.420 C
C  41 AMPLIFIER         55.392 C
C  45 AMPLIFIER         64.931 C
C  50 HFHE TC IN        29.791 C
C  52 TEMP OUT          30.379 C
C  55 PRESSURE IN       41.515 PSIG
C  61 PAO FLOWRATE       3.723 KG/MIN
C  62 PAO DENSITY       0.7854 KG/L
C  80 VAC IN             28.33 VAC IN
C  81 AMP IN              1.413 AMP
C  82 WATTS IN           40.034 W

END SCAN GROUP 1      12 JUL 95  14:50:36


BEGIN SCAN GROUP 1    12 JUL 95  14:50:43
HYD. TESTS

C   1 BORDER BARRIER    35.070 C
C   2 BORDER BARRIER    34.159 C
C   3 BORDER BARRIER    33.458 C
C   4 BORDER BARRIER    32.574 C
```

```
C    5 BORDER BARRIER    30.694 C
C    6 BORDER BARRIER    39.399 C
C    7 BORDER BARRIER    30.753 C
C    8 BORDER BARRIER    30.765 C
C   11 BARRIER HTR       30.926 C
C   12 BARRIER HTR       35.258 C
C   13 BARRIER HTR       33.898 C
C   14 BARRIER HTR       33.350 C
C   15 BARRIER HTR       32.209 C
C   22 AMPLIFIER         50.639 C
C   24 AMPLIFIER         51.197 C
C   27 AMPLIFIER         50.135 C
C   30 AMPLIFIER         53.528 C
C   38 AMPLIFIER         55.620 C
C   40 AMPLIFIER         54.371 C
C   41 AMPLIFIER         55.261 C
C   45 AMPLIFIER         65.016 C
C   50 HFHE TC IN        29.773 C
C   52 TEMP OUT          30.247 C
C   55 PRESSURE IN       41.820 PSIG
C   61 PAO FLOWRATE       3.761 KG/MIN
C   62 PAO DENSITY       0.7855 KG/L
C   80 VAC IN             28.32 VAC IN
C   81 AMP IN              1.422 AMP
C   82 WATTS IN          40.263 W

END SCAN GROUP 1     12 JUL 95  14:50:46


BEGIN SCAN GROUP 1   12 JUL 95  14:50:53
HYD. TESTS

C    1 BORDER BARRIER    35.006 C
C    2 BORDER BARRIER    34.136 C
C    3 BORDER BARRIER    33.506 C
C    4 BORDER BARRIER    32.548 C
C    5 BORDER BARRIER    30.671 C
C    6 BORDER BARRIER    39.359 C
C    7 BORDER BARRIER    30.769 C
C    8 BORDER BARRIER    30.757 C
C   11 BARRIER HTR       30.896 C
C   12 BARRIER HTR       35.285 C
C   13 BARRIER HTR       33.871 C
C   14 BARRIER HTR       33.309 C
C   15 BARRIER HTR       32.182 C
C   22 AMPLIFIER         50.639 C
C   24 AMPLIFIER         51.169 C
C   27 AMPLIFIER         50.149 C
C   30 AMPLIFIER         53.654 C
C   38 AMPLIFIER         55.867 C
```

```
C  40 AMPLIFIER          54.385 C
C  41 AMPLIFIER          55.140 C
C  45 AMPLIFIER          64.869 C
C  50 HFHE TC IN         30.038 C
C  52 TEMP OUT           30.413 C
C  55 PRESSURE IN        42.029 PSIG
C  61 PAO FLOWRATE        3.744 KG/MIN
C  62 PAO DENSITY        0.7853 KG/L
C  80 VAC IN              28.32 VAC IN
C  81 AMP IN              1.413 AMP
C  82 WATTS IN           40.028 W

END SCAN GROUP 1      12 JUL 95  14:50:56


BEGIN SCAN GROUP 1    12 JUL 95  14:51:03
HYD. TESTS

C   1 BORDER BARRIER    34.869 C
C   2 BORDER BARRIER    34.111 C
C   3 BORDER BARRIER    33.537 C
C   4 BORDER BARRIER    32.538 C
C   5 BORDER BARRIER    30.676 C
C   6 BORDER BARRIER    39.378 C
C   7 BORDER BARRIER    30.732 C
C   8 BORDER BARRIER    30.747 C
C  11 BARRIER HTR       30.901 C
C  12 BARRIER HTR       35.263 C
C  13 BARRIER HTR       33.876 C
C  14 BARRIER HTR       33.313 C
C  15 BARRIER HTR       32.187 C
C  22 AMPLIFIER         50.621 C
C  24 AMPLIFIER         51.122 C
C  27 AMPLIFIER         49.994 C
C  30 AMPLIFIER         53.643 C
C  38 AMPLIFIER         55.724 C
C  40 AMPLIFIER         54.429 C
C  41 AMPLIFIER         55.347 C
C  45 AMPLIFIER         64.848 C
C  50 HFHE TC IN        29.785 C
C  52 TEMP OUT          30.376 C
C  55 PRESSURE IN       41.896 PSIG
C  61 PAO FLOWRATE       3.746 KG/MIN
C  62 PAO DENSITY       0.7855 KG/L
C  80 VAC IN             28.31 VAC IN
C  81 AMP IN             1.413 AMP
C  82 WATTS IN          40.014 W

END SCAN GROUP 1      12 JUL 95  14:51:06
```

```
BEGIN SCAN GROUP 1    12 JUL 95   14:51:13
HYD. TESTS

C    1 BORDER BARRIER    35.041 C
C    2 BORDER BARRIER    34.130 C
C    3 BORDER BARRIER    33.444 C
C    4 BORDER BARRIER    32.542 C
C    5 BORDER BARRIER    30.665 C
C    6 BORDER BARRIER    39.382 C
C    7 BORDER BARRIER    30.707 C
C    8 BORDER BARRIER    30.736 C
C   11 BARRIER HTR       30.893 C
C   12 BARRIER HTR       35.238 C
C   13 BARRIER HTR       33.865 C
C   14 BARRIER HTR       33.303 C
C   15 BARRIER HTR       32.176 C
C   22 AMPLIFIER         50.593 C
C   24 AMPLIFIER         51.165 C
C   27 AMPLIFIER         50.171 C
C   30 AMPLIFIER         53.496 C
C   38 AMPLIFIER         55.628 C
C   40 AMPLIFIER         54.321 C
C   41 AMPLIFIER         55.065 C
C   45 AMPLIFIER         64.939 C
C   50 HFHE TC IN        29.973 C
C   52 TEMP OUT          30.261 C
C   55 PRESSURE IN       41.818 PSIG
C   61 PAO FLOWRATE       3.821 KG/MIN
C   62 PAO DENSITY       0.7853 KG/L
C   80 VAC IN             28.33 VAC IN
C   81 AMP IN             1.413 AMP
C   82 WATTS IN          40.034 W

END SCAN GROUP 1      12 JUL 95   14:51:16


BEGIN SCAN GROUP 1    12 JUL 95   14:51:23
HYD. TESTS

C    1 BORDER BARRIER    34.788 C
C    2 BORDER BARRIER    34.059 C
C    3 BORDER BARRIER    33.486 C
C    4 BORDER BARRIER    32.471 C
C    5 BORDER BARRIER    30.582 C
C    6 BORDER BARRIER    39.300 C
C    7 BORDER BARRIER    30.665 C
C    8 BORDER BARRIER    30.665 C
C   11 BARRIER HTR       30.834 C
C   12 BARRIER HTR       35.182 C
```

```
C  13 BARRIER HTR       33.795 C
C  14 BARRIER HTR       33.247 C
C  15 BARRIER HTR       32.120 C
C  22 AMPLIFIER         50.543 C
C  24 AMPLIFIER         51.058 C
C  27 AMPLIFIER         49.916 C
C  30 AMPLIFIER         53.608 C
C  38 AMPLIFIER         55.714 C
C  40 AMPLIFIER         54.361 C
C  41 AMPLIFIER         55.279 C
C  45 AMPLIFIER         64.767 C
C  50 HFHE TC IN        29.770 C
C  52 TEMP OUT          30.331 C
C  55 PRESSURE IN       41.820 PSIG
C  61 PAO FLOWRATE       3.797 KG/MIN
C  62 PAO DENSITY       0.7855 KG/L
C  80 VAC IN             28.33 VAC IN
C  81 AMP IN             1.413 AMP
C  82 WATTS IN          40.034 W

END SCAN GROUP 1      12 JUL 95  14:51:26

BEGIN SCAN GROUP 1    12 JUL 95  14:51:33
HYD. TESTS

C   1 BORDER BARRIER    34.919 C
C   2 BORDER BARRIER    34.034 C
C   3 BORDER BARRIER    33.378 C
C   4 BORDER BARRIER    32.449 C
C   5 BORDER BARRIER    30.587 C
C   6 BORDER BARRIER    39.276 C
C   7 BORDER BARRIER    30.655 C
C   8 BORDER BARRIER    30.655 C
C  11 BARRIER HTR       30.827 C
C  12 BARRIER HTR       35.201 C
C  13 BARRIER HTR       33.784 C
C  14 BARRIER HTR       33.237 C
C  15 BARRIER HTR       32.110 C
C  22 AMPLIFIER         50.587 C
C  24 AMPLIFIER         51.051 C
C  27 AMPLIFIER         49.906 C
C  30 AMPLIFIER         53.505 C
C  38 AMPLIFIER         55.597 C
C  40 AMPLIFIER         54.369 C
C  41 AMPLIFIER         55.288 C
C  45 AMPLIFIER         64.790 C
C  50 HFHE TC IN        29.691 C
C  52 TEMP OUT          30.308 C
C  55 PRESSURE IN       41.805 PSIG
C  61 PAO FLOWRATE       3.789 KG/MIN
```

```
C  62 PAO DENSITY      0.7855 KG/L
C  80 VAC IN            28.31 VAC IN
C  81 AMP IN            1.413 AMP
C  82 WATTS IN         40.008 W

END SCAN GROUP 1     12 JUL 95  14:51:36

BEGIN SCAN GROUP 1   12 JUL 95  14:51:43
HYD. TESTS

C   1 BORDER BARRIER   35.008 C
C   2 BORDER BARRIER   34.067 C
C   3 BORDER BARRIER   33.411 C
C   4 BORDER BARRIER   32.479 C
C   5 BORDER BARRIER   30.602 C
C   6 BORDER BARRIER   39.308 C
C   7 BORDER BARRIER   30.703 C
C   8 BORDER BARRIER   30.688 C
C  11 BARRIER HTR      30.842 C
C  12 BARRIER HTR      35.204 C
C  13 BARRIER HTR      33.803 C
C  14 BARRIER HTR      33.255 C
C  15 BARRIER HTR      32.113 C
C  22 AMPLIFIER        50.587 C
C  24 AMPLIFIER        51.131 C
C  27 AMPLIFIER        50.140 C
C  30 AMPLIFIER        53.408 C
C  38 AMPLIFIER        55.543 C
C  40 AMPLIFIER        54.290 C
C  41 AMPLIFIER        55.059 C
C  45 AMPLIFIER        64.962 C
C  50 HFHE TC IN       29.842 C
C  52 TEMP OUT         30.175 C
C  55 PRESSURE IN      41.819 PSIG
C  61 PAO FLOWRATE      3.716 KG/MIN
C  62 PAO DENSITY      0.7854 KG/L
C  80 VAC IN            28.32 VAC IN
C  81 AMP IN            1.422 AMP
C  82 WATTS IN         40.256 W

END SCAN GROUP 1     12 JUL 95  14:51:46

BEGIN SCAN GROUP 1   12 JUL 95  14:51:53
HYD. TESTS

C   1 BORDER BARRIER   34.882 C
C   2 BORDER BARRIER   34.067 C
C   3 BORDER BARRIER   33.479 C
C   4 BORDER BARRIER   32.479 C
C   5 BORDER BARRIER   30.632 C
```

```
C    6 BORDER BARRIER    39.320 C
C    7 BORDER BARRIER    30.729 C
C    8 BORDER BARRIER    30.703 C
C   11 BARRIER HTR       30.872 C
C   12 BARRIER HTR       35.216 C
C   13 BARRIER HTR       33.817 C
C   14 BARRIER HTR       33.270 C
C   15 BARRIER HTR       32.158 C
C   22 AMPLIFIER         50.537 C
C   24 AMPLIFIER         51.109 C
C   27 AMPLIFIER         50.115 C
C   30 AMPLIFIER         53.577 C
C   38 AMPLIFIER         55.776 C
C   40 AMPLIFIER         54.290 C
C   41 AMPLIFIER         55.005 C
C   45 AMPLIFIER         64.828 C
C   50 HFHE TC IN        30.021 C
C   52 TEMP OUT          30.328 C
C   55 PRESSURE IN       41.793 PSIG
C   61 PAO FLOWRATE       3.842 KG/MIN
C   62 PAO DENSITY       0.7853 KG/L
C   80 VAC IN             28.30 VAC IN
C   81 AMP IN             1.413 AMP
C   82 WATTS IN          40.001 W

END SCAN GROUP 1      12 JUL 95  14:51:56

BEGIN SCAN GROUP 1    12 JUL 95  14:52:03
HYD. TESTS

C    1 BORDER BARRIER    34.786 C
C    2 BORDER BARRIER    34.042 C
C    3 BORDER BARRIER    33.483 C
C    4 BORDER BARRIER    32.472 C
C    5 BORDER BARRIER    30.607 C
C    6 BORDER BARRIER    39.269 C
C    7 BORDER BARRIER    30.678 C
C    8 BORDER BARRIER    30.692 C
C   11 BARRIER HTR       30.846 C
C   12 BARRIER HTR       35.194 C
C   13 BARRIER HTR       33.792 C
C   14 BARRIER HTR       33.245 C
C   15 BARRIER HTR       32.118 C
C   22 AMPLIFIER         50.541 C
C   24 AMPLIFIER         51.031 C
C   27 AMPLIFIER         49.903 C
C   30 AMPLIFIER         53.553 C
C   38 AMPLIFIER         55.645 C
C   40 AMPLIFIER         54.387 C
C   41 AMPLIFIER         55.277 C
```

```
C  45 AMPLIFIER          64.793 C
C  50 HFHE TC IN         29.680 C
C  52 TEMP OUT           30.340 C
C  55 PRESSURE IN        41.968 PSIG
C  61 PAO FLOWRATE        3.776 KG/MIN
C  62 PAO DENSITY        0.7855 KG/L
C  80 VAC IN              28.31 VAC IN
C  81 AMP IN              1.413 AMP
C  82 WATTS IN           40.008 W

END SCAN GROUP 1      12 JUL 95  14:52:06

BEGIN SCAN GROUP 1    12 JUL 95  14:52:13
HYD. TESTS

C   1 BORDER BARRIER    34.987 C
C   2 BORDER BARRIER    34.062 C
C   3 BORDER BARRIER    33.390 C
C   4 BORDER BARRIER    32.462 C
C   5 BORDER BARRIER    30.584 C
C   6 BORDER BARRIER    39.288 C
C   7 BORDER BARRIER    30.682 C
C   8 BORDER BARRIER    30.655 C
C  11 BARRIER HTR       30.809 C
C  12 BARRIER HTR       35.169 C
C  13 BARRIER HTR       33.770 C
C  14 BARRIER HTR       33.208 C
C  15 BARRIER HTR       32.096 C
C  22 AMPLIFIER         50.531 C
C  24 AMPLIFIER         51.089 C
C  27 AMPLIFIER         50.109 C
C  30 AMPLIFIER         53.395 C
C  38 AMPLIFIER         55.595 C
C  40 AMPLIFIER         54.298 C
C  41 AMPLIFIER         54.959 C
C  45 AMPLIFIER         64.889 C
C  50 HFHE TC IN        29.956 C
C  52 TEMP OUT          30.230 C
C  55 PRESSURE IN       41.822 PSIG
C  61 PAO FLOWRATE       3.672 KG/MIN
C  62 PAO DENSITY       0.7853 KG/L
C  80 VAC IN             28.32 VAC IN
C  81 AMP IN             1.413 AMP
C  82 WATTS IN          40.021 W

END SCAN GROUP 1      12 JUL 95  14:52:16

STOPPED SCANNING      12 JUL 95  14:52:17
*******************************************************************************
```

D.2 Output File

The following file shows the output file from the data reduction program, LAB. This particular file is for the coolant temperature of 30°C, flow rate of 3.75 kg/min, and a heat load of 40 W. This file shows the individual data points for all 15 measurements.

```
**************************************************************************
12 JUL 95
   1 BORDER BARRIER      35.171  35.034  35.010  35.136  34.876  35.070
35.006  34.869  35.041  34.788  34.919  35.008  34.882  34.786  34.987
   2 BORDER BARRIER     34.246  34.206  34.196  34.210  34.132  34.159
34.136  34.111  34.130  34.059  34.034  34.067  34.067  34.042  34.062
   3 BORDER BARRIER     33.586  33.564  33.595  33.539  33.573  33.458
33.506  33.537  33.444  33.486  33.378  33.411  33.479  33.483  33.390
   4 BORDER BARRIER     32.658  32.621  32.611  32.611  32.545  32.574
32.548  32.538  32.542  32.471  32.449  32.479  32.479  32.472  32.462
   5 BORDER BARRIER     30.796  30.745  30.749  30.719  30.668  30.694
30.671  30.676  30.665  30.582  30.587  30.602  30.632  30.607  30.584
   6 BORDER BARRIER     39.496  39.445  39.450  39.421  39.370  39.399
39.359  39.378  39.382  39.300  39.276  39.308  39.320  39.269  39.288
   7 BORDER BARRIER     30.867  30.813  30.832  30.805  30.739  30.753
30.769  30.732  30.707  30.665  30.655  30.703  30.729  30.678  30.682
   8 BORDER BARRIER     30.879  30.827  30.817  30.805  30.753  30.765
30.757  30.747  30.736  30.665  30.655  30.688  30.703  30.692  30.655
  11 BARRIER HTR        31.006  30.984  30.989  30.944  30.907  30.926
30.896  30.901  30.893  30.834  30.827  30.842  30.872  30.846  30.809
  12 BARRIER HTR        35.423  35.328  35.277  35.362  35.296  35.258
35.285  35.263  35.238  35.182  35.201  35.204  35.216  35.194  35.169
  13 BARRIER HTR        33.978  33.941  33.946  33.919  33.882  33.898
33.871  33.876  33.865  33.795  33.784  33.803  33.817  33.792  33.770
  14 BARRIER HTR        33.433  33.394  33.386  33.357  33.320  33.350
33.309  33.313  33.303  33.247  33.237  33.255  33.270  33.245  33.208
  15 BARRIER HTR        32.292  32.267  32.260  32.216  32.193  32.209
32.182  32.187  32.176  32.120  32.110  32.113  32.158  32.118  32.096
  22 AMPLIFIER          50.832  50.667  50.659  50.729  50.679  50.639
50.639  50.621  50.593  50.543  50.587  50.587  50.537  50.541  50.531
  24 AMPLIFIER          51.308  51.225  51.214  51.247  51.169  51.197
51.169  51.122  51.165  51.058  51.051  51.131  51.109  51.031  51.089
  27 AMPLIFIER          50.274  50.166  50.061  50.267  50.012  50.135
50.149  49.994  50.171  49.916  49.906  50.140  50.115  49.903  50.109
  30 AMPLIFIER          53.598  53.777  53.616  53.578  53.636  53.528
53.654  53.643  53.496  53.608  53.505  53.408  53.577  53.553  53.395
  38 AMPLIFIER          55.690  55.950  55.708  55.777  55.702  55.620
55.867  55.724  55.628  55.714  55.597  55.543  55.776  55.645  55.595
  40 AMPLIFIER          54.435  54.427  54.459  54.381  54.420  54.371
54.385  54.429  54.321  54.361  54.369  54.290  54.290  54.387  54.298
```

```
  41 AMPLIFIER          55.297  55.277  55.428  55.110  55.392  55.261
55.140  55.347  55.065  55.279  55.288  55.059  55.005  55.277  54.959
  45 AMPLIFIER          65.143  64.938  64.969  64.984  64.931  65.016
64.869  64.848  64.939  64.767  64.790  64.962  64.828  64.793  64.889
  50 HFHE TC IN         29.912  30.040  29.783  30.071  29.791  29.773
30.038  29.785  29.973  29.770  29.691  29.842  30.021  29.680  29.956
  52 TEMP OUT           30.273  30.499  30.385  30.348  30.379  30.247
30.413  30.376  30.261  30.331  30.308  30.175  30.328  30.340  30.230
  55 PRESSURE IN        41.744  41.857  41.613  41.755  41.515  41.820
42.029  41.896  41.818  41.820  41.805  41.819  41.793  41.968  41.822
  61 PAO FLOWRATE        3.687   3.755   3.701   3.746   3.723   3.761
3.744   3.746   3.821   3.797   3.789   3.716   3.842   3.776   3.672
  62 PAO DENSITY         0.785   0.785   0.785   0.785   0.785   0.785
0.785   0.785   0.785   0.785   0.785   0.785   0.785   0.785   0.785
  80 VAC IN             28.300  28.320  28.340  28.320  28.330  28.320
28.320  28.310  28.330  28.330  28.310  28.320  28.300  28.310  28.320
  81 AMP IN              1.413   1.413   1.413   1.413   1.413   1.422
1.413   1.413   1.413   1.413   1.413   1.422   1.413   1.413   1.413
  82 WATTS IN           39.994  40.028  40.047  40.028  40.034  40.263
40.028  40.014  40.034  40.034  40.008  40.256  40.001  40.008  40.021
*************************************************************************
```

D.3 Summary File

The following file is the summary file consisting of the averaged values of the 15 measurments for the entire range of flow rates and heat loads for a given temperature. This particular file represents the averaged values for a coolant temperature of 30°C. The summary file is obtained one line at a time by the data reduction program. For this particular summary program the averaged values are presented in the following form:

Flow Rate & Heat Load	c 1	c 2	c 3	c 4	c 5
c 6	c 7	c 8	c 11	c 12	c 13
c 15	c 22	c 24	c 27	c 30	c 38
c 40	c 41	c 45	c 50	c 52	
c 55	c 61	c 80	c 81	c 82	

Where the channels represent the following:

c 1 - c 15	Surface Temperatures (°C)
c 22 - c 45	Amplifier Temperatures (°C)
c 50 & c 52	Coolant Inlet and Outlet Temperatures (°C)
c 55	Pressure Drop across the HFHE (psi)
c 61	Mass Flow Rate (kg/min)
c 80	Voltage (V)
c 81	Current (A)
c 82	Input Power (W)

File BT6

****

f7p1	33.923	33.444	33.097	32.475	31.274
36.633	31.338	31.348	31.474	34.284	33.461
33.146	32.420	43.150	43.485	42.883	44.955
46.120	44.884	45.795	51.371	30.011	30.416
23.410	2.730	0.785	21.424	0.931	19.940
f9p1	34.002	33.524	33.173	32.578	31.416
36.686	31.490	31.498	31.622	34.357	33.543
33.227	32.518	43.233	43.549	42.954	44.999
46.182	44.878	45.806	51.423	30.125	30.515
27.165	2.979	0.785	21.489	0.930	19.983
f10p1	33.812	33.341	33.011	32.435	31.327
36.455	31.397	31.403	31.529	34.159	33.350
33.041	32.364	42.966	43.281	42.690	44.713
45.886	44.680	45.523	51.113	30.046	30.389
32.251	3.250	0.785	21.396	0.927	19.842
f11p1	33.668	33.201	32.857	32.303	31.217
36.315	31.279	31.294	31.418	34.009	33.205
32.904	32.231	42.832	43.178	42.564	44.622
45.797	44.614	45.453	51.040	29.936	30.300
35.817	3.458	0.785	21.400	0.927	19.846
f12p1	33.529	33.065	32.729	32.168	31.105
36.174	31.171	31.181	31.300	33.857	33.047
32.747	32.077	42.777	43.102	42.494	44.544
45.732	44.652	45.383	51.046	29.880	30.236
40.433	3.690	0.785	21.449	0.931	19.972
f12p1	33.738	33.293	32.975	32.415	31.387
36.378	31.458	31.460	31.586	34.070	33.267
32.966	32.325	43.015	43.324	42.725	44.762
45.962	44.824	45.590	51.261	30.162	30.502
46.638	4.034	0.785	21.465	0.933	20.020
f1p2	37.558	36.603	35.812	34.385	31.350
42.589	31.459	31.440	31.585	38.148	36.592
35.925	34.399	53.834	54.427	53.295	56.789
58.906	56.158	58.334	67.928	29.877	31.019
3.364	1.062	0.785	28.332	1.399	39.622
f2p2	37.132	36.189	35.398	34.102	31.277
42.053	31.371	31.359	31.511	37.694	36.160
35.515	34.041	53.195	53.730	52.675	56.151
58.257	55.786	57.717	67.308	29.982	30.906
5.240	1.292	0.785	28.290	1.401	39.629
f3p2	36.694	35.796	35.053	33.837	31.253
41.427	31.348	31.337	31.494	37.194	35.720
35.104	33.708	52.393	52.907	51.898	55.321
57.396	55.205	56.871	66.307	30.065	30.838
7.981	1.516	0.785	28.121	1.389	39.066
f4p2	36.290	35.417	34.716	33.531	31.092
40.938	31.186	31.170	31.338	36.775	35.335
34.734	33.385	51.818	52.320	51.311	54.694
56.750	54.647	56.224	65.607	29.900	30.570
9.947	1.727	0.785	28.135	1.391	39.149
f5p2	36.360	35.469	34.773	33.612	31.252
40.990	31.351	31.332	31.495	36.783	35.333
34.732	33.400	52.071	52.557	51.528	54.996
57.094	55.041	56.559	66.081	30.172	30.801
13.129	2.000	0.785	28.192	1.401	39.478
f6p2	36.077	35.222	34.542	33.424	31.165
40.675	31.262	31.251	31.409	36.504	35.062
34.473	33.181	51.787	52.308	51.271	54.708
56.820	54.864	56.266	65.819	30.147	30.692
16.215	2.239	0.785	28.191	1.403	39.551
f7p2	35.755	34.895	34.230	33.161	31.001
40.279	31.098	31.085	31.247	36.141	34.719
34.140	32.886	51.346	51.853	50.834	54.251
56.346	54.618	55.824	65.364	30.045	30.545
20.180	2.555	0.785	28.154	1.393	39.212

f8p2	35.584	34.742	34.091	33.033	30.934
40.130	31.028	31.013	31.178	35.964	34.541

33.966	32.731	51.328	51.840	50.799	54.269
56.386	54.677	55.861	65.497	29.989	30.475
23.839	2.804	0.785	28.337	1.415	40.098
f9p2	35.510	34.654	34.004	32.982	30.959
39.977	31.042	31.039	31.198	35.838	34.424
33.853	32.662	51.171	51.694	50.647	54.114
56.227	54.596	55.718	65.358	30.026	30.496
28.482	3.059	0.785	28.347	1.412	40.034
f10p2	35.338	34.550	33.892	32.891	30.924
39.787	31.012	31.005	31.169	35.687	34.288
33.729	32.561	50.935	51.449	50.397	53.882
55.997	54.431	55.472	65.054	30.061	30.506
32.305	3.250	0.785	28.247	1.403	39.628
f11p2	35.337	34.504	33.876	32.902	30.996
39.733	31.079	31.075	31.233	35.644	34.257
33.711	32.562	50.873	51.400	50.364	53.803
55.912	54.432	55.401	65.008	30.087	30.519
36.281	3.462	0.785	28.346	1.410	39.974
f12p2	35.042	34.201	33.577	32.613	30.735
39.444	30.818	30.816	30.971	35.334	33.937
33.385	32.253	50.718	51.245	50.182	53.666
55.798	54.436	55.301	65.011	29.932	30.382
41.696	3.766	0.785	28.337	1.415	40.100
f1p3	40.349	38.986	37.812	35.816	31.474
47.364	31.594	31.549	31.724	41.092	38.901
37.949	35.788	63.152	63.800	62.362	67.158
70.208	66.275	69.504	82.994	29.898	31.408
2.855	0.945	0.785	33.985	1.799	61.135
f2p3	39.690	38.330	37.173	35.298	31.213
46.554	31.321	31.288	31.466	40.316	38.153
37.215	35.120	62.396	63.067	61.604	66.461
69.501	65.821	68.837	82.350	29.876	31.155
4.649	1.213	0.785	34.061	1.807	61.542
f3p3	38.903	37.583	36.496	34.747	31.027
45.536	31.135	31.107	31.287	39.430	37.321
36.415	34.435	61.324	61.995	60.530	65.371
68.383	65.017	67.749	81.178	29.923	30.932
8.031	1.513	0.785	33.932	1.798	61.014
f4p3	38.575	37.282	36.230	34.531	30.980
45.136	31.084	31.056	31.246	39.073	36.969
36.080	34.155	60.944	61.673	60.215	64.997
68.055	64.840	67.375	80.933	29.977	30.834
10.473	1.768	0.785	33.908	1.789	60.669
f5p3	38.270	37.004	35.982	34.308	30.876
44.831	30.978	30.953	31.141	38.752	36.661
35.782	33.888	60.721	61.423	59.944	64.801
67.841	64.635	67.199	80.750	29.923	30.743
12.653	1.933	0.785	33.995	1.798	61.130
f6p3	37.936	36.651	35.617	34.056	30.820
44.310	30.920	30.895	31.082	38.297	36.238
35.376	33.559	60.206	60.904	59.418	64.249
67.279	64.280	66.649	80.210	29.925	30.647
16.798	2.272	0.785	33.897	1.797	60.922
f7p3	37.843	36.540	35.517	34.006	30.874
44.144	30.971	30.946	31.134	38.155	36.099
35.247	33.467	60.095	60.802	59.300	64.144
67.166	64.284	66.558	80.163	29.975	30.642
19.969	2.481	0.785	33.909	1.794	60.847
f8p3	37.608	36.373	35.412	33.893	30.877
43.919	30.983	30.952	31.139	37.956	35.914
35.074	33.336	59.914	60.625	59.145	63.979
67.049	64.108	66.380	80.012	30.059	30.681
23.583	2.747	0.785	34.021	1.801	61.267
f9p3	37.394	36.166	35.216	33.741	30.813
43.653	30.908	30.888	31.075	37.721	35.696
34.676	33.168	59.604	60.307	58.813	63.692
66.724	63.896	66.081	79.649	29.979	30.595
26.475	2.943	0.785	33.994	1.796	61.064
f10p3	37.065	35.850	34.921	33.492	30.681
43.262	30.781	30.759	30.946	37.356	35.350
34.540	32.890	59.283	59.976	58.471	63.351

66.380	63.634	65.760	79.351	29.875	30.463
32.891	3.283	0.785	33.953	1.792	60.842
f11p3	37.024	35.805	34.870	33.503	30.772
43.179	30.856	30.847	31.029	37.284	35.306
34.505	32.891	59.148	59.867	58.376	63.203
66.234	64.018	65.595	79.218	29.946	30.507
36.789	3.506	0.785	33.889	1.784	60.472
f13p3	36.891	35.711	34.826	33.487	30.913
43.024	31.001	30.993	31.175	37.173	35.193
34.410	32.871	59.039	59.746	58.245	63.122
66.164	63.685	65.522	79.092	30.002	30.558
46.953	4.057	0.785	34.065	1.793	61.097
f3p4	41.394	39.688	38.276	36.021	31.210
49.798	31.330	31.284	31.499	42.014	39.290
38.121	35.578	69.875	70.756	68.855	74.995
78.890	74.315	78.128	95.303	29.925	31.239
7.350	1.469	0.785	38.618	2.092	80.759
f4p4	40.958	39.314	37.960	35.769	31.204
49.289	31.330	31.284	31.494	41.495	38.842
37.682	35.213	69.441	70.201	68.427	74.606
78.499	74.104	77.762	94.988	30.113	31.270
10.084	1.733	0.785	38.707	2.089	80.828
f5p4	40.515	38.883	37.565	35.440	31.078
48.741	31.214	31.153	31.369	41.042	38.347
37.210	34.805	68.968	69.990	68.018	74.161
78.124	73.976	77.313	94.737	30.180	31.154
13.100	1.960	0.785	38.802	2.091	81.115
f6p4	39.888	38.304	37.030	34.974	30.797
48.009	30.917	30.869	31.086	40.370	37.728
36.616	34.274	68.199	69.104	67.234	73.355
77.311	73.398	76.528	93.856	30.034	30.953
16.311	2.227	0.785	38.598	2.085	80.453
f7p4	39.374	37.783	36.528	34.562	30.587
47.329	30.711	30.661	30.879	39.774	37.153
36.061	33.798	67.436	68.393	66.526	72.561
76.501	72.891	75.717	93.146	29.863	30.632
20.463	2.529	0.785	38.656	2.088	80.703
f8p4	39.197	37.638	36.406	34.458	30.585
47.197	30.704	30.659	30.874	39.599	36.975
35.888	33.660	67.498	68.403	66.498	72.694
76.637	73.035	75.899	93.339	29.842	30.632
23.912	2.759	0.785	38.785	2.094	81.203
f9p4	39.139	37.612	36.424	34.532	30.826
47.048	30.945	30.899	31.118	39.516	36.933
35.863	33.706	67.295	68.216	66.305	72.489
76.428	73.075	75.691	93.123	30.128	30.854
28.858	3.057	0.785	38.774	2.096	81.242
f11p4	38.596	37.056	35.861	34.065	30.532
46.368	30.640	30.603	30.819	38.849	36.319
35.268	33.189	66.701	67.618	65.680	71.925
75.848	72.755	75.142	92.615	29.938	30.651
37.274	3.497	0.785	38.720	2.094	81.083
f12p4	38.316	36.828	35.691	33.916	30.498
46.069	30.613	30.578	30.795	38.622	36.170
35.064	33.040	66.277	67.228	65.315	71.469
75.414	72.484	74.667	92.160	29.935	30.569
41.997	3.776	0.785	38.769	2.093	81.116
f13p4	38.375	36.857	35.700	33.974	30.625
46.035	30.734	30.703	30.914	38.609	36.108
35.076	33.079	66.298	67.241	65.315	71.508
75.446	72.511	74.713	92.178	30.025	30.670
46.062	3.985	0.785	38.772	2.090	81.008
f5p5	42.486	40.480	38.852	36.254	30.926
52.551	31.065	31.000	31.246	43.067	39.769
38.359	35.417	77.421	78.557	76.235	83.770
88.661	83.542	87.751	109.110	29.910	31.097
13.648	2.001	0.785	43.410	2.350	102.020
f7p5	41.519	39.565	38.018	35.591	30.692
51.278	30.832	30.768	31.019	41.961	38.737
37.383	34.608	76.029	76.992	74.853	82.362
87.215	82.515	86.346	107.578	29.909	30.907
20.195	2.519	0.785	43.286	2.343	101.410

f9p5	41.057	39.121	37.616	35.326	30.742
50.625	30.858	30.817	31.060	41.390	38.215
36.896	34.250	75.424	76.581	74.233	81.739
86.577	82.088	85.706	106.979	29.976	30.836
27.852	2.990	0.785	43.146	2.340	100.963
f10p5	40.840	38.960	37.369	35.147	30.708
50.315	30.819	30.778	31.017	41.080	37.932
36.626	34.040	75.207	76.304	73.966	81.567
86.400	82.032	85.359	106.823	29.940	30.803
32.405	3.208	0.785	43.244	2.342	101.279
f11p5	40.261	38.418	37.014	34.783	30.491
49.770	30.625	30.563	30.808	40.606	37.484
36.191	33.677	74.637	75.734	73.442	80.973
85.810	81.741	84.942	106.153	29.897	30.760
37.227	3.496	0.785	43.214	2.343	101.250
f12p5	40.199	38.363	36.958	34.787	30.607
49.629	30.720	30.679	30.923	40.524	37.403
36.127	33.659	74.462	75.697	73.309	80.735
85.663	81.399	84.674	106.036	30.083	30.758
41.720	3.707	0.785	43.110	2.340	100.884
f13p5	40.190	38.297	36.871	34.773	30.703
49.504	30.812	30.775	31.014	40.405	37.310
36.050	33.628	74.381	75.499	73.133	80.691
85.505	81.350	84.671	105.942	30.056	30.777
46.661	4.026	0.785	43.233	2.344	101.327

****

D.4 Data Reduction Program

The following program represents the data reduction program LAB. This program contains one input, the data output file of the Fluke data logger, and two outputs, the data output file and the summary file.

```
************************************************************
PROGRAM LAB
*     This is a data conversion program for Mike Cutbirth
*     written 7/1/95
         REAL X1(30,30),SD(30),AVGFILE(30)
         CHARACTER
C*1,A(5)*50,A1(2,30)*15,FILNM1*10,FILNM2*10
         CHARACTER FILNM3*10,IDNEW*10,IDOLD*10
         INTEGER Y(30)
         PRINT*,'ENTER THE FILENAME OF THE DATA FILE      '
         READ*, FILNM1
         OPEN (UNIT=8,FILE=FILNM1,STATUS='OLD')
         PRINT*,'ENTER THE FILENAME OF THE NEW DATA FILE  '
         READ*, FILNM2
         OPEN (UNIT=9,FILE=FILNM2,STATUS='UNKNOWN')
*************************************************************
*       THIS BLOCK READS IN THE FIRST DATA SET              *
*************************************************************
*
*
         DO 10, I=1,5
                 READ (8,100) A(I)
   10    CONTINUE
         J=1
         DO 20, I=1,30
                 READ (8,110) C,Y(I),A1(1,I),X1(J,I),A1(2,I)
                 IF(C.NE."C") THEN
                         K=I-1
                         GOTO 21
                 ENDIF
   20    CONTINUE
   21    CONTINUE
*
*************************************************************
*
*   THIS BLOCK CHECKS TO SEE IF ADDITIONAL DATA SETS
*
*    EXISTS AND READS THEM
*
```

```
*****************************************************************
*
*
*
        DO 40, J=2,30
        I=1
        DO 23, M=1,15
        READ(8,125,ERR=22) C,X1(J,I)
   22   CONTINUE
        IF(C.EQ."S") GOTO 50
        IF(C.EQ."C") GOTO 25
   23   CONTINUE
   25   CONTINUE
        DO 30, I=2,K
                READ(8,130) X1(J,I)
   30   CONTINUE
   40   CONTINUE
   50   CONTINUE
*
*****************************************************************
****
*    THIS BLOCK PRINT THE DATA IN THE NEW FORMAT
*
*****************************************************************
****
*
*
        K1=J-1
        WRITE(9,135) A(3)
        DO 60, I=1,K
                WRITE(9,140) Y(I),A1(1,I),(X1(K2,I),K2=1,K1)
   60   CONTINUE
        CLOSE(8)
*
*****************************************************************
***
*    THIS BLOCK CALCULATES AND PRINTS THE AVERAGES AND RMS
*
*****************************************************************
***
*
*
*        WRITE(9,*)
C        WRITE(9,*) '       RMS AND AVERAGES  '
         DO 80, I=1,K
         X2=0.0
         DO 70, J=1,K1
                 X2=X2+X1(J,I)
   70   CONTINUE
         X2AVG=X2/REAL(K1)
```

```
          AVGFILE(I)=X2AVG
          DO 72, J=1,K1
                  SD(J)=SQRT((X1(J,I)-X2AVG)**2)
   72    CONTINUE
C          WRITE(9,140) Y(I),A1(1,I),(SD(J),J=1,K1)
C          WRITE(9,150) X2AVG
C          WRITE(9,*)
   80    CONTINUE
          PRINT*, '  DATA CONVERSION COMPLETED  '
          CLOSE(9)
*************************************************************
*
*       THIS BLOCK PRINTS AVERAGES IN A DIFFERENT FILE
*       AFTER PREVIOUS RUNS
*************************************************************
**
         PRINT*
         PRINT*,'   ENTER FILENAME FOR ACCUM. AVERAGE FILE'
         PRINT*
         READ*, FILNM3
         PRINT*, '  ENTER INDENTIFIER NAME FOR THIS RUN'
         PRINT*
         READ*, IDNEW
         OPEN(UNIT=10, FILE=FILNM3, STATUS='UNKNOWN')
         DO 90, I=1,150
                 READ(10,160,END=91) IDOLD, AVGOLD
   90    CONTINUE
   91    CONTINUE
         WRITE(10,170) IDNEW,(AVGFILE(J),J=1,K)
         CLOSE(10)
*************************************************************
**
*
  100    FORMAT(19X,A12)
  110    FORMAT(A1,1X,I3,1X,A15,1X,E7.3,1X,A7)
  120    FORMAT(A1)
  125    FORMAT(A1,21X,E7.3)
  130    FORMAT(22X,E7.3)
  135    FORMAT(6X,A12)
  140    FORMAT(1X,I3,1X,A15,1X,30F8.3)
  150    FORMAT(1X,'AVERAGE = ',F15.3)
  160    FORMAT(A10,F15.3)
  170    FORMAT(A10,30F15.3)
         END
*************************************************************
```

APPENDIX E

UNCERTAINTY ANALYSIS

To fully evaluate the equations that were developed from curve fitting the experimental data, such as the radial heat loss due to conduction equation and the temperature difference between the wall and fluid, a least squares analysis was performed on the deviation between the experimental data and the curve fitted data for each equation. However, this analysis does not apply for equations developed by using previous equations instead of experimental data. Examples of these equations include the thermal resistance equation and the thermal performance equation. It is assumed that the uncertainty of these equations are the sum of the uncertainties of these equations used for their development. For example, the uncertainty of the thermal resistance is the equivalent of the uncertainty of the wall temperature equation. Furthermore, the uncertainty of the thermal performance equation is the sum of the uncertainty for the thermal resistance equation and the hydraulic performance equation.

E.1 Uncertainty for the Heat Loss Equation

A least squares analysis was performed for the radial heat loss equation, seen in Equation (3.18). This analysis is described in section 2.2.3. The experimental data can be seen in Appendix F.

$$\frac{\dot{Q}_{loss}}{\dot{Q}_{applied}} = \phi_1 + \left(\phi_2 + \phi_3 e^{(\phi_4 T)}\right) e^{\left[\left(\phi_5 + \phi_6 e^{(\phi_7 T)}\right)\dot{m}\right]} \qquad (3.18)$$

However, the coefficients, ϕ, are dependent on the applied heat load. Therefore, for this least squares analysis, the equation for each applied heat load must evaluated. The results of this analysis is presented using the standard deviation of the curve fitted data, shown in the heat loss per heat applied and in percentage of the deviation to the experimental data. In addition, the maximum error and the corresponding flow rate are presented. These results are shown in Table E.1, for the standard deviation, and Table E.2, for the maximum errors. As can be seen from these tables, the standard deviation of the error of the curve fit is less than 1.0% for each heat load. Furthermore, the maximum error is less 0.002 $\dot{Q}_{loss} / \dot{Q}_{applied}$.

Table E.1 Uncertainties for the Heat Loss Equation.

	-10°C	0°C	10°C	20°C	30°C	40°C
		Standard	Deviation	in W/W		
20 W	0.00100	0.00034	0.00047	0.00073	0.00050	0.00074
40 W	0.00085	0.00066	0.00054	0.00121	0.00037	0.00119
60 W	0.00066	0.00077	0.00054	0.00097	0.00100	0.00055
80 W	0.00096	0.00055	0.00055	0.00064	0.00060	
100 W	0.00035	0.00047	0.00082	0.00046		
		Standard	Deviation	in %		
20 W	0.503	0.147	0.205	0.372	0.277	0.407
40 W	0.498	0.283	0.271	0.623	0.188	0.683
60 W	0.377	0.392	0.298	0.539	0.576	0.322
80 W	0.594	0.273	0.256	0.330	0.341	
100 W	0.218	0.272	0.450	0.251		

Table E.2 Maximum Error for the Heat Loss Equation.

			-10°C	0°C	10°C	20°C	30°C	40°C
20 W	max. error		-0.0016	-0.0008	-0.0009	0.0010	-0.0005	-0.0008
	@flow rate	kg/hr	60	90	75	60	240	225
40 W	max. error		-0.0012	0.0011	0.0011	-0.0018	-0.0007	0.0018
	@flow rate	kg/hr	120	75	240	195	120	180
60 W	max. error		0.0013	0.0014	-0.0010	0.0019	0.0015	0.0008
	@flow rate	kg/hr	180	60	60	240	195	195
80 W	max. error		0.0013	0.0012	-0.0015	-0.0012	-0.0013	
	@flow rate	kg/hr	150	60	240	240	240	
100 W	max. error		0.0005	0.0007	-0.0015	0.0008		
	@flow rate	kg/hr	180	90	75	105		

E.2 Uncertainty for the Temperature Difference Equation

A least squares analysis was performed for the radial heat loss equation, seen in Equation (3.20).

$$T_w - T_f = \lambda_0 + \left(\lambda_1 + \lambda_2 e^{(\lambda_3 m)}\right)\dot{Q} \qquad (3.20)$$

The constants λ_n are independent of the flow rate, heat load, and fluid temperature and have the following values: λ_0 (2.25), λ_1 (0.19779), λ_2 (0.19968), and λ_3 (-0.013115). In addition, the mass flow rate is in kg/hr, and the heat load is in W/cm^2. The experimental data for this equation can be seen in Table E.3. The results of this analysis is presented using the standard deviation of the curve fitted data, shown in the heat loss per heat applied and in percentage of the deviation to the experimental data. In addition, the maximum error and the corresponding flow rate are presented. These results are shown in Table E.4, for the standard deviation and the maximum errors. As can be seen from these tables, the standard deviation of the error of the curve fit is less than 4.3% for each heat load. Furthermore, the maximum error is less 10.44%. However, this large maximum error occurs for the heat load of 20 W, at which the temperature difference is relatively small.

Table E.3 Data for the Temperature Difference Equation.

Heat Load	20 W			40 W			60 W		
Flow Rate	Net Heat Load	T_w-T_f (Actual)	T_w-T_f (fitted)	Net Heat Load	T_w-T_f (Actual)	T_w-T_f (fitted)	Net Heat Load	T_w-T_f (Actual)	T_w-T_f (fitted)
kg/hr	W	°C (K)	°C (K)	W	°C (K)	°C (K)	W	°C (K)	°C (K)
60	15.719	6.615	6.788	32.180	11.620	11.540	48.764	16.487	16.328
75	15.892	6.218	6.580	32.445	11.025	11.090	49.097	15.817	15.627
90	16.059	5.845	6.411	32.718	10.595	10.728	49.486	15.216	15.073
105	16.211	5.680	6.273	32.851	10.174	10.403	49.822	14.841	14.614
120	16.219	6.187	6.129	33.128	9.827	10.173	49.898	14.431	14.184
135	16.366	6.095	6.043	33.344	9.599	9.978	50.183	14.096	13.881
150	16.410	6.094	5.954	33.497	9.384	9.810	50.561	13.908	13.662
165	16.505	5.993	5.893	33.628	9.2443	9.672	50.701	13.744	13.441
180	16.615	5.916	5.849	33.653	9.230	9.540	50.754	13.888	13.245
195	16.378	5.863	5.743	33.434	9.275	9.380	50.672	13.745	13.056
210	16.462	5.797	5.715	33.602	9.186	9.323	50.719	13.633	12.926
225	16.533	5.717	5.693	33.717	8.982	9.271	50.879	13.489	12.844
240	16.559	5.649	5.667	33.766	8.762	9.218	50.826	13.265	12.739

Table E.3 (cont.)

Heat Load	80 W			100 W					
Flow Rate	Net Heat Load	T_w-T_f (Actual)	T_w-T_f (fitted)	Net Heat Load	T_w-T_f (Actual)	T_w-T_f (fitted)			
kg/hr	W	°C (K)	°C (K)	W	°C (K)	°C (K)			
60	65.822	21.146	21.252	82.480	25.786	11.540			
75	66.334	20.406	20.324	83.017	25.009	11.090			
90	66.850	19.484	19.573	83.517	24.030	10.728			
105	67.093	18.788	18.901	83.981	23.130	10.403			
120	67.413	18.369	18.374	84.409	22.401	10.173			
135	67.732	17.899	17.949	84.801	21.952	9.978			
150	67.935	17.564	17.584	85.157	21.528	9.810			
165	68.115	17.329	17.285	85.476	21.210	9.672			
180	68.389	17.113	17.065	85.760	20.973	9.540			
195	68.263	16.658	16.808	86.007	20.697	9.380			
210	68.362	16.415	16.641	86.218	20.321	9.323			
225	68.515	16.295	16.517	86.393	20.102	9.271			
240	68.516	16.220	16.389	86.532	19.931	9.218			

Table E.4 Uncertainties for the Temperature Difference Equation.

		20 W	40 W	60 W	80 W	100 W
Standard Deviation	°C	.262	.295	.435	.123	.130
	%	4.29	2.90	2.93	0.66	0.57
Maximum Error	°C	-0.593	-0.456	0.707	-0.226	-0.177
	%	-10.44	-5.21	5.22	1.37	0.89
@ Flow Rate	kg/hr	105	240	210	210	240

APPENDIX F

RADIAL CONDUCTED HEAT LOSS

The raw data, the curve fit coefficients, and the curve fits for the radial heat loss due to conduction are presented in this appendix. This data represents the heat loss due to the simplification of applying a heat load to one CHIC at a time. Futhermore, the radial heat loss is presented as a function of the mass flow rate and coolant temperature for various applied heat loads. The analytical model for the radial heat loss is presented as a ratio of the heat loss to the applied heat load and is equivalent to an exponential decay function with the coolant temperature and the mass flow rate as the dependent variables. However, the coefficients shown in the following equation are dependent on the applied heat load, and shown in Table F.1.

$$\frac{\dot{Q}_{loss}}{\dot{Q}_{applied}} = \phi_1 + \left(\phi_2 + \phi_3 e^{(\phi_4 T)}\right) e^{\left(\left(\phi_5 + \phi_6 e^{(\phi_7 T)}\right)\dot{m}\right)}$$

Furthermore, Figures F.1 through F.5 show the curve fits for the various equations. Finally, the raw data for these curves is presented in Tables F.2 through F.6.

Table F.1. Curve Fit Coefficients for the Radial Heat Loss

	Curve Fit Coefficients						
Applied Heat Load	ϕ_1	ϕ_2	ϕ_3	ϕ_4	ϕ_5	ϕ_6	ϕ_7
20 W	0.143	0.290	-0.621	-0.0050	-0.0048	-0.612	-0.0180
40 W	0.134	0.280	-0.470	-0.0035	-0.0048	-0.489	-0.0177
60 W	0.128	0.265	-0.376	-0.0029	-0.0052	-0.419	-0.0173
80 W	0.125	0.189	-0.253	-0.0032	-0.0035	-0.121	-0.0116
100 W	0.119	0.119	-0.786	-0.0011	-0.0047	-0.377	-0.0170

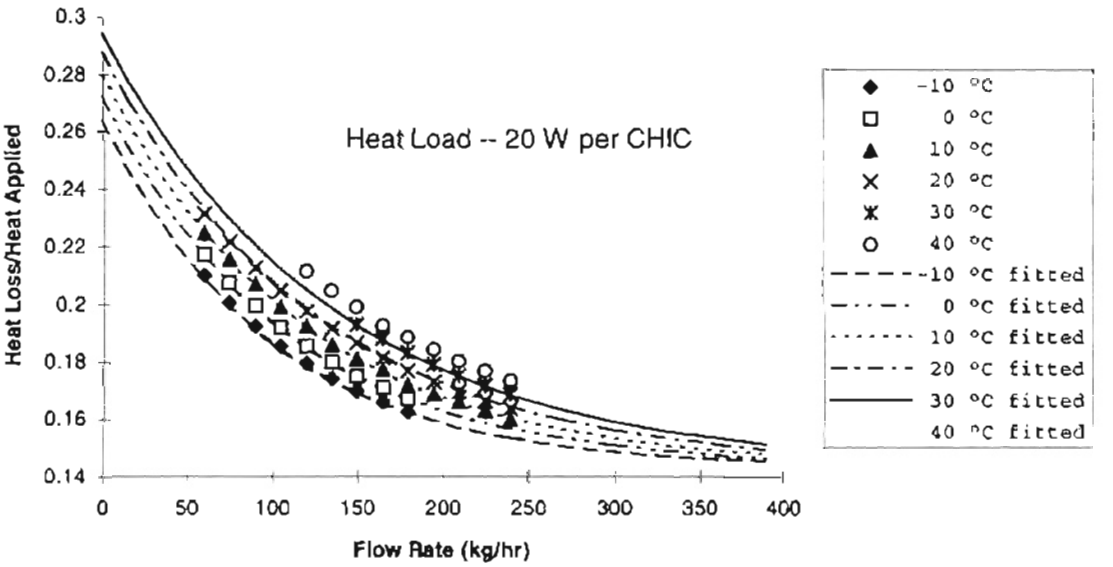

Figure F.1. Radial Heat Loss Due to Conduction Heat Transfer for an Applied Heat Load of 20 W.

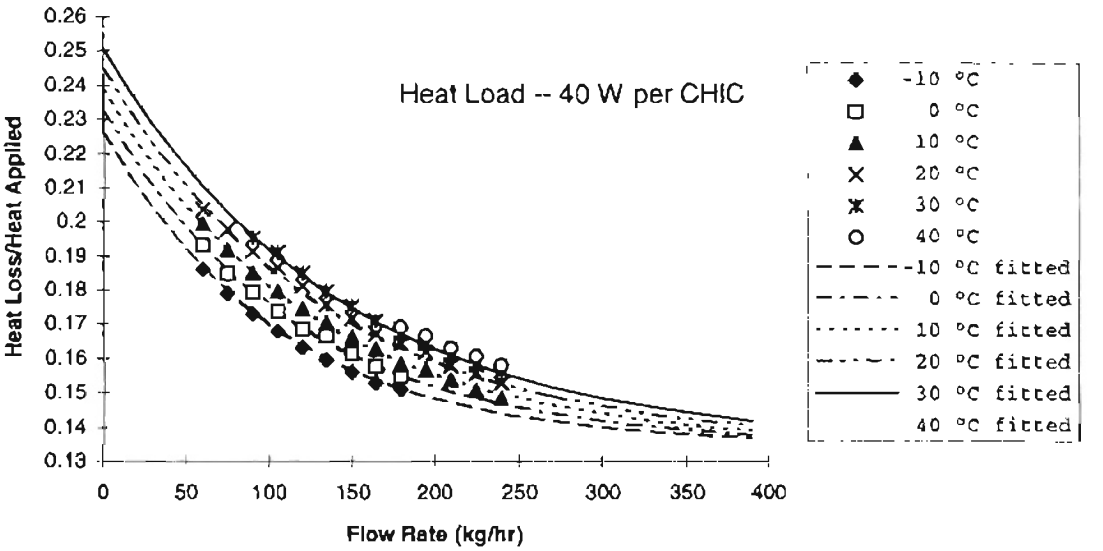

Figure F.2. Radial Heat Loss Due to Conduction Heat Transfer for an Applied Heat Load of 40 W.

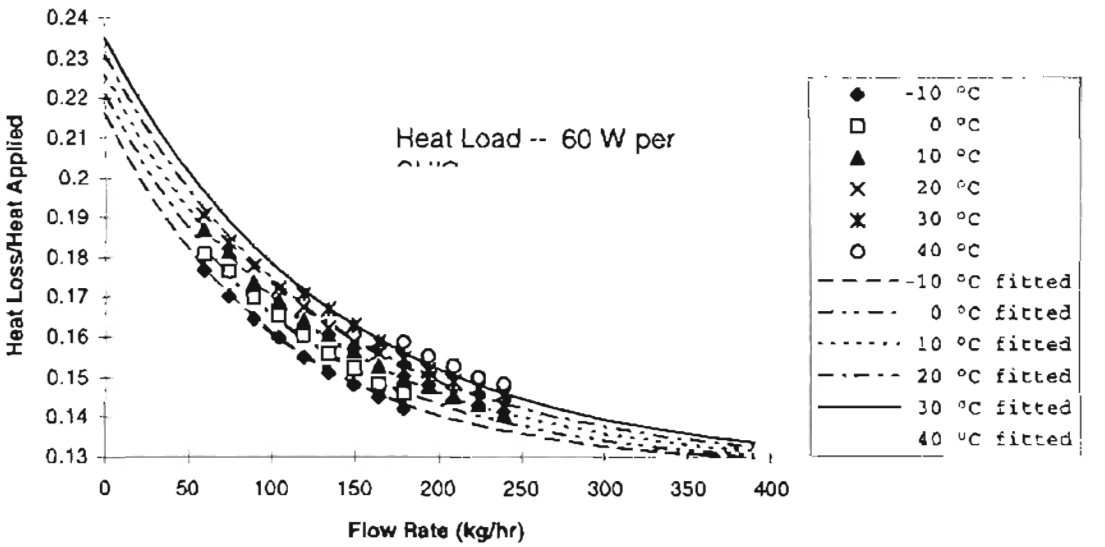

Figure F.3. Radial Heat Loss Due to Conduction Heat Transfer for an Applied Heat Load of 60 W.

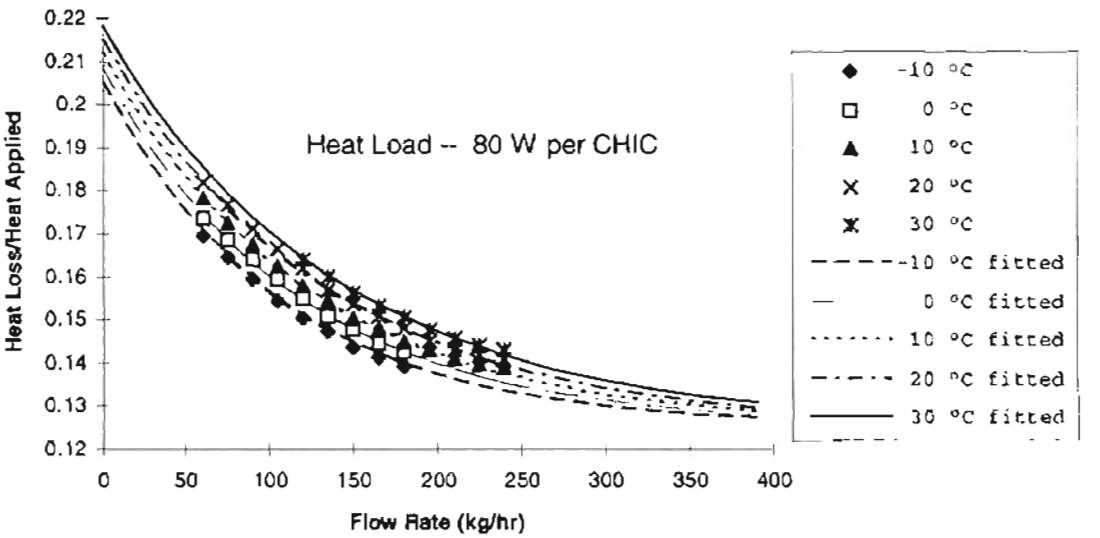

Figure F.4. Radial Heat Loss Due to Conduction Heat Transfer for an Applied Heat Load of 80 W.

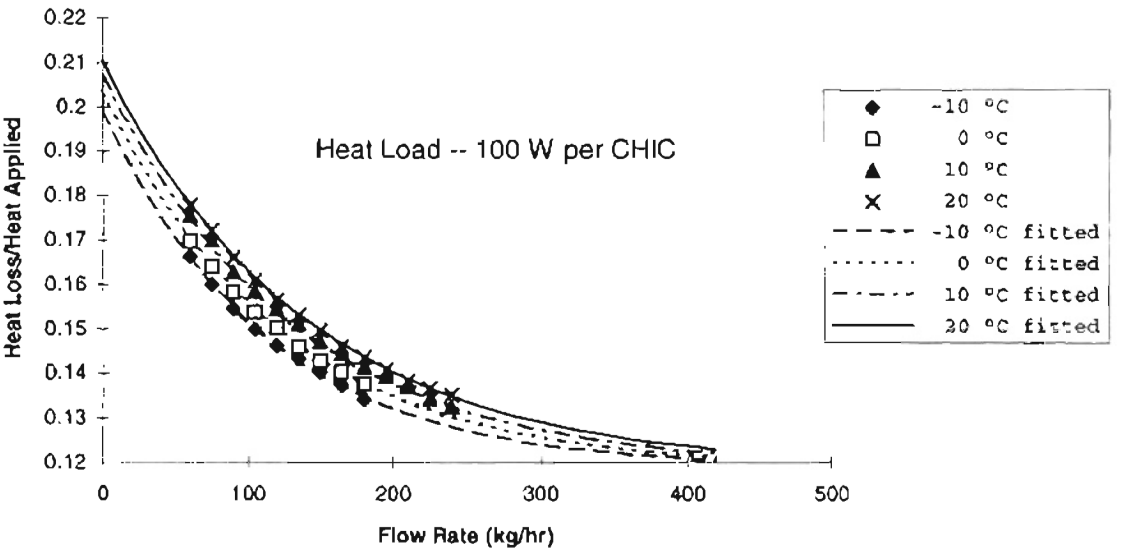

Figure F.5. Radial Heat Loss Due to Conduction Heat Transfer for an Applied Heat Load of 100 W.

Table F.2. Curve Fit Data for the Radial Heat Loss for an Applied Heat Load of 20 W.

Heat Loss /Heat Applied						
Flow Rate	Coolant Temperature					
kg/hr	-10°C	0°C	10°C	20°C	30°C	40°C
60	0.210	0.217	0.225	0.232		
75	0.201	0.208	0.216	0.222		
90	0.193	0.200	0.207	0.213		
105	0.186	0.192	0.199	0.205		
120	0.179	0.186	0.193	0.198		
135	0.174	0.180	0.186	0.192		
150	0.170	0.175	0.181	0.187	0.193	0.199
165	0.166	0.171	0.177	0.181	0.188	0.193
180	0.163	0.167	0.172	0.177	0.183	0.189
195			0.169	0.173	0.179	0.184
210			0.166	0.169	0.175	0.180
225			0.163	0.167	0.172	0.177
240			0.160	0.164	0.169	0.173

Table F.3. Curve Fit Data for the Radial Heat Loss for an Applied Heat Load of 40 W.

Heat Loss /Heat Applied						
Flow Rate	Coolant Temperature					
kg/hr	-10°C	0°C	10°C	20°C	30°C	40°C
60	0.186	0.193	0.199	0.204		
75	0.179	0.185	0.191	0.198		
90	0.173	0.180	0.185	0.191		
105	0.168	0.174	0.180	0.187		
120	0.163	0.169	0.175	0.181	0.185	
135	0.160	0.165	0.171	0.176	0.180	
150	0.156	0.162	0.167	0.172	0.175	
165	0.153	0.158	0.163	0.168	0.171	
180	0.151	0.155	0.159	0.164	0.167	0.169
195			0.156	0.162	0.164	0.168
210			0.154	0.158	0.161	0.163
225			0.151	0.156	0.158	0.161
240			0.149	0.153	0.156	0.158

Table F.4. Curve Fit Data for the Radial Heat Loss for an Applied Heat Load of 60 W.

Heat Loss /Heat Applied						
Flow Rate	Coolant Temperature					
kg/hr	-10°C	0°C	10°C	20°C	30°C	40°C
60	0.177	0.181	0.187	0.191		
75	0.171	0.176	0.181	0.184		
90	0.165	0.170	0.174	0.178		
105	0.160	0.165	0.169	0.172		
120	0.155	0.160	0.164	0.168	0.171	
135	0.151	0.156	0.161	0.163	0.167	
150	0.148	0.152	0.157	0.159	0.163	
165	0.145	0.149	0.153	0.156	0.159	
180	0.142	0.146	0.150	0.152	0.155	0.159
195			0.148	0.150	0.152	0.156
210			0.145	0.146	0.149	0.153
225			0.143	0.145	0.147	0.150
240			0.140	0.143	0.146	0.148

Table F.5. Curve Fit Data for the Radial Heat Loss for an Applied Heat Load of 80 W.

Heat Loss /Heat Applied						
Flow Rate	Coolant Temperature					
kg/hr	-10°C	0°C	10°C	20°C	30°C	40°C
60	0.169	0.173	0.178	0.182		
75	0.165	0.169	0.172	0.177		
90	0.159	0.164	0.167	0.171		
105	0.154	0.159	0.163	0.166		
120	0.150	0.155	0.158	0.162	0.164	
135	0.147	0.151	0.154	0.157	0.160	
150	0.144	0.148	0.150	0.154	0.156	
165	0.141	0.145	0.148	0.151	0.153	
180	0.139	0.142	0.145	0.148	0.151	
195			0.143	0.145	0.148	
210			0.141	0.143	0.146	
225			0.140	0.142	0.144	
240			0.139	0.141	0.143	

Table F.6. Curve Fit Data for the Radial Heat Loss for an Applied Heat Load of 100 W.

Heat Loss /Heat Applied						
Flow Rate	Coolant Temperature					
kg/hr	-10°C	0°C	10°C	20°C	30°C	40°C
60	0.166	0.170	0.176	0.178		
75	0.160	0.164	0.170	0.172		
90	0.155	0.158	0.163	0.166		
105	0.150	0.154	0.158	0.161		
120	0.146	0.150	0.155	0.157		
135	0.143	0.146	0.151	0.153		
150	0.140	0.143	0.147	0.150		
165	0.137	0.140	0.144	0.146		
180	0.134	0.138	0.142	0.143		
195			0.139	0.141		
210			0.137	0.138		
225			0.135	0.137		
240			0.133	0.135		

VITA

J. Michael Cutbirth

Candidate for the Degree of

Master of Science

Thesis: ANALYSIS OF THE HYDRAULIC AND THERMAL PERFORMANCE FOR THE HIGH FLUX HEAT EXCHANGER

Major Field: Mechanical Engineering

Biographical:

Personal Data: Born in Austin, Texas, September 3,1972, the first son of Dr. James W. and Dr. Denise M. Cutbirth.

Education: Graduated from Edmond Memorial High School, Edmond, Oklahoma in May 1990; received a Bachelor of Science Degree in Mechanical Engineering from the Oklahoma Sate University in May 1994; completed the requirements for a Master of Science Degree in Mechanical Engineering from Oklahoma State University in May 1996.

Professional Experience: Research Engineer, Wright Laboratories, Wright-Patterson AFB, May 1994, to August 1994. Teaching Assistant, Department of Mechanical and Aerospace Engineering, Oklahoma State University, August 1994, to December 1995; Research Assistant, Department of Mechanical and Aerospace Engineering, Oklahoma State University, January 1995, to December 1995. Engineering Science 2223 Section 5 Discussion Instructor, Department of Mechanical and Aerospace Engineering, Oklahoma State University, August 1995, to December 1995.

Professional Societies: Continuing member of the American Society of Mechanical Engineers and the Pi Tau Sigma Honory Society.